# UNIVERSITY OF GENOA
## POLYTECHNIC SCHOOL

**DIME - Department of Mechanical, Energy, Management and Transportation Engineering**


PhD in Machine and System Engineering for Energy, the Environment and Transport
Curriculum Mathematical Engineering and Simulation

**PhD Thesis**
XXXVI Course

# "Simulation tools for design and analysis of CO2-based innovative energy plants"


**Supervisors:**
Prof. Alberto Traverso
Prof. Mario Ferrari

**Candidate:**
Simone Maccarini


May 2024

# UNIVERSITÀ DEGLI STUDI DI GENOVA
## SCUOLA POLITECNICA

**DIME - Dipartimento di Ingegneria Meccanica, Energetica, Gestionale e dei Trasporti**


Dottorato di Ricerca in Ingegneria delle Macchine e dei Sistemi per l'Energia, l'Ambiente e i Trasporti
Curriculum Ingegneria Matematica e Simulazione

**Tesi di Dottorato**
XXXVI Ciclo

# "Strumenti di simulazione per il progetto e l'analisi di sistemi energetici evolventi anidride carbonica"


**Supervisori:**
Chiar.mo Prof. Alberto Traverso
Chiar.mo Prof. Mario Ferrari

**Candidato:**
Simone Maccarini


Maggio 2024

# Contents

# Abstract

In an energy scenario where climate change and geopolitical concerns drive the energy production and utilisation towards decarbonisation strategies, the need to exploit energy sources in efficient ways as well as to manage electrification of processes, is paramount.

In this context, power plants evolving supercritical carbon dioxide (sCO2) can be an efficient, cost-effective, and fast-response solution. Being firstly studied for nuclear applications, these cycles offer a variety of design choices and possible application that need to be analysed and evaluated to identify the best performances and the most profitable applications.

Some of the tools that can be used to assess the performances of such variety of designs of these plants can be the heat and mass balances and the cost analyses to be performed upon them.

Starting from the logical structure of a software tool pre-existing at the Thermochemical Power Group at the University of Genova, the TEMP-EVO tool has been developed and it is illustrated in the present dissertation. This is a tool enabling modular simulation of equipment to be assembled to obtain the desired process configuration. Once the desired layout is chosen, thermodynamic design and optimisation analyses can be performed, to evaluate performances and profitability.

The tool is structured in blocks, separating the process definition, its thermodynamic resolution, and its economical evaluation. The modules developed are presented, together with the integration methods and the possible solvers that have been chosen and developed. Some applications of the tool to cycles evolving sCO2 are presented thermoeconomic results to evaluate different cycle layouts and compare solutions.

# 1 Introduction

## 1.1 Background

Since the industrial revolution, the world energy demand, and therefore fossil fuels consumption, have increased progressively. As a direct consequence, the concentration of greenhouse gases has reached alarming levels, potentially impacting onto the climate of our planet [1] [2]. From 1901 the average surface temperature (which definition and measurement is anyway controversial) of Earth has been increasing with 0.7 – 0.9 °C/century, reaching values of 1.5 – 1.8 °C/century after 1975 [3]. These alterations have potentially endangered the equilibrium of the planet in many ways, e.g. causing a significant worldwide reduction of glaciers [4] and accelerating desertification of drylands [5]. Climate change, combined with emission and deposition of pollutants has impacted both aquatic and terrestrial ecosystems due to their detrimental effect on vegetation and wildlife [6].

Energy policies, mainly of Europe, have addressed decarbonization and reduction of pollutant emissions, shifting the focus of both industries and researchers working in the energy systems field on the development of environmentally sustainable power generation systems. The European Union (EU) research programme Horizon 2020, which had run from 2014 to 2020, put close attention on climate action and development of clean and efficient energy systems and transports [7]. The European Green Deal, a set of measures launched by the European Commission in 2019, has the ambitious goal of achieving zero net greenhouse gas emissions within the EU by 2050, replacing fossil power plants with renewable energy systems [8]. The Green Deal is expected to drive the EU towards a sustainable, potentially climate-neutral, and circular economy [9], also thanks to the new research programme Horizon Europe [10], which will fund research programs between 2021-2027 across the EU members, and the new funding plan NextGenerationEU [11], established

after the COVID-19 pandemic. In the United States (US), renewable energy policies are often promoted individually by the States themselves, more than by the federal government, leading to different scenarios. For example, California set the goals of producing 60% of clean energy by 2030 and of reaching 100% electric retail sales from clean energy systems by 2045. Similarly, the New York government planned to achieve a carbon-neutral economy by 2040, widely adopting clean energy systems [12]. China has also promoted clean energy systems through five-year plans [12], and, according to [13] it could reach 35% of clean energy production by 2030, becoming the biggest user of clean energy in the world.

For these reasons, in the last decades the installed capacity of renewable energy systems showed a strong growing trend [14].

Within the renewable energy mix [15], a huge part consists of the contribution of VRE (Variable Renewable Energy), which represents the energy deriving from renewable sources characterized by non-programmability and non-dispatchability due to their fluctuating nature, such as wind and solar. On the contrary, sectors such as hydroelectric, biomass and even geothermal (which can be considered an approximately constant source) can be controlled without particular variations. The integration of increasingly higher shares of VRE into energy systems is essential for decarbonisation, allowing to continue to meet the growing demand for energy, globally. Thanks to falling costs and supportive policies, the penetration of VRE in the energy mix has increased significantly in recent years. However, the use of non-programmable energies presents a challenge for operators and regulators of electricity production systems [16]. In fact, given that there are rigid constraints on frequency maintenance on the network, this unpredictability of renewable sources, due to variations in atmospheric conditions to which VRE is linked by definition, is a highly disadvantageous aspect that involves balancing problems between demand and the production of electricity.

The energy transition mostly represents a necessary change in the management of energy fluxes, in particular due to VREs, which anyway comes at a cost; any technological advancement will be fundamental to try to achieve most of the ambitious objectives that the world has to set for itself.

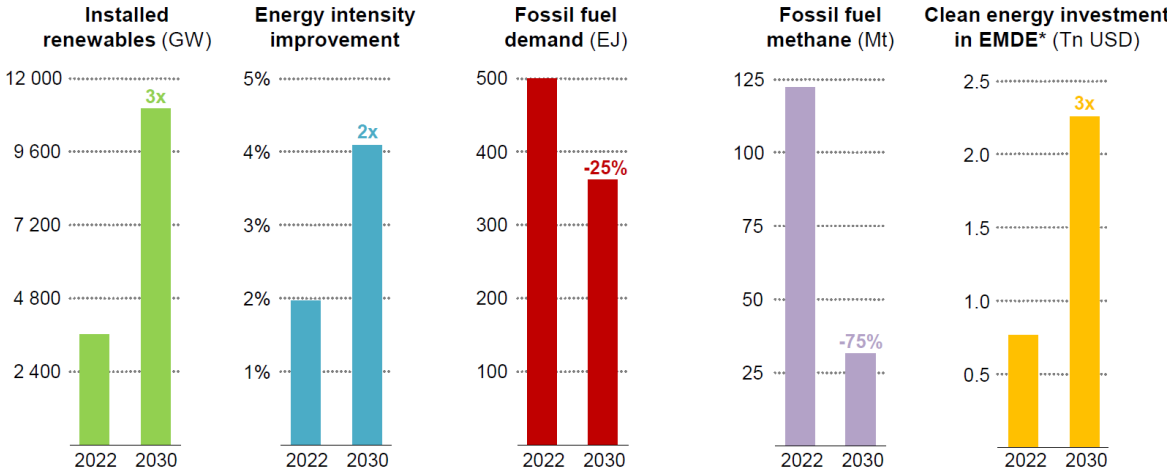


*Figure 1 – Worldwide needed efforts to contain the global temperature rise of 1.5°C considering the Net Zero by 2050 Scenario of the World Energy Outlook by IEA* [1].
**EMDE = emerging market and developing economies*

## 1.2 Power Systems evolving sCO2

As said, climate change and evolving economic interests are leading many countries towards energy policies more focused on an energy transition, in which an increasing share of the energy used comes from a renewable or green sources [15]. Especially in the electrical energy production field, this induces not only the optimisation of the traditional power production plants, but also the research towards new technologies or new fields of application.

In this context, the power plants evolving supercritical carbon dioxide (sCO2) are a field of interest of research institutions and industry in the last decade [17], following the study by Dostal [18][19] , that sparked again the interest on this technology, after the initial studies of Angelino [20] and Feher [21]. The main idea is to design a cycle similar to the gas Brayton one but letting the

compressor working in an high-density region (similarly to what happens in a Rankine cycle) in order to minimise the compression work and thus to increase the efficiency with respect to traditional technology [22].

### 1.2.1 Properties of Carbon dioxide in supercritical state

The choice to use a fluid in supercritical conditions and in particular $CO_2$ was dictated by the advantages that this brought compared to other fluids taken into consideration.

Among these, the fact of having the critical point at a temperature of 31.1 °C stands out, which guarantees reduced thermal stress on the "cold side" of the cycle and allows the use of a refrigerant fluid at temperatures that are not excessively low, accessible in many parts of the world, and a critical pressure of 73.8 bar, a reasonably permissible value which however does not allow high pressure ratios due to technological limits placed on the maximum pressure of the cycle.

Furthermore, carbon dioxide is neither toxic, nor flammable, nor highly corrosive and is stable at high temperatures and economically convenient, given its abundant availability. By working close to the critical point, in particular at the compressor inlet, and at even higher pressures, there is a high density ρ of the fluid which allows a double advantage related to the small dimensions required of the operating machine and the energy needed to compress the fluid, significantly lower than that of a classic Brayton cycle operating a perfect gas.

One of the main problems of sCO2 is represented by its specific heat value cp, which shows maximum trends at a fixed pressure as a function of the temperature, around the critical point, with a progressive reduction in the value of the maximum peak as the pressure increases (Figure 2). This does not allow the adoption of typical thermodynamic simplifying hypotheses, which in most cases consider constant cp, requiring the implementation of complex thermodynamic libraries within the calculation codes.

In terms of control and stability of the thermodynamic conditions within the system, constant monitoring of the state of the operating fluid is required: any variation in the properties of the fluid around the critical point can compromise the correct functionality of the system itself.

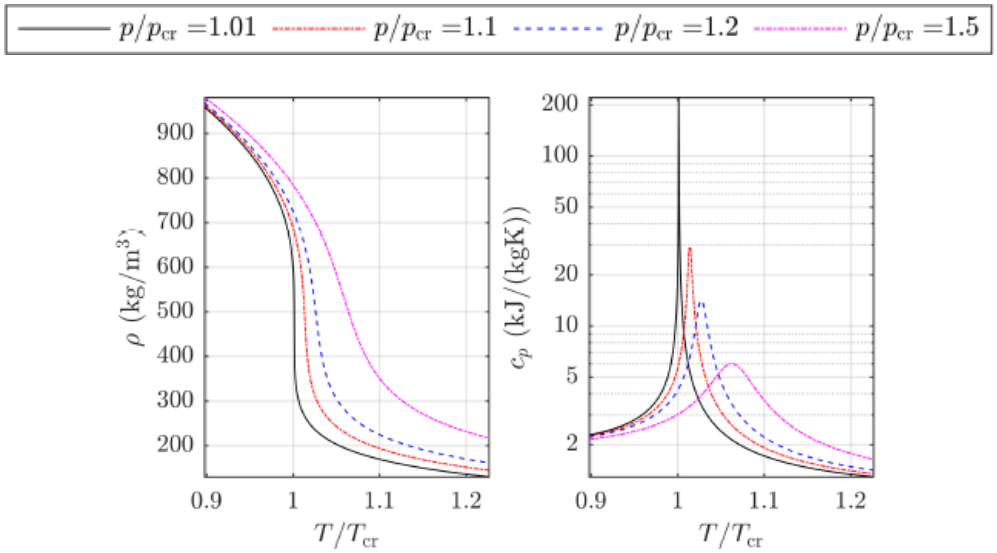


*Figure 2 - Behaviour of $CO_2$ in proximity of the critical point for density and specific heat at constant pressure* [17]

Before analysing the different design solutions, it is necessary to focus on the operating conditions that can be found within transcritical and supercritical cycles. The thermodynamic cycle can in fact be defined as supercritical when all the transformations take place with the operating fluid in pressure and temperature conditions higher than the critical point. However, if the fluid is also in conditions lower than the critical state, it is possible to speak of a transcritical cycle. The development of this second category of cycles has found interest in engineering research as it is capable of significantly increasing the expansion ratio and, in the case of complete condensation cycles, it offers the possibility of replacing the compressor with a pump in order to reduce the work spent in the compression phase. However, the main problem lies in the need to be able to cool the $CO_2$ below 31.1 °C, which makes it a solution that is not always practical.

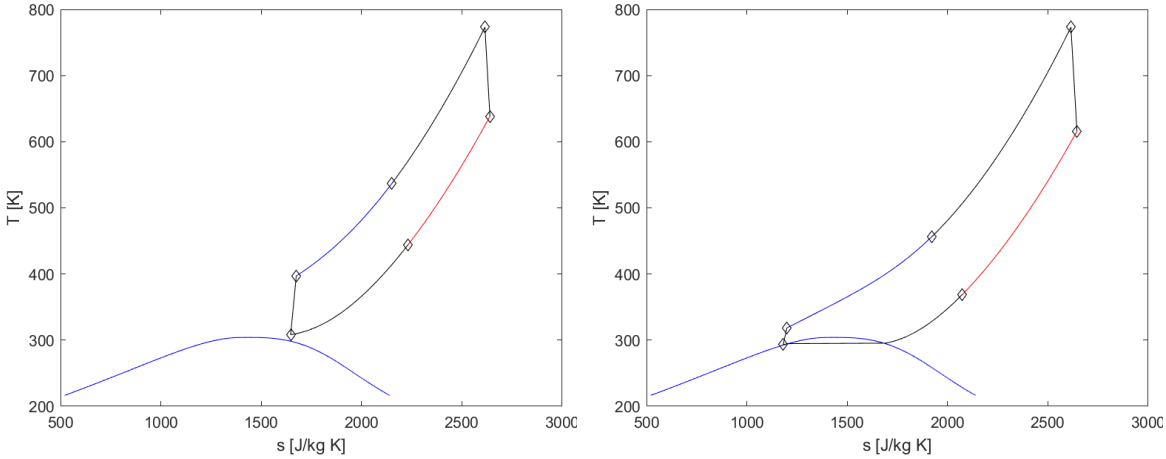


*Figure 3 - Supercritical Brayton cycle (a) and transcritical Rankine cycle (b)*

Alternatively, solutions have been proposed in which the $CO_2$ is enriched with other fluids in order to alter its thermodynamic properties. In particular, two possible paths have been identified: the first involves lowering the critical point in order to guarantee greater expansion capacity in the supercritical state, while the second takes into consideration the possibility of increasing the critical temperature to allow condensation at higher temperatures than the classic ones. Their limited diffusion is due to the need for further specific studies relating to the stability and behaviour of $CO_2$, a fluid which is well known from its use in the industrial field as a solvent, when it is mixed with other compounds.

### 1.2.2 Layouts

The sCO2 cycles are a flexible technology, allowing for many different possible cycle configurations [23], and thus they appear to be interesting in several application fields. This is also due to the extended range of possible operating range in terms of maximum temperature, ranging from the 200°C [24] of the so-called transcritical cycles (tCO2) to the most efficient configurations at 900°C [25]. This last feature makes it possible to find many different application areas for sCO2 cycles, such as waste heat recovery [26][27], or bottoming cycles to a gas turbine [28][29], nuclear plants [30], fossil fuelled power plants [31],

concentrated solar power (CSP) [32][33][34][35] and geothermal [36]. Another foreseen field of application is that of the thermomechanical energy storages, where they can be used with two cycles, one heat pump to convert electricity to thermal energy in order to charge a thermal energy storage, and a power cycle to reconvert the stored thermal energy into electricity; different ways to apply this concept can be found in [37], [38], [39], and [40].

One of the main downsides of these cycles is the high value of the operating pressures [17] that has consequences also on the material selection, due to the combined stress that affects the components when the high pressures are coupled with the high temperatures. This also has an impact on the maximum allowable values of pressure ratio, that limit the efficiency. Moreover, the expected high efficiencies [22] can be achieved only close to the critical point, which leads to a problematic design and management, especially of the main compressor.

For what concern the most studied supercritical cycles, it is possible to take advantage of the classification that was performed by Ahn et al. [22], who noted that all the configurations studied have the simple recovered cycle as their reference cycle. Two macro groups have been outlined based on the characteristics of the flow, i.e. the presence or absence of a $CO_2$ flow split. For the single-flow cycles the most studied ones are:

- Simple Recuperated Cycle
- Intercooling Cycle
- Reheating Cycle
- Pre-compressed Cycle
- Inter-recuperation Cycle
- Split Expansion Cycle

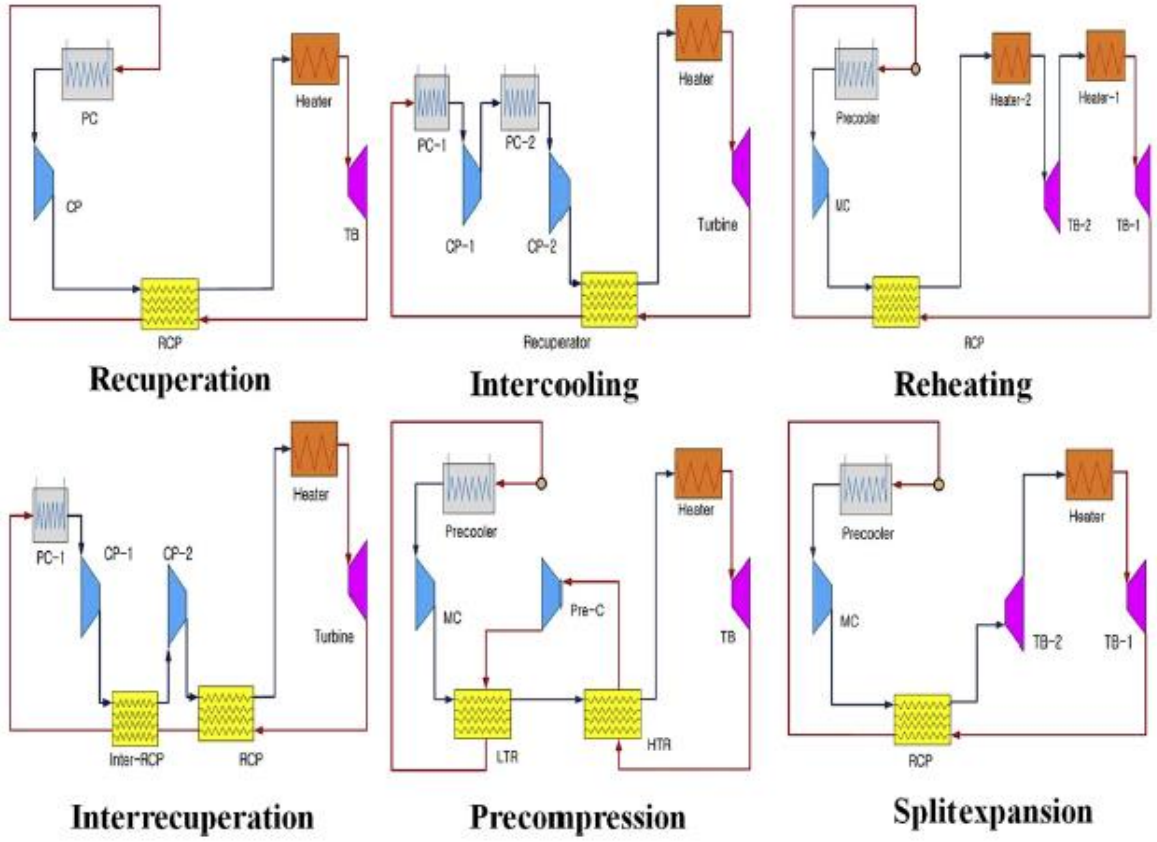


*Figure 4 – Single-flow plant layouts* [22]

Intercooling and Reheating are adopted, respectively, to minimize the compression work and to maximize the expansion work. The high enthalpy content at the turbine outlet allows heat recovery to be carried out in different ways, in fact the remaining cycles proposed exploit different energy recovery techniques which depend on the position of the recuperators.

The development of double flow cycles was dictated by the fact that, inside the recuperators of single flow cycles, the thermal profiles of the hot and cold sides tend to move apart due to the imbalance of thermal capacities, compromising the effectiveness specific to the heat exchanger. This solution allows for different flow rates between the two sides of the recuperator, effectively counteracting this undesirable effect. The most studied cycles in this category are:

- Recompressed Cycle
- Cycle with Preheating

- Cascade Cycle
- Dual Recuperated Cycle
- Dual Split Dual Expansion Cycle

Among these, the recompressed cycle is the one capable of reaching the highest efficiency values: the cycle minimizes the energy expenditure required from the upper source thanks to an optimal ability to exploit heat recovery, made possible by a balance of thermal capacities between the hot and cold fluids inside the low temperature recuperator. Instead, the other layouts maximize the temperature difference recorded between the input and output of the heater, reporting a propensity for use in waste heat recovery (WHR) systems. In fact, since the temperature difference is directly proportional to the energy recovery capacity from an external source, the performance achieved by a cycle such as the recompressed one would be inadmissible for this application.

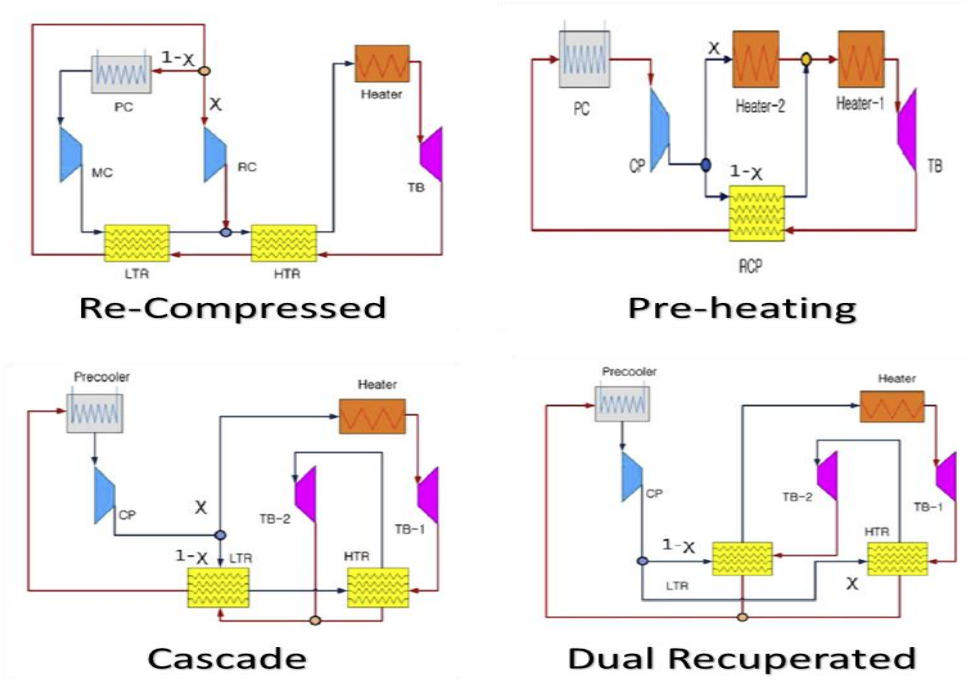


*Figure 5 – Split-flow plant layouts* [22]

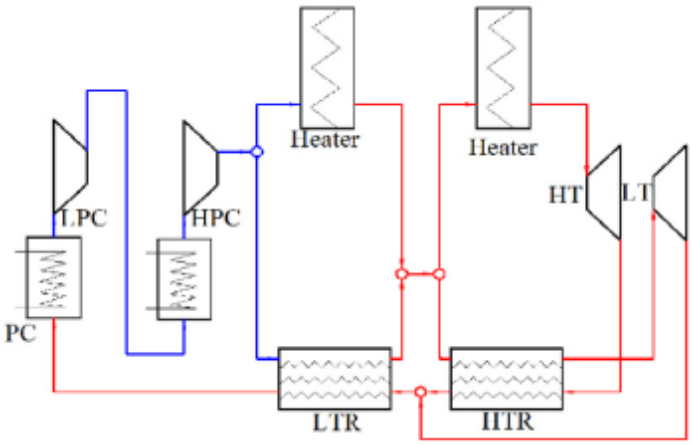


*Figure 6 - Dual split dual expansion plant layout* [41]

### 1.2.3 Typical equipment

The simplest plant layout is the recovered Brayton cycle, whose main components are the turbomachinery, turbine and compressor, and the heat exchangers, heater, cooler and recuperator. The other layouts include various combinations of the same basic components. The high operating pressures and densities can allow a significant miniaturization in the required dimensions of all components, at gas path level, with a consequent reduction in the cost and space required for the system. From these observations it is possible to understand how the selection of materials used for manufacturing all components, aimed at this plant sector, must take into account their thermo-mechanical specifications, compatibly with operating pressures and temperatures.

#### *1.2.3.1 Turbomachinery*

The degree of compactness of the machines leads to high power densities and, to cope with a reduction in their efficiency, the turbomachines must rotate at high speeds in the case of low power output. The high pressure differences that are recorded within the individual stages introduce the need to be able to cope with new challenges aimed at innovative design of blades, casing and bearings

of the machine itself. Once the size of the system has been defined, although an increase in the pressure ratio leads to an increase in cycle efficiency, there is a reduction in isentropic efficiency of the turbomachinery due to the increase in the enthalpy load between different stages. It follows that correct plant optimization must also take into account the efficiency of the machine in different operating conditions. It is good practice to choose radial turbomachinery below sizes of 10 MW, with rotation speeds above 30000 rpm [17], while axial turbomachinery configurations may become suitable for higher power sizes and lower speeds.

#### *1.2.3.2 Heat Exchangers*

In sCO2 systems the heat exchangers strongly influence the efficiency of the cycle and the size of the system. The main problem is to maintain adequate compactness, knowing how to resist the thermo-mechanical stresses induced by pressure gradients and high temperatures. In a simple recovered cycle you can find three different heat exchangers:

- Heater, in order to guarantee a heat exchange with the hot source;
- Cooler, which guarantees the cooling of the working fluid;
- Recuperator, implemented to exploit the high enthalpy content at the turbine exit, due to the low pressure ratio of the cycle, thus increasing the efficiency of the cycle.

By comparing the characteristics of different exchangers on the market, it was possible to identify several types that satisfy the specific requests reported above.

For what concerns the heater, the type of exchanger depends on the nature of the heat exchange: if the source is a fuel and the heat transmission is of the radiant type, the most suitable exchanger is similar to those used in boilers in steam cycles, while if the transmission is only of the convective type, such as for WHR applications, the most common one is the Shell and Tube type or the Hairpin type.

Instead, for the recuperator, the innovative Printed Circuit Heat Exchanger (PCHE) technology is optimal for this use. The PCHE are made up of a series of overlapping flat plates which, through channels obtained by removing material, are alternately crossed by hot fluid and cold fluid with counter-current heat exchange.

There may also be solutions where two hot plates are alternated with a single cold one; in most cases the section that characterizes the canals is semicircular. These are compact and structurally robust, managing to guarantee excellent performance in extreme working conditions; on the other hand, this compactness causes high pressure losses, which must be managed to obtain the optimal system configuration. Unfortunately, these exchangers involve complex cleaning procedures due to the small size of the channels and the entirely welded structure; for all the aforementioned reasons, the most common types of exchangers are often applied, such as those of the hairpin, shell and tube type, especially microtube, or plate-fin ones.

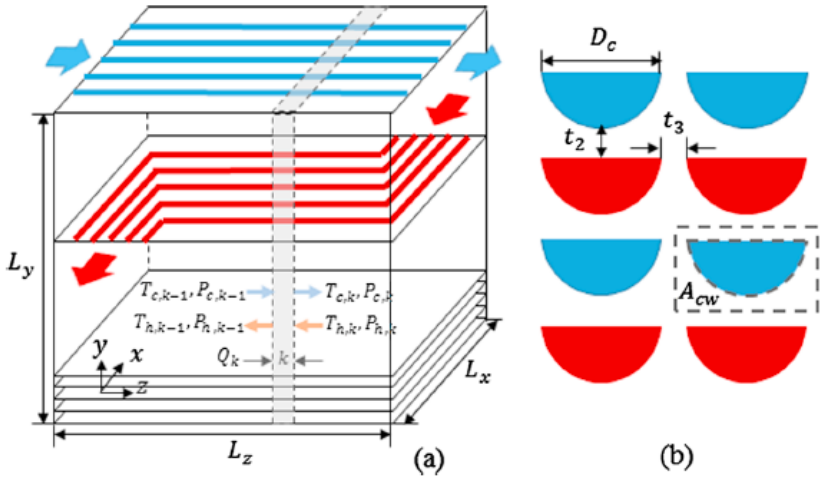


*Figure 7 – Printed Circuit heat exchanger (PCHE)* [22]

Compared to heaters and recuperators, the pressures and temperatures to which the cooler is subject are significantly lower, resulting in less attention being paid to the selection of materials used for manufacturing. The refrigerant fluid used can be made up of water (wet cooling) or air (dry cooling), or intermediate situations based on the heating of the air and evaporation of water

(wet surface air cooler WSAC, see Figure 8), paving the way for different heat exchange configurations. If the fluid used is air, the pressures that can be adopted by the $CO_2$ at the lower source must have higher values when compared to those with water exchangers. Due to the high difference in specific heat between $CO_2$ and air, the latter requires high flow rates in order to balance the heat capacities in the exchanger, and requires a choice of ad hoc heat exchangers. On the contrary, when water is used during cooling, the problems mentioned above do not occur, allowing lower operating pressures for $CO_2$ and the use of the more common plate exchangers.

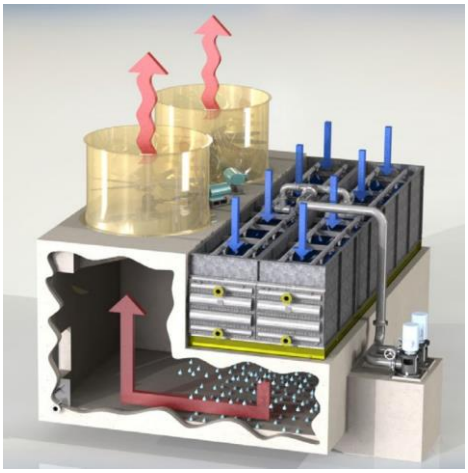

*Figure 8 – Alfa Laval's Wet Surface Air Cooler (WSAC)* [42]

### 1.2.4 Aspects of dynamics and test facilities

As said, these systems have some tight operational constraint and are characterised by peculiar transient phenomena that occur during load changes. Consequently, it is also crucial to study the dynamic behaviour of an sCO2 plant to assess its actual capabilities and advantages with respect to more traditional power plants, and design a control system that is both responsive and efficient.

Several studies have delved into the performance of sCO2 cycles under varying loads and dynamic conditions, as detailed in [17]. However, only a few of these studies have been validated thus far, and typically on a small scale [43][44]. Inventory control is commonly favoured for its efficiency, despite its slower response and stability concerns due to mass injections or withdrawals [45].

Meanwhile, turbine flow bypass or throttling is considered for rapid transients near the design point, although this approach often sacrifices efficiency [46]. Furthermore, studies propose a dual-shaft configuration to enable control over the main compressor speed (and consequently flow), resulting in efficient load management with reduced complexity [47].

Applications of control systems can be observed in the STEP project and the Echogen EPS100 unit, detailed respectively in [48] and [49]. In the latter, a relatively simple control system is applied to a real-world scenario, utilizing a compressor bypass valve, turbine throttling valve, and inventory system to respectively control compressor speed (and mass flow rate), power output, and cycle lower pressure. Recent studies have systematically explored cycle operating strategies. For instance, [27] conducts a comprehensive analysis for WHR applications, examining both variable and constant inventory systems, while [50] reviews key aspects of part-load analyses and explores the behaviour of a recompressed cycle with dry cooling, including the influence of ambient temperature. A similar study is also presented in [51], which also considers the impact of molten salts tanks. The influence of the control strategies implemented on the power block on a CSP solar receiver is briefly analysed in [52].

To evaluate the practical implementation of these cycles, several small loops are operational worldwide, such as [53] [54] [55] [56] [57] [44] [58], with a few projects aiming to construct complete pilot plants, notably the STEP project in the US [59] [60].

In Europe, many research projects aim to study and develop novel equipment for this technology, and in particular the SOLARSCO2OL EU Project [61] [62], in which the University of Genoa is partner, aims to develop and build the first MW—scale demonstration plant of a sCO2 power block coupled with molten salts coming from a CSP plant in Europe.

## 1.3 Aim of present work

As briefly shown in the description of sCO2 plants, these systems are seen as a possible technology able to be applied to many different applications in the energy production and storage fields. At the same time, the more traditional, affordable and established technology of the benchmark technology of the steam Rankine cycle (but also the ones working with organic fluids), poses questions on where and how the sCO2 plants can find a spot in the energy production market.

For these reasons, questions arise on what the best applications of these cycles can be, and on what the possible best layout configurations and their performances can be, both in terms of efficiency and cost-effectiveness, as well as for what concern their operational performances.

To try to answer these questions, it was necessary to develop a thermo-economic tool able to analyse sCO2 cycles in different configurations and for different applications, and to be able as well to compare them with more traditional plants in a comparative way. For what concerns the operational performances of such plants, at the same time a dynamic tool had to be developed, in order to evaluate the possibility of the study of the dynamic behaviour of such plants and evaluate their dynamic performances.

# 2 The TEMP-EVO tool

The thermodynamic cycles presented in the previous chapter mainly take advantage of the peculiar changes in thermophysical properties of carbon dioxide. Since several possible configurations exist, choosing the most appropriate or performative one depends on the specific application, and it is of paramount importance for designing of plants and decision making.

Different commercially available software tools, less or more general-purpose, allow the user to perform cycle design and heat and mass balances, such as Ebsilon [63], Gate Cycle [64], IPSEpro [65], Thermoflow [66], Aspen Plus [67], or ProSim [68]. Since late 90s, the Thermochemical Power Group of the University of Genova developed a tool called Web-based ThermoEconomic Modular Program [69], written in Fortran and consisting of several libraries to perform thermoeconomic evaluations of complex energy systems mainly working with fluids with perfect gas behaviour: the original code was equipped with a web-based visual interface in the early 2000s. In order to update the internal W-TEMP tool, and to integrate the possibility to analyse systems working with fluids with real-gas behaviour, similarly to the $CO_2$-based ones, a newer version of such thermoeconomic tool, the ThermoEconomic Modular Program EVOlution (TEMP-EVO), has been developed and is presented in this chapter.

The TEMP-EVO software is developed in the MATLAB® programming environment. This simulation tool has evolved in order to analyse and optimize the thermo-economic performance of different supercritical $CO_2$ cycles and is capable of evaluating evolving fluids with perfect or real gas behaviour, including change of phase, through the integration of CoolProp, an open-source library of thermophysical properties [70]. Furthermore, it has been also implemented the possibility to connect to the REFPROP [71] library to obtain analyses also working with fluids with peculiar compositions. In particular for

carbon dioxide, in these libraries the Span and Wagner equation of state is used [72].

TEMP-EVO is a modular software, as each component of the system considered is represented by a set of functions that calculate the input and/or output parameters, basing on fundamental thermodynamic evaluations carried out within the component itself and subsequently assembled at system level, combining all components; in this way, the different modules can be both analysed separately or assembled in various ways to evaluate any desired layout.

## 2.1 Tool general structure

The TEMP-EVO tool can be used to compute a thermodynamic cycle, open or closed, or more generally a process, despite still missing, at present, some capabilities that were not of paramount interest in the study of sCO2 cycle, like the implementation of a changing composition of the fluid (e.g. combustor, chemical reactor, etc.).

A graphical interface is not present yet, and thus the user has to rely on the direct interaction between the user and the MATLAB scripts: however, the visual interface is planned to be realised within 2025, through professional ICT suppliers, and it will be based on MATLAB GUI library, therefore allowing future upgrades on single-software basis. It basically consists of a series of predefined scripts, in which some parts can be modified, and a collection of routines representing either the implemented components of thermodynamic processes (e.g.: a turbine, an heat exchanger), the *component functions*, or a routine used to automatise the set-up or solve of the desired process, like the *solver functions*, or again the routines that compute further results, like the *cost functions*.

The logic flow with which the tool operates is illustrated in Figure 9.

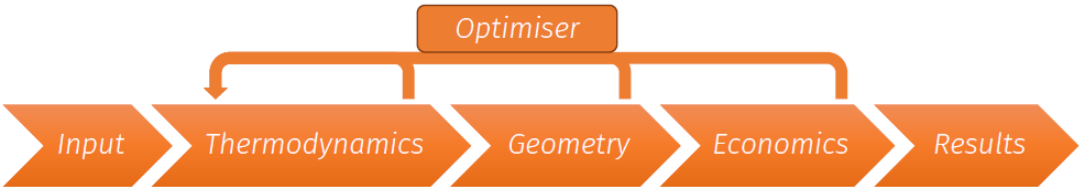


*Figure 9 - General logic flowchart of the TEMP-EVO tool*

First of all, the user has to define externally what is the desired process or the desired thermodynamic cycle to be analysed, and enumerate all the thermodynamic steady state points of the process. After that, a function representing the list of the necessary component-functions that need to be computed can be created, or it can be chosen among the predefined ones (some thermodynamic cycles are already pre-implemented). With this information, the inputs of the process can be provided to the tool, in slightly different ways, depending on the chosen thermodynamic resolution method. The inputs that the user has to provide are all those necessary to define a unique thermodynamic solution to the system to be analysed. Thus, these inputs represent all the assumptions relative to the thermodynamic states of the fluids involved and the operational-performance characteristics of the existing machines. These include, for example, all the fluids evolving in the components, some thermodynamic properties in a specific point (e.g.: a desired temperature), or a property that can be assumed to be heavily dependent on how a component is made or operated (and thus called "Component Property"), like a mass split percentage of a three-way valve, or the efficiency of a turbine.

When all the initial steps are completed, the user can run the script relative to the thermodynamic resolution, that takes information from the inputs to iterate the computation of the function of the cycle (or the process) until convergence to the solution, within a pre-defined numerical tolerance. If a solution cannot be computed, the script immediately warns that some parameters are either in excess or are missing; if the calculation may start but cannot converge, the vector of the variables is returned to the user, to identify what are the conditions

that do not allow the solution to exist. Of course it is also possible that a physical solution can exist, but the solver is not able to identify it; several solvers have been implemented to increase the robustness of the tool, but in case of unsuccess of the solver, modifications of specific parameters can help in identifying the problem.

Following the thermodynamic resolution, all the properties of the desired process are known (e.g. mass flow, pressure, temperature), and thus, upon such a defined thermodynamic solution, a more detailed analysis can be made. The first step is to carry out a preliminary design of heat exchangers or other components involved in the process. The heat exchangers (HEXs) are always solved, inside the thermodynamic resolution, with 0D (or in some cases 1D) models that compute the exchange of heat for a counter-current HEX. The geometry resolution thus simply computes all the heat exchangers in detail, depending on the geometrical input values that the user selected, such as the desired type and the information on tube dimensions and velocity. The geometry routine thus computes the area of the exchanger through the calculation of the heat exchange coefficients, and it serves as a basis for the cost estimations. It is further important to underline that this calculation serves as a first selection and design, and while its results (such as the actual pressure drops) can be used to initialise the inputs to a new calculation of the same process, an internal iteration combining the thermodynamics and the geometry it is not possible, at the moment, since this would complicate the solver. On the other hand, as far as thermodynamic principles are conserved and real transformations are calculated, e.g. avoiding any internal negative pinch point, the preliminary design is necessary only for the following economic evaluations, and not for determining the cycle performance,.

Finally, the tool allows for economic evaluation of the converged thermodynamic solution. After the thermodynamic and geometrical resolution, the sizes of the components (e.g. in terms of the area of heat exchangers, or of power for the machines, etc.) are found, and they are used as the main scaling parameters on

the cost functions, used to compute the purchase equipment cost (PEC) of the components involved in the analysed process. With this approach, it is then possible to compute the capital and operational expenditures, and to estimate the key parameters from the investment point of view, such as the internal rate of return or the payback period.

Every time a group of results is generated, (namely, the thermodynamic, or the geometrical, or the economical ones), it is possible to use them for an optimisation on selected parameters, or to just have a look at a sensitivity analysis on the influence of target variables on the key performance indicators (such as the efficiency, or the total cost, etc.). As said, this is done through a predefined MATLAB script, modified according to what the user wants to study, that allows to show a sensitivity on up to 4 parameters at once, or to find the optimal value of a performance indicator given the variation of a certain number of decision variables. The optimisation process relies on the functions for global optimisation natives to MATLAB, such as "patternsearch", "surrogateopt", or "ga", thus ensuring a flexible choice to the user, reliable behaviour of the solver and a more trustworthy solution.

### 2.1.1 Background – The W-TEMP Tool

This simulation tool presented in this thesis represents the latest evolution of W-TEMP (Web-based ThermoEconomic Modular Program) [69], a code developed almost 20 years ago by the Thermochemical Power Group (TPG), research group of the University of Genova, Italy, in order to study and optimise complex energy systems, to analyse their performance and feasibility, both technically and economically. For this reason, detailed software has been developed for a complete and automatic thermoeconomic analysis of power and cogeneration plants of different types, concepts and sizes. However, the original tool had the limitation that only water could be included with real-gas behaviour. The recent interest towards supercritical $CO_2$ cycles, as well as

Organic Rankine Cycles, motivated the need to extend the approach to real-gas systems.

From the beginning of this work, the basic idea was to regenerate the original tool on a different and more modern software basis, for instance from Fortran to MATLAB, retaining a modular approach in order to allow free development by all users, and including the possibility to simulate a variety of working fluids with real-gas behaviour.

The original code W-TEMP currently offers more than 90 modules and is capable of simulating different types of energy systems, from conventional systems (i.e. combined cycle) to advanced concepts (humid air cycle, hybrid fuel cell system, integrated biomass gasification plant, etc.), automatically providing the user with thermodynamic, exergetic and economical both on the internal structure of the layout and on the system as a whole.

W-TEMP allows the thermoeconomic and exergoeconomic analysis of numerous energy cycles: steam, gas turbine, combined and advanced (mixed gas-steam cycles, integrated biomass gasification plant, SOFC and MCFC fuel cells, hybrid cycles, partial oxidation, chemical recovery cycles, solar-integrated combined cycles).

The system to be calculated is defined as a set of interconnected components, whose operational characteristics and mass and energy balances, in the design state, are calculated sequentially until the conditions (pressure, temperature, flow rate, etc.) at all interconnections converge on a stable value.

The code is developed in FORTRAN, and it is able to evaluate the performance of cycles evolving user-defined fluids, through the indication of the composition of the fluid itself, and the definition of a polynomial function for the main physical properties. 28 different working fluids can be selected and are available as semi-ideal gas (ideal compressibility factor but variable specific heat), with the only exception of water, for which real-gas effects are fully included (ASME Steam Tables).

The W-TEMP code is also equipped with an energy system optimization tool with different objective functions: the most important are thermal efficiency and the cost of electricity.

In the W-TEMP software, in addition to the complete thermoeconomic evaluation, the environmental analysis of power plants is also available. The code allows the user to evaluate the effects, for example, on the final cost of electricity and on the internal rate of return of the system caused by the introduction of charges on polluting emissions or taxation of fuels. In this regard, W-TEMP is also a powerful tool for evaluating the advantages and disadvantages of policy actions from a microeconomic and macroeconomic perspective. Finally, the software is equipped with the complete Carbon Exergy Tax (CET) procedure, proposed by TPG as an effective rule to control $CO_2$ emissions, penalizing the most inefficient systems.

## 2.2 General Concepts of the Thermodynamic Analysis in TEMP-EVO

The thermodynamic analysis in TEMP-EVO consists in the resolution of the thermodynamic process that is the object of interest, and thus defining all the properties of the system respecting the basic heat and mass balances, according to the intrinsic thermophysical properties of the working fluid in each point, the characteristics or efficiency of components, external energy transfers or losses, etc.

A central feature is the so-called *General Matrix of Properties* (GenProps Matrix), which is a table (in the tool it is technically a matrix, despite not being used as it mathematically) that collects all the information on the properties of the evolving fluid, in each point of the analysed system. Since it is not used in matrix computations but acts as a database of information, it can be updated and expanded with all the properties that can be relevant for the specific system. The rows of the table represent the thermodynamic points of the desired cycle, and the columns represent the properties. The properties are stored in basic

units of measurement relative to the international system, but a second table is also present, copied from it and scaled towards a more "engineering-common" system. At the present moment, the following properties are implemented:

1. Pressure in [Pa] or in [bar];
2. Temperature in [K] or in [°C];
3. Specific Enthalpy in [J/kg] or in [kJ/kg];
4. Specific Entropy in [J/kgK] or in [kJ/kgK];
5. Mass flow rate in [kg/s] in both tables;
6. Quality its value ∈[0,1] only if the point is two-phase, otherwise its value is equal to -1;
7. Density in [kg/m$^3$] in both tables;
8. Exergy in [J/kg] or in [kJ/kg];

| | p | T | h | s | m | x | ρ | ex | ... |
|---|---|---|---|---|---|---|---|---|---|
| 1 | | | | | | | | | |
| 2 | | | | | | | | | |
| ... | | | | | | | | | |
| n | | | | | | | | | |

*Figure 10 - Representation of the General Properties Matrix*

Alongside with the General Properties Matrix, a vector of fluid information is also a similar central feature. In fact, it is defined again as a table (in the tool it is a cell vector data type) containing the fluid features in each point of the process. The rows are, as before, the thermodynamic points of the system, while the columns are the fluid name, followed by its characteristics, if relevant, represented as functions of the temperature. In fact, many times it is sufficient

for the most common non-pure technical fluids (such as, for example, some commercial molten salts used as heat transfer fluid) to have their properties represented only as a function of the temperature of the fluid itself.

Usually, the fluid name is defined so that it can be directly used within the integrated library of CoolProp (or REFPROP), by passing a string of characters indicating the name; for example, for carbon dioxide the fluid name can be 'co2' and this will be used in all the computations related to the specific process point. In this case, no further information for this fluid would be necessary. Otherwise, if the fluid is, for instance, a binary molten salt that is not present in the CoolProp library, the user can give as input the value 'userdefined' as the fluid name, and the characteristics of the fluid will be added to the following columns for that fluid, in the form of vector of coefficients that have to be used to compute them. The characteristics that can be introduced in this way are:

1. Specific heat $C_p$ in [J/kgK]
2. Density $\rho$ in [kg/m$^3$]
3. Dynamic viscosity $\mu$ in [Pa·s]
4. Thermal conductivity $\lambda$ in [W/mK]

The specific heat, density and the thermal conductivity are derived from three coefficients *a*, *b* and *c*, while the dynamic viscosity only by two, and they can be computed with the following simple polynomial equations, where the temperature $T$ is expressed in degrees Celsius:

$$C_p = a + b \cdot T + c \cdot T^2 \quad (1)$$

$$\rho = a + b \cdot T + c \cdot T^2 \quad (2)$$

$$\mu = a \cdot T^b \quad (3)$$

$$\lambda = a + b \cdot T + c \cdot T^2 \quad (4)$$

Thanks to the integration with REFPROP, it is also possible to define mixtures, predefined by the user with fixed composition, to be used as working fluid.

Thus, each point is linked to a predefined specific fluid, and this is actually a limit to upgrade the tool in order to be able to address also problems where a change in composition is present, such as in the case of combustion. One way, despite not present yet, could be to upgrade the fluid information so that it can be also gathered from a table similar to the properties matrix, but dedicated to the composition of the fluid, and then allowing some specific component (such as a combustor) to modify and compute these modifications. At present, detailed analysis of cycles with variable compositions is retained as main capability of the original W-TEMP tool.

| | 1 | 2 | 3 | 4 | 5 |
|---|---|---|---|---|---|
| 1 | 'co2' | 0 | 0 | 0 | 0 |
| 2 | 'co2' | 0 | 0 | 0 | 0 |
| 3 | 'co2' | 0 | 0 | 0 | 0 |
| 4 | 'co2' | 0 | 0 | 0 | 0 |
| 5 | 'co2' | 0 | 0 | 0 | 0 |
| 6 | 'co2' | 0 | 0 | 0 | 0 |
| 7 | 'userdefined' | [1430,0,0] | [2240,-0.27... | [1.3721e+0... | [0.5200,0,0] |
| 8 | 'userdefined' | [1430,0,0] | [2240,-0.27... | [1.3721e+0... | [0.5200,0,0] |

*Figure 11 - Example of the fluid vector*

Some properties relevant for the thermodynamic resolution are not actually properties of the evolving fluid, and thus are not related to a specific thermodynamic point, and thus their data cannot be stored neither into the Properties Matrix nor into the fluid vector, but are intrinsic to or descriptive of a specific equipment type. For this reason, in the tool these properties are called *Component Properties* ("CompProps", and stored into the structure of each component) and can be, for instance, a percentage of split of a certain mass flow, a machinery efficiency, or an effectiveness or a temperature difference inside an heat exchanger. At the present moment they are all collected in a single vector during iterations.

Finally, also a vector containing all the powers exchanged by each component is present and named *Powers vector*, and it is used to collect this type of information, to be later exported and used after the thermodynamic resolution, or to be used in iterations within the solution computation.

The main thermodynamic performance indicators, such as efficiency of or net power produced by the analysed cycle, are dependent on the specific configuration, and thus are not standardized but are computed for each cycle configuration post-processing the data from the properties table. Then this information is simply collected or it can even be used as objective of an optimisation procedure.

To summarise, from a practical point of view, to set up the thermodynamic solution of the cycle using the TEMP-EVO tool it is necessary to proceed with the following steps:

1. Define externally the cycle or the process to be analysed, assigning a number to each thermodynamic state. Then report the system into the tool by initialising a predefined cycle or assembling the various component modules by calling their respective input functions and define component interfaces (this step will be automated through a visual interface within 2025).
2. Initialise the information related to the evolving fluids and choose the library from which the thermophysical properties are obtained, or define them through coefficients to compute their physical properties. For each module, it is possible to set a different fluid (or two for the heat exchangers) passing through the component.
3. Set the values of only the known parameters (properties) of the components (efficiency, pressure losses, etc.), to be saved to structures that define each component. Set the values of only the known thermodynamic properties (pressure, temperature, etc.) in the relative points. The values of these two groups (called degrees of freedom of the

system) have to be chosen so that a unique solution is possible for the energy system.

4. Initialise every property with some initial guess value, close enough to the solution so that it can be used by the corresponding functions (it is not recommended to put values outside the order of magnitude of the real solution, or of opposite sign). These will be used by the solvers to start the iterations, that will stop when the residuals of the calculation tend to zero. The more stable the model, the easier convergence will be achieved despite the initial values being defined far from the final cycle. To define the initial conditions, it is necessary to assume flow, pressure and temperature values for all points of the cycle. For the properties of the components (e.g.: turbine expansion ratio), a standard initial value is already implemented in the code but, however, the user is free to modify them.
5. Once the system has been initialised, it is possible to recall the functions of all the components, that implement the pressure, energy and flow balance equations of the various modules to find the solution of the system, obtaining the thermodynamic data (pressure, temperature, enthalpy, mass flow rate, entropy, exergy, density, etc.) for each point of the cycle defined at the beginning.

### 2.2.1 Introduction to the mathematical methods

Having described the general logic of how the tool is structured, in particular for the computation of the thermodynamic results, which mainly consists of a heat and mass balances, it is possible to illustrate the general concepts of how calculations are performed.

The process is simulated in the tool as an ensemble of components, each of which is constituted by characteristic equations. Thus, the process itself is made of a set of equations that have to be calculated, and three methods can be generally

identified to perform the heat and mass balance on them, namely *sequential*, *equation-oriented*, and *semi-parallel*, as described, for instance, in [73].

A *sequential method* consists of performing the computation of each component in sequence, performing then at least one or, depending on the equations dependencies, even more iteration loops. This was the approach used in the original W-TEMP software tool. These iterations can be not so easy to implement with a modular approach, being case-specific, and very time-consuming and sometimes lead to divergence of the simulation tool.

To avoid problems of iterations, an *equation-oriented approach* based on a system of equations can be used, also to increase the modularity of the tool. In this method all equations representing the entire system are collected in a matrix and solved simultaneously. On the other hand, with this kind of method problems on the convergence can arise mainly depending on the initial guesses used as inputs to the numerical solvers of the system of equations. One approach to avoid this kind of problem could be to build the plant in smaller segments and use the resolved data from the segments as the starting values for the solver.

Finally, a combination of the two methods discussed is also possible, called *semi-parallel method*. The sequential method is here used to solve as many variables as possible for the general system of equations, and to increase the quality of the initial guesses to be used by a solver following the equation-based approach.

The methods illustrated in this thesis are original re-elaborations of the first two methods outlined above with the first one being very close to the logic implemented in the original W-TEMP, and the second one applied to direct resolution of the whole plant and not only a sequential resolution of the components: it will be called *complete system* approach in the following. The last method has not been implemented, and could be objective of future work, but some changes are made to the second-type logic to increase the robustness of the equation-oriented (or system-oriented) resolution.

## 2.3 Modelling approach

As said, the structure of the TEMP-EVO tool is organised so that the analysis of the system, and its configuration, can be flexible, and this is guaranteed through the modularity of the tool itself. The desired system is made up by assembling the modules relative to the main real equipment that is needed for it (calling each of them from the predefined library).

Each module of a component (Figure 12) is defined by its characteristic equations to compute thermodynamic and thermophysical properties such as pressure, temperature, enthalpy, etc. It is then connected via inlet and outlet "ports" to other components, to be able to assemble every possible thermodynamic cycle.


*Figure 12 - Schematics representing two components; a turbomachine (left) and a heat exchanger (right)*

The aforementioned library is basically made of a series of functions, where each one reports the resolution of simple thermodynamic equations related to a specific piece of equipment. Each component is modelled as a function that receives all the properties related to the component itself, both from its inlets and its outlets , calculated at the previous iteration, plus its intrinsic characteristics, and returns a way to compute the next step of the iteration, depending on which solver has been selected.

More in detail, though being also inspired by the object-oriented programming, at the present moment the code is structured so that each component is neither a unique function nor exactly a software object, but it is anyway defined with a

software structure and two functions that describe the component type, similarly to the methods of an object. The structure contains the main information on how the component interacts with the others and the main data strictly related to the component, also called component properties (CompProps). Then, two functions allow to initialise or solve the component, depending on the iteration status. The first of these functions is the *Inputs function*, and allows to define the component, by simply inserting the main interactions, like inlets and outlets of the component, and the values of those component properties that are classified as parameters, meaning that they are fixed in the initial phase by the user and not computed as results. The result is the definition of the structure of a defined component of the desired type. For example, a compressor operating between points 1 and 2 of the cycle is defined with the function relative to its component type and a structure is created named, for instance, "COM1" (or as desired).

The second function of each component type consists of the main characteristic equations that need to be solved to define how the component operates. Since certain components can be represented through different possible functions, depending on how many parameters are needed to define it in that specific case, it is good practice that the user selects the function that allows the resolution of the desired data for the component using the simplest function available, avoiding unnecessary computations and iterations to solve equations to find variables that are not relevant to be fixed in the analysis. Once the desired cycle is computed, then a complete description of all the variables can be obtained a posteriori, even though not included in the computational process. For example, an heat exchanger can be represented by a function that only resolves the heat exchange equation, or which also computes the temperature difference between the two fluids. So, if the temperature difference is fixed as an imposed value by the user, and thus can be called a "degree of freedom" of the system and it is used to start the calculation of the other parameters, it is necessary to use the function that also computes such a parameter. Otherwise, the information on the temperature difference can be obtained a posteriori after the thermodynamic

problem is solved, and thus it is possible to simplify the model and remove a variable and the related equation from the system, to enhance converge speed.

### 2.3.1 General-purpose structures and functions

As described before, each component is described through the definition of certain parameters that are collected in a software structure. This is generally called *structure of the component* (Component_Str) and it has the name selected by the user for the specific component. In Figure 13 it is shown the structure for a compressor named "COM1", provided as an example. The main software variables inside the structure are the inlet and outlet ports of the component, that are used as index to connect the component to the thermodynamic point of the cycles between which it operates, and thus also to the rows of the matrix of properties described in the previous chapter. It can also be seen the software variable "k_Comp", which represents the index on which the information related to the component starts within the vector of the component properties. This is a way to uniquely identify where the information of each component is stored.

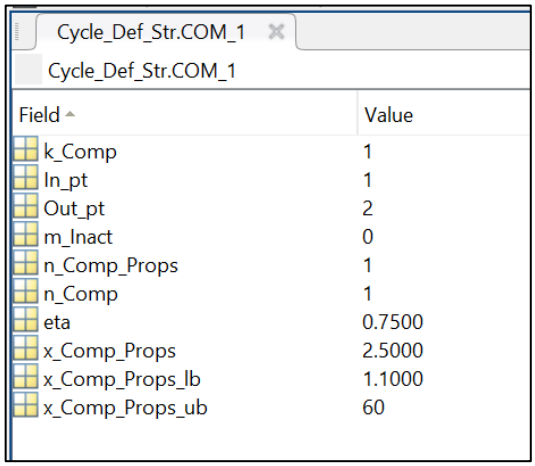


*Figure 13 - Detail of the structure of the compressor COM_1*

All the structures of the components are then collected, together with other information, in a single structure representing the main information of a specific cycle, and thus called *structure of cycle definition* (Cycle_Def_Str). In Figure 14

it is shown an example of such a structure, in which it can be seen the presence of four component structures, together with the initial guess values for the component properties vector (X_Comp_Props_IC, to be further discussed later on), and the *components matrix*, which is presented in detail in Figure 15. This matrix shows for each column the information relative to each component, and thus simply collect all the data of how the different modules interact. It is also shown that a single component can have different fluids or different inlets and outlets.

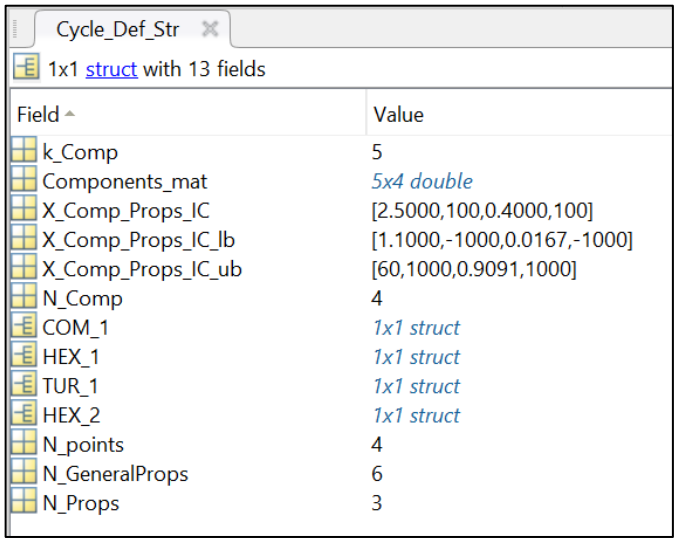


*Figure 14 - Detail of the structure of cycle definition*

| | 1 | 2 | 3 | 4 | |
|---|---|---|---|---|---|
| 1 | 1 | 2 | 3 | 4 | Index k_Comp |
| 2 | 1 | 2 | 3 | 4 | Inlet point of fluid A |
| 3 | 2 | 3 | 4 | 1 | Outlet point of fluid A |
| 4 | 0 | 0 | 0 | 0 | Inlet point of fluid B |
| 5 | 0 | 0 | 0 | 0 | Outlet point of fluid B |

*Figure 15 - Detail of the components matrix*

All the data here presented into the *structure of cycle definition* (Cycle_Def_Str) are the outputs of all the functions that are run to define the cycle, generally

called *Inputs functions*. Through them the user can specify how the modules are connected to which thermodynamic point, and then the initialisation for the system to be analysed is formed. It can also be stored and used with other instances of the same cycle, even if the values of the degrees of freedom are then changed, and for the same reason it is necessary to run these functions only once for each sensitivity or optimisation analysis.

Other general purpose functions are those that are used to compute the thermophysical properties of the working fluids. These are simply called *property calculation functions* (fCalc) and their organisation is similar. They compute one property (for example, a temperature) given other two independent properties (for example, a pressure and an enthalpy). If the fluid exists in CoolProp or REFPROP these libraries are used; otherwise, the fluid is 'userdefined' and the information retained in the fluid vector is used to compute the desired property.

### 2.3.2 Detailed component functions

The component functions are the functions in which are actually implemented the basic characteristic equations. These functions are called by the solvers to provide the results to be used in the next iteration step. Some of the components implemented are presented in the following, together with the implicit form of the equations used. Usually the subscript 1 indicates the inlet of the component, while the subscript 2 indicates the outlet of the component.

- Compressor.
  It performs the compression of the working fluid within the desired boundaries;

$$p_2 - p_1 \cdot \beta_c = 0 \qquad (5)$$

$$h_2 - h_1 - \left(f_{h_{2s}}(p_1, p_2, h_1) - h_1\right)/\eta_c = 0 \qquad (6)$$

$$m_2 - m_1 = 0 \quad (7)$$

- Turbine.

  It performs the expansion of the working fluid within the desired boundaries;

$$p_2 - p_1 \cdot \beta_e = 0 \quad (8)$$

$$h_2 - h_1 - \left(f_{h_{2s}}(p_1, p_2, h_1) - h_1\right) \cdot \eta_t = 0 \quad (9)$$

$$m_2 - m_1 = 0 \quad (10)$$

- Valve_Merge.

  It simulates the mixing between two flows (inlets 1 and 2, outlet 3) having the same fluid composition by solving the energy balance;

$$m_3 h_3 - m_2 h_2 - m_1 h_1 = 0 \quad (11)$$

$$m_3 - m_2 - m_1 = 0 \quad (12)$$

- Valve_Splitter.

  It simulates a valve splitting the flow in two different pipes (inlet1, outlets 2 and 3);

$$m_3 - \xi_{split} m_1 = 0 \quad (13)$$

$$m_3 - m_2 - m_1 = 0 \quad (14)$$

- Valve_Isoenthalpic.

  It simulates the pression reduction of a fluid passing through an isenthalpic valve.

$$p_2 - p_1 \cdot (1 - \Delta p) = 0 \quad (15)$$

$$h_2 - h_1 = 0 \quad (16)$$

- Shaft.

  It computes an energy balance of the powers between two machines, typically a compressor (C) and a turbine (T). It allows a connection between the two machines imposing the same power generated and absorbed on the shaft.

$$m_T(h_{2T} - h_{1T}) \cdot \eta_{mech} + m_C(h_{2C} - h_{1C})/\eta_{mech} = 0 \quad (17)$$

- Inventory. Only used in the passing-information logic, to select and transmit a value of mass flow in a cycle. Integrated in the machines in the complete-system logic.
- Loop Closer. Only used in the passing-information logic, to recirculate the information of mass flow in open cycles.

### 2.3.3 Detailed heat exchanger functions

Heat exchangers have relevant roles in power cycles, therefore they are explained in this dedicated paragraph as implemented in the tool. The subscript 1 indicates the inlet of the component, while the subscript 2 indicates the outlet of the component. The subscript A indicates the hot fluid, while the subscript 2 indicates the cold fluid.

- HEX_Half.

  It computes only one side of an heat exchanger, thus only the enthalpy variation and pressure drop of only one stream flow, and the heat ceased or the heat absorbed to obtain that variation.

$$p_2 - p_1 \cdot (1 - \Delta p) = 0 \quad (18)$$

$$h_2 - h_1 - (Q_{exch}/m_1) = 0 \quad (19)$$

$$m_2 - m_1 = 0 \quad (20)$$

- HEX_SimpleRecup.

  It computes a simple countercurrent heat exchanger between working fluids, namely a recuperator. It implements the effectiveness $\varepsilon$ of the heat exchanger as a variable, and the efficiency $\eta$ representing the thermal losses to ambient.

$$p_{2A} - p_{1A} \cdot (1 - \Delta p_A) = 0 \quad (21)$$

$$p_{2B} - p_{1B} \cdot (1 - \Delta p_B) = 0 \quad (22)$$

$$h_{2A} - h_{1A} - (Q_A/m_A) = 0 \quad (23)$$

$$h_{2B} - h_{1B} - (Q_B/m_B) = 0 \quad (24)$$

$$m_{2A} - m_{1A} = 0 \quad (25)$$

$$m_{2B} - m_{1B} = 0 \quad (26)$$

  Where:

$$Q_{max} = f_{Q_{max}}(p_{1A}, p_{1B}, h_{1A}, h_{1B}, m_{1A}, m_{1B}) \quad (27)$$

$$Q_A = -Q_{max} \cdot \varepsilon \quad (28)$$

$$Q_A = Q_{max} \cdot \varepsilon \cdot \eta \quad (29)$$

- HEX_Recup.

  It computes a countercurrent heat exchanger between working fluids, namely a recuperator. It implements the effectiveness of the heat exchanger as a variable. It also allows to compute the temperature differences between the hot and cold fluids at the inlets of the fluids. It adds the following equations with respect to the previous function:

$$T_{1A} - T_{2B} - \Delta T_{@InletA} = 0 \qquad (30)$$

$$T_{2A} - T_{1B} - \Delta T_{@InletB} = 0 \qquad (31)$$

- HEX_General.

  Quasi-1D function that computes a countercurrent heat exchanger between working fluids, namely a recuperator. It implements the effectiveness of the heat exchanger as a variable. It also allows to compute the temperature differences between the hot and cold fluids at the inlets of the fluids. It allows the computation of a possible internal temperature difference (pinch point - *pp*) between the fluids. To be used if an internal pinch point is possible due to variations of the physical properties of the fluid, as the specific heat or change of phase. Requires good initial guesses to converge. The $Q_{max}$ is now computed through a minimisation algorithm with a function able to spot an internal pinch point if present. Also the function to compute the actual pinch point runs an algorithm that includes a minimisation. The components adds the following equations with respect to the previous function:

$$Q_{max} = f_{1D_{Q_{max}}}(p_{1A}, p_{1B}, h_{1A}, h_{1B}, m_{1A}, m_{1B}) \qquad (32)$$

$$Y_{\Delta T_{pp}} - \Delta T_{pp} = 0 \qquad (33)$$

  Where:

$$Y_{\Delta T_{pp}} = f_{\Delta T_{pp}}(p_{1A}, p_{1B}, h_{1A}, h_{1B}, m_{1A}, m_{1B}, h_{2A}, h_{2B}, \dots) \quad (34)$$

- HEX_Connector.
  Similarly to the Shaft function, it allows to connect two functions, in this case two HEX_Half functions, by only adding the information on how the heat is exchanged. Different types of HEX_Connectors can be used, which add more equations to the system. Here are presented all the possible equations implemented.

$$m_A(h_{2A} - h_{1A}) \cdot \eta_{HEX} + m_B(h_{2B} - h_{1B}) = 0 \quad (35)$$

$$T_{1A} - T_{2B} - \Delta T_{@InletA} = 0 \quad (36)$$

$$T_{2A} - T_{1B} - \Delta T_{@InletB} = 0 \quad (37)$$

$$Y_{\Delta T_{pp}} - \Delta T_{pp} = 0 \quad (38)$$

## 2.4 Thermodynamic Analysis – The passing-information logic

As previously mentioned, the resolution of the thermodynamic analysis consists of finding values of all the properties of the system in a single solution, to be considered as the design point of the desired process, and upon that make the evaluations on the key performance parameters.

One way to solve the thermodynamic system in TEMP-EVO, and the first developed, is to use the thermodynamic resolution characterised by the "passing-information" logic. This is similar to the sequential logic that has been presented in the previous chapter, and it is the same logic used in the pre-existing W-TEMP tool.

This main logic basically consists of the independent computation of each component, and the transmission of the data that are computed by each of them to the connected components. Thus a flow of information has to be determined a priori, depending on what are the variables selected to be independent.

This solver uses the functions of the components presented in the previous chapter to allow the modularity of the tool, but the characteristic equations inside the component are solved in an explicit way, and thus a characterisation of the "functioning cases" of each component has been made within each component function. This means that, depending on the property that is selected to be one of the so-called "degrees of freedom" of the system (which are basically the independent variables upon which the computation of the whole system is determined), the characteristic equations inside each component are solved explicitly based on what is known (the independent variables) to compute what needs to be determined (the dependent variables). Thus, all the data computed by each component are stored, and thus a first iteration is solved when all the component functions are called by the main solver. Then, all the data coming from one component will be used, during the next iteration, by the others that are connected to the first one, and in this way the information is said to be transmitted.

Figure 16 represents a schematics of how the tool is structured using this sequential logic, together with its interaction with the part of the tool related to the economic analysis. At the beginning, some initial guess value are used; the solver is not sensitive to these values and thus can be chosen quite randomly, but anyway they have to exist within the boundaries of the calculation of the thermodynamic properties, otherwise problems can arise especially when the properties are computed through the use of external libraries, such as CoolProp and REFPROP. These values are used to initialise the matrix of properties, which is used, together with the cycle specifications, in the computation of all the equations of each component.

The cycle specifications are set by the user through the use of the input functions, and consists of all the information needed both to uniquely define a specific cycle and to define how the information is transferred from one component to another. For example, the cycle specifications will contain the information on the pressures and temperatures that are required in some thermodynamic points, or a characteristic of a component, such as its efficiency, as well as what is the solving-case of each component, which will determine how the same characteristics equations are solved, for example if a property has to be computed at the inlet or at the outlet.

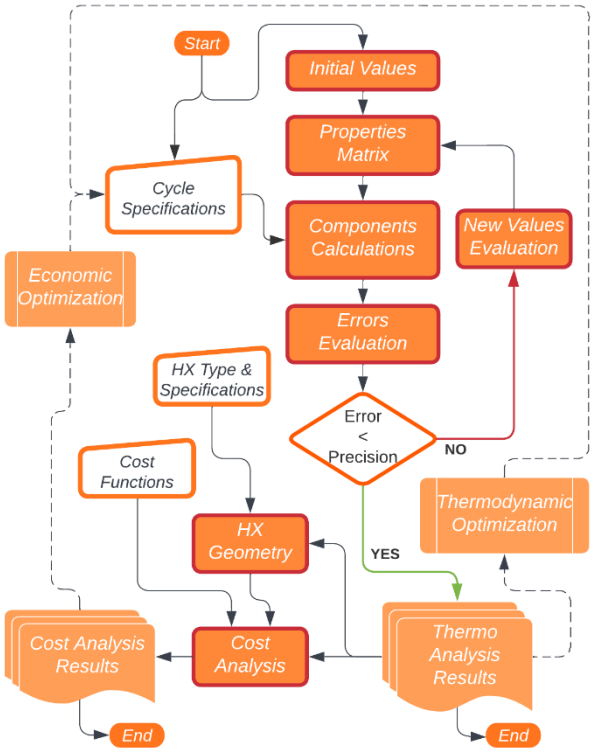


*Figure 16 - Structure of the calculation code*

Once combined the cycle specifications and the initial values, and after the computation of each component, the actual thermodynamic calculation phase can start, which is of iterative type based on the convergence of all the thermodynamic points, within a certain tolerance band defined by the user.

Each component takes the information from the cycle specifications and from the matrix of properties, and computes its outputs that are then stored in a newer version of the properties matrix. The following formulas present the iteration process that occurs. The values of the properties matrix to be used in the next iteration (k+1) are then computed as a weighted mean of the values used for the calculation of each component (*old*) and the values computed by each component (*new*), within the same k-th iteration. The iterations stops when the error function, as defined below, reaches the non-dimensional precision threshold (*prec*) defined by the user.

$$Props^{(k+1)} = a_{new} \cdot Props_{new}{}^{(k)} + a_{old} \cdot Props^{(k)} \tag{39}$$

$$s.t.: \qquad a_{new} + a_{old} = 1 \tag{40}$$

$$err = \sum_{ij} \frac{\left|Props\_new_{ij} - Props_{ij}\right|}{\frac{Props\_new_{ij} + Props_{ij}}{2}} \leq prec \tag{41}$$

In this way, since the information from the independent variable is always imposed by the cycle specifications, and the components start computing from those values, this system basically consists of a transmission of information from the independent variable to the dependent ones, through the characteristic equations of each module. Thus, a flow of information is created, that links all the variables of the same type (all the pressures, the temperatures, enthalpies, etc. in each point), that finally leads to the complete resolution.

This operating logic requires that information is transmitted from component to component, as illustrated schematically in Figure 17, taking a simple recuperated closed Brayton cycle as an example. For example, if a turbomachine sets an outlet pressure, then the pressure information (in blue) will be transmitted "forward", i.e. in a way consistent with the direction of the real mass flow rate (in green); vice versa, setting an inlet pressure means transmitting information "backward", i.e. in the opposite way to the direction of the mass flow rate. The same concept is applied for the transmission of information related to

enthalpy, temperature and, where necessary, quality, for which the heat exchangers set a value, and the transmission of information is schematically represented in the figure in red.

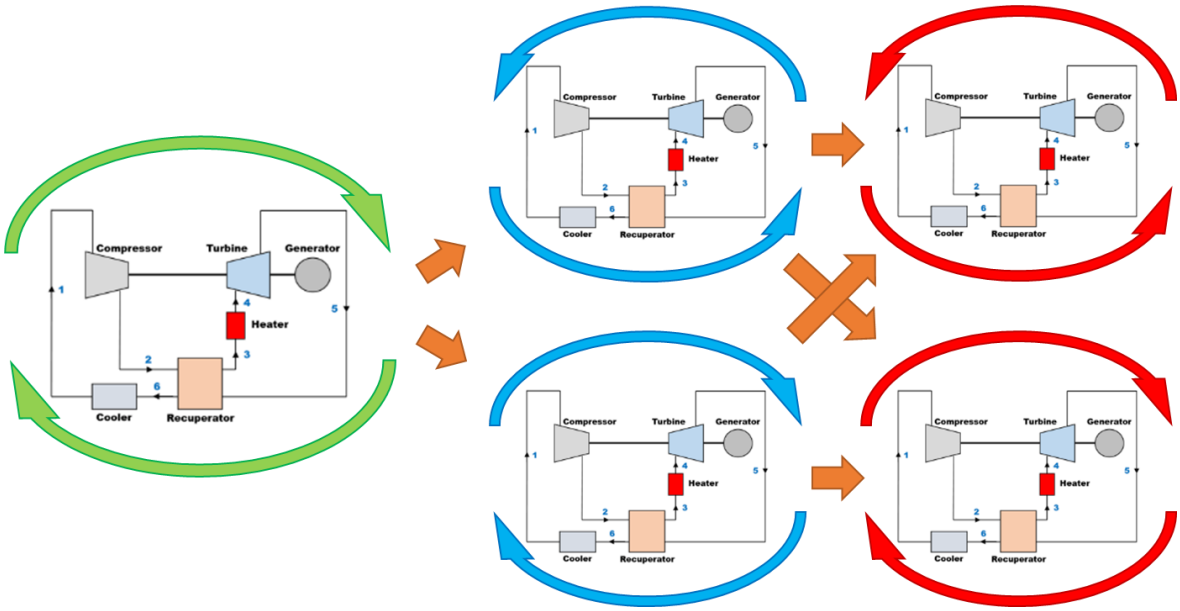


*Figure 17 - Example of the logic of information transmission of the degrees of freedom of the system*

Moreover, each component can transmit pressure and enthalpy/temperature information both forward and backward, and this allows flexibility in the choice of the degrees of freedom of the system, and the possibility to the study both power cycles and inverse cycles.

As previously briefly mentioned, the choice of the forward or backward transmission is made through the selection of parameters called "*cases*", that determine how the characteristic equations of each module have to be solved.

When setting the layout to be calculated, the user will therefore select different "*operating cases*" for each component, which will therefore determine the methods to set the degrees of freedom of the system and therefore the transmission of information. A consequence of this is that, since the definition of the operating cases is linked to the definition of what is an independent variable in the cycle, the solution of the equations of a module is linked to the

definition of the independent variable. Thus, a variable is basically defined within a component, and not externally, and the components are linked to some specific property; this means that, while a module can compute all the possible property types of the system, at their inlet and outlet ports, on the other hand it can start the computation only from some of them (and define the remaining set of them). More specifically, the machines have to define the pressure information, while the heat exchangers have to define the energy information, in the form of temperature, enthalpy, or quality, at their inlet or outlet points, but not both.

In particular, for the heat exchangers, it is possible to use different definitions for heaters, coolers, and recuperators, or also to use a single function designed to characterize the operation of any counter-current heat exchanger. But the user has to select which case to use, which will result, for instance, in the computation of a mass flow rate, given all the temperatures (with only one set by the user as an independent variable, and the others taken from the iterations of nearby components), or vice versa on the computation of the outlet temperatures, given the temperatures at the inlets and both the mass flows, or the exchange area, etc.

The advantages of this solution method is that it is extremely fast, with only fractions of seconds, or few seconds, used to compute a moderately complex cycle. This is especially useful to perform sensitivity analysis and optimisation, since for these several computations of the same cycle are needed. Moreover, this solver is also well robust and rarely diverges during calculations. For this reason, it is not necessary to operate any complex adaptation of the initial guesses, and also this is an advantage when optimisation analyses are performed.

The disadvantages are mainly linked to the definition of a new process, for which it is necessary to think on how the information is transferred from one component to another, and this also happens whenever a different degree of freedom is selected for the same configuration, thus, for example, if the user

wants to select the outlet temperature instead of the inlet one, for the same module. Another disadvantage is that adding a new component is not straightforward, since all the possible operating cases of the module have to be included for it to be used in all possible applications. Finally, another limitation linked to the solver is that also the thermodynamic properties to be used as independent variables are defined within the components, and only one for each component.

## 2.5 Thermodynamic Analysis – The new complete system logic

### 2.5.1 Mathematical approach

To overcome the difficulties of the passing-information logic, also another method to compute the thermodynamic analysis was developed in this thesis, called *complete-system* method. This can be defined as an equation-oriented method, and it basically consists of assembling the characteristics equations of all the modules of the desired process into a single system of nonlinear algebraic equations, which is then resolved using different numerical methods. The present logic is shown in Figure 18, and it can be seen as it only affects the thermodynamic resolution, while the following rest can proceed using the same approach of the passing-info logic.

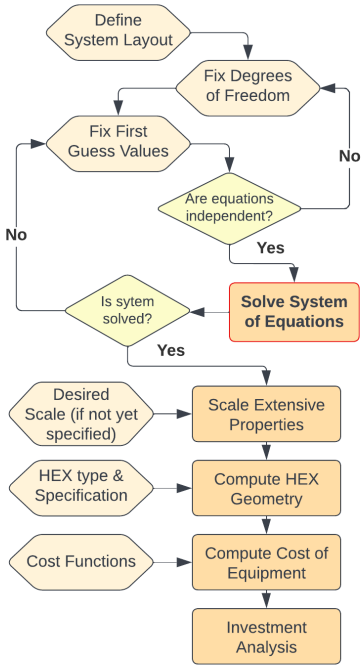


*Figure 18 – Logic flowchart of the complete tool, considering the complete-system logic*

The main drawbacks of the passing-information method are that the user has to select the cases that each module has to operate depending not only on how a system or a cycle is assembled, but also on what are the variables selected as independent, upon which the computation of the entire system is performed. This is particularly difficult to manage without a graphical interface, and for this reason another logic has been also developed, which solves the entire system analysed as a whole, but keeping the same structure to be able to interface with the rest of the tool, and to be able to switch between the use of the two different logics to solve the thermodynamic problem.

The first difference with respect to the logic previously explained is that in the complete system the parameters have to be defined externally to the components. In this way the replicability of the same cycle to be used in different analyses is enhanced. Another difference is that the *cases* of the modules have not to be defined anymore, since the resolution of the characteristic equations is in implicit form. These two main changes to the logic allow the user not to be

bounded by the resolution logic, but instead allow the resolution of any possible combination of system assembling and parameters definition. This generalises the approach with respect to the passing-info logic, but also transfers the complexity of the thermodynamic solver from the cycle composition, and cases and parameters definition, to the actual mathematical solver, and for this reason this logic needs a more rigorous mathematical structure with respect to the previous one.

For example, if a system would require a compressor to reach a certain value of its outlet temperature, given its inlet point, with the passing-info logic an internal iteration would have been necessary, with another component setting the outlet pressure of the compressor and the implementation of a system to iterate until the required outlet temperature is found; this implementation also has to be specific of this combination of component assembling and parameters definition, and could not work when the same compressor is desired to be computed with a constraint on the outlet pressure, for instance. By moving to the complete-system logic, the complexity of the desired flow of information is thus tackled by the general solver, which solves the equations implicitly, and thus implements the component iterations together with the iterations of the whole system, and does not need a specific system configuration explicitly stating the iteration order needed in that specific situation. Moreover, if the user then wants to design the same system based on the definition of the outlet pressure instead of the outlet temperature of the compressor, in the complete-system logic, the same assembly of modules can be used, only performing a switch on what is the independent variable and what is, instead, a dependent one.

At this point, before proceeding with the detailed description of the complete-system logic, it could be good to show the main advantages and disadvantages that led to the development of a second different solving logic.

### 2.5.2 Pros and cons

One of the main advantages of the *complete-system* logic is the enhanced freedom for the user to select any combination of independent variables that allow for a unique solution for the design of the desired process. Another one is that each cycle assembling is independent from the definition of what variables will be used as independent, and thus it can be used to performed different analyses, once one of possible the combinations of variables is selected. In particular, this is especially useful since a graphical interface has not been developed. Moreover, since the properties are defined outside of the modules, the simulation of only portions of the desired process is allowed, or even a single component; this is also useful to decouple a more complex system into easier solvable subsystems. Then, since the resolution of each component is based on the resolution of its characteristics equations in implicit form, the addition of new modules representing new components is easier that in the passing-info logic, where also the definition of all the cases is necessary. Finally, when the system converges to a result, it is ensured to be a true solution, otherwise the residuals of the characteristic equations would not be close to zero; this is not ensured with the passing-info logic, and several checks are implemented in that to ensure that the result is a real solution and not affected by mistaken choices of the *cases* by the user. Moreover, in both the logics, if the result is a true solution to the system, given the constraints implemented, it is also ensured that it is the only physically acceptable solution.

The main disadvantages of the complete-system logic is that the complexity of the solution is transferred to the solver. This means that, while the problem definition (meaning the definition of the assembling and of the parameters) is more straightforward, finding the solution requires a more structured and robust mathematical approach. In general, with respect to the passing-info logic, the dependence on the initial guesses is increased, and they could need to be treated before being used by the actual solver, and for the same reason the robustness of the solver is not intrinsic, but could be particularly stressed in the

layouts involving many nonlinear characteristic equations; to tackle this aspect, a system to rank and re-order the system of equations has been also implemented.

### 2.5.3 Definition of the mathematical problem

Since the objective of the thermodynamic resolution is to find all the thermodynamic states and all the components' properties, these are central concepts in the resolution logic.

Starting from the definition of the properties matrix as in the previous chapters, that has to be modified in order to be managed by the mathematical solver. With the present logic, the distinction between the previously defined general properties matrix (so the table of all the possible thermodynamic parameters of the system for each thermodynamic point) and the properties variables matrix becomes clear, the latter being a matrix that only implements all the parameters that can be selected to be independent variables of the system. Namely, among all the possible parameters, only the values of pressure, enthalpy and mass flow rate in each thermodynamic point were selected to be used within the computations: the other parameters are derived from these. In fact, two independent thermodynamic properties are sufficient to define a thermodynamic state, in our case pressure and enthalpy were selected, to allow also the study of two-phase flow, were pressure and temperature are not independent; together with these two, also the mass flows are fundamental to compute the exchanges of energy (powers) in the components.

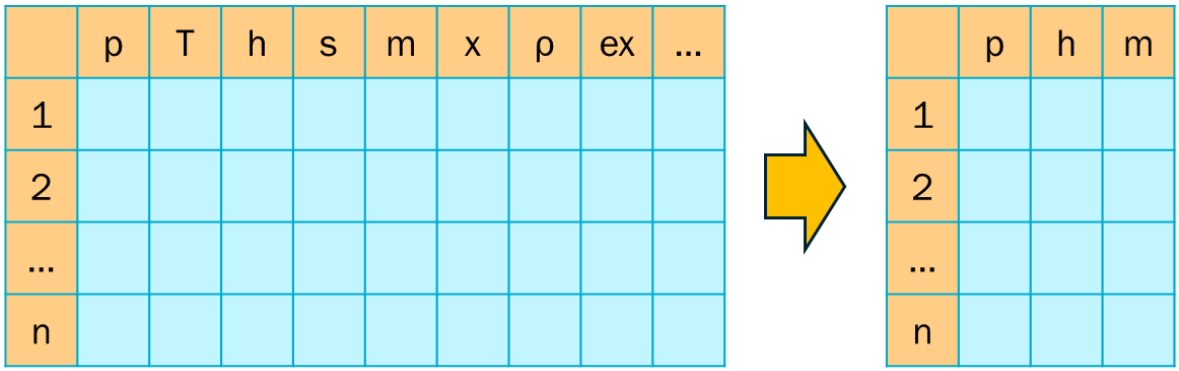


*Figure 19 – From the General Props Matrix to the Props (Variables) Matrix*

Together with the thermodynamic properties of each point, a thermodynamic cycle is also defined by the properties of components employed in their characteristics equations. These are defined within the components and are collected in a single vector named "X_Comp_Props". These could be theoretically be all computed by the solver if the rest of the problem is defined to obtain a unique solution; for example, if both pressures are fixed at the inlet and at the outlets of a machines, its pressure ratio is dependent on these decision and is obtained through calculations, same for the case of an heat exchanger or a valve, its pressure drop depends on the decisions on the pressures. At the same time, these cases are not the same, because the pressure drop across an heat exchanger is a result of how well it is designed, while the pressure ratio of a machine is more a possible design variable. For this reason, the components properties of each module are divided into *parameters* and *actual variables*, the former being defined a priori by the user depending on the expected results (like the non-dimensional pressure drop that is estimated across an heat exchanger), and the latter being either a result of the computation of the system or an independent variable that is used to define the cycle (such as the pressure ratio of a compressor, or the pressure drop of an isenthalpic valve). Thus, among all the *component properties*, the *parameters* will compare into the characteristic equations of the different equipment always and only as fixed parameters, while those that are classified as *variables* will be part of the variables of the characteristic equations or the closure equations, or could be selected as part of

the degrees of freedom of the system (thus mathematically becoming fixed parameters).

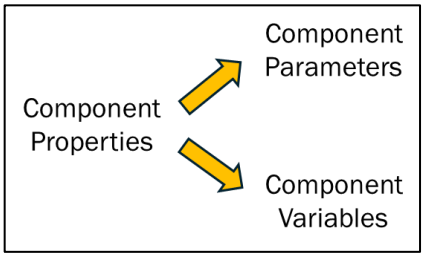


*Figure 20 - Logical distinction of component properties into parameters and variables*

In this way, among all the properties of the system, it has been possible to identify the variables, those that actually enters the computation system of the solver. All the variables are collected into a vector of the variables "X", to be used by the solver. The thermodynamic variable properties come from the properties matrix (the one only with p, h and m) and the variable properties of each thermodynamic point are listed into a row vector (X_Props). This is then assembled with the row vector that collects all the components variables from the modules, as shown in Figure 21.


*Figure 21 - Assembly of the vector of the variables X, composed of the thermodynamic properties that can be variables (p, h, m), and of the component properties that can be variables of the system (so excluding the parameters)*

A similar process is used to assemble the functions of the system, and in this way it has been possible to maintain the modular approach of the tool. In order to build a system of equations, that has later to be solved, all the characteristic equations, as presented in the modelling chapter, are assembled together by appending the equations of the next component below the equations of the previous one. The result in the code is actually the assembling of the residuals of the characteristic equations, which are solved in implicit form, for the i-th iteration.

Each module function also computes the part of the Jacobian of the system relative to the specific component, which consists of the partial derivatives, at the i-th iteration, of each characteristic functions, with respect to each variables. In particular, only the variables that appear in each function will possibly give a non-zero result, and since in each function can only appear the variable relative to the inlets and outlets of the component, the Jacobian have the form of a sparse matrix. The partial derivatives are exact when it is possible to derive the function implemented, and so it was possible to code the derivative expression inside each component; otherwise, the derivative is computed numerically, considering a step size $h$ equal to the 3% of the value of the variable of interest. In this way it was possible to automate the process with a consistent approach to partial derivative calculations. The choice of the value of 3% followed different tests performed by the author and is also the result of compromise between what value can work better for different variables type; moreover, this value seems accurate especially when used for computation of enthalpy values, which is the primary case in which this method is applied. In particular, the value can also be increased by the user, but choosing too high values for this percentage step can cause the computation to be less precise. On the other hand, a lower value can cause difficulties in the numerical evaluation of the derivative, leading to possible errors due to the different values that are encountered during the iteration and due to the higher influence of round-off errors.

This concept is presented in Figure 22. In this way it is possible to maintain the modularity of the calculation code, with the system of equations being a vector of residuals of all the equations, merged with the "append" function, so independently of the number and type of components. In a similar way, the Jacobian of the system is also created, which will turn out to be a sparse matrix, and which can be necessary to calculate the solution, depending on the solver used among the implemented ones.

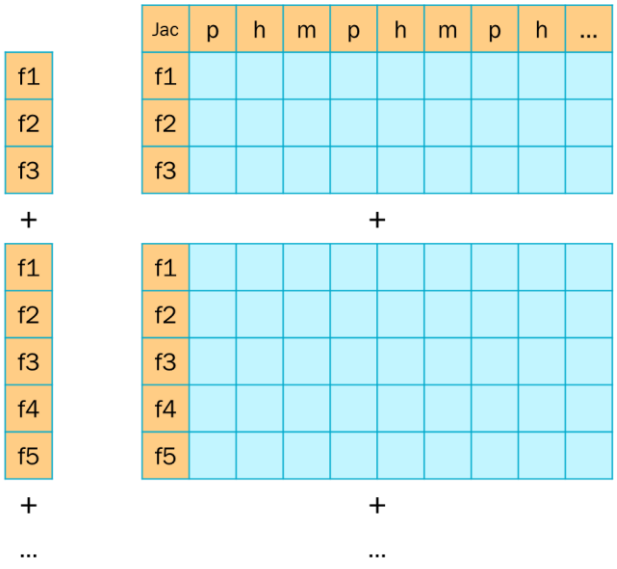


*Figure 22 - Assembly of the vector of the functions-residuals "F" (left) and of the Jacobian of the system "J" (right)*

It should be now clearer what has been presented in the modelling chapter, where different component functions were available for the same real component (for instance, an heat exchanger). In fact, in order to solve the system of equations it is necessary to set all or almost all the variables contained in the characteristic equations as variables of the system. Thus, depending on the component variables that are needed or of interest for the user (for example, a temperature difference at one side of the heat exchanger), also the corresponding equations have to be added to the system, to be able to solve it. Vice versa, it has no meaning to add an equation if not strictly necessary or if the value of the variable that is computed in that equation is not interesting to be set by the user. The use of the appropriate input functions, when defining the process, is of paramount importance to correlate the components properties and the characteristic equations in which they are used, so that the user can select the desired module, and automatically all the component variables that actually are used in the characteristic equations are created and initialised in the component. Otherwise, it would not be possible to have the same number of

equations and of independent variables, and the system would be impossible to be solved.

At this point, a system of equations is formed, which, in the code, is translated into a vector X containing all the variables, a vector F and a matrix J containing all the residuals of the characteristic equations and the partial derivatives of all the equations with respect to each variable, respectively, both computed with the first guess values of the variables.

The system so obtained is not squared, since the number of variables (all the possible variables of the process) is greater than the number of the characteristic equations. To be able to solve the system, the same number is required for both, and thus a number of independent variables has to be chosen equal to the difference between the lengths of the two vectors. So after the system is formed in this way, the user can select which are the independent variables for the process, also called "*boundary conditions*" in the tool, though it is inappropriate mathematically. It has been chosen this wider term instead of simply "independent variable" because it could cause confusion between what is a variable and what is not. In fact, to provide a simple example, the user could choose to set a desired temperature in a point to be one of the design conditions of the system, but a temperature is not present in the variable of the system of equations, because enthalpy is actually used; similarly, the user could select a pressure to be a design parameter, and in this case that is also a possible variable of the system of equations.

The boundary conditions are collected into a matrix for the properties of the fluid (the GenPropsBC matrix, in Figure 23), and in a vector for the component properties (the X_CompPropsBC). These contain NaN values, that, when the user sets a boundary condition, the specific element is overwritten in the BC arrays. They are later used to solve the system.

| | 1 | 2 | 3 | 4 | 5 |
|---|---|---|---|---|---|
| 1 | 85 | 523 | NaN | NaN | 1 |
| 2 | NaN | 623 | NaN | NaN | NaN |
| 3 | NaN | NaN | NaN | NaN | NaN |
| 4 | NaN | 373 | NaN | NaN | NaN |

*Figure 23 - Example of the GenPropsBC matrix for few thermodynamic points*

So the boundary conditions, which are the values of the design parameters chosen by the user, are used to make the system squared, to make it solvable. This can be done in two ways, both implemented.

(i) The more general approach to boundary conditions is to transform each boundary condition into a closure equation, that is then added to the system (with the *append* function), which is helpful to add a design parameter not already considered a variable of the system of equations, such as a temperature. The following equations provide two examples of formation of a closure equation.

$$p_i = 100 \quad \rightarrow \quad p_i - 100 = 0 \tag{42}$$

$$T_i = 100 \quad \rightarrow \quad f_T(p_i, h_i) - 100 = 0 \tag{43}$$

(ii) A second approach to boundary conditions making the system squared is to reduce the number of the actual variables of the system. If a variable (e.g., a pressure at a point) is also chosen as a boundary condition, its value is not needed to be iterated in the system, since it is already appointed by the user. Thus it is possible to reduce the effective number of variables, by removing those which are also design conditions. This operation is shown in the following figure and in the tool it is called "*boundary conditions filtering*".

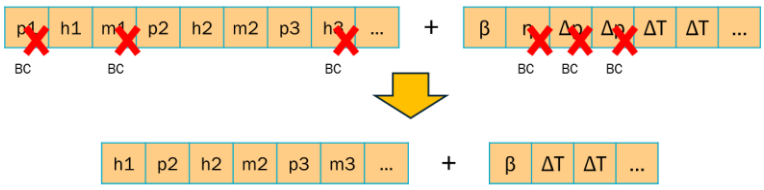


*Figure 24 - Representation of the BC Filtering*

Therefore, if initially the system consists of a vector of variables X with $n$ values, and a vector of functions F with $m$ values, and a $m \times n$ Jacobian matrix, with $m < n$, the final squared system will be formed by a vector X with $k$ values, a vector F with $k$ values, and a $k \times k$ Jacobian matrix, with $m \leq k \leq n$.

An effective way to do the "boundary conditions filtering" operation, since it has to be done also during each iteration, is found to be made through the use of the "reduction" matrix (RED). This is simply a matrix of 1s and 0s, used to select only the columns of X (and J) that are the effective variables of the system of equations.

$$\underbrace{X_{RED}}_{[k\times 1]} = \underbrace{RED}_{[k\times n]} \cdot \underbrace{X}_{[n\times 1]} \tag{44}$$

$$\underbrace{Jac_{RED}}_{[k\times k]} = \underbrace{Jac}_{[k\times n]} \cdot \underbrace{RED^T}_{[n\times k]} \tag{45}$$

The squared Jacobian obtained in this way is also used to perform a control on the independence of the design conditions chosen by the user. In fact, a generic point X (which means, a generic combination of the values of the vector of the variables X) will result in an invertible Jacobian if the system of equations can be solved. Thus, before proceeding with the iterations, a check on the rank of the Jacobian is performed.

In fact, a warning is returned to the user, before the iterations can begin, if the system cannot be solved, and this happens either if the user has selected too many or too few boundary conditions, resulting in a non-squared system, or if the user selected two or more dependent conditions, which results in a squared system, with the value of the rank of the Jacobian lower than its size $k$.

It is also important to underline that a low Jacobian rank may occur when, in a specific point X, some values of the Jacobian decay to zero, due to the values used to perform the calculation in that point. For this reason, it is important to adjust the initial guess values, also called "initial conditions" in the tool, though it is inappropriate mathematically. This is done by calling some functions, called "check" functions, that simply randomise or move the initial guesses to more suitable values, for example by modifying the values of enthalpies at the inlets and outlets of an heat exchanger if they are the same or too close each other.

When the system is formed and squared (same number of equations and of variables), and it is verified that it is solvable, the actual iterative procedure can start.

The most simple solver implemented is a modification of the Newton method, which was initially developed mainly in order to check the proper functioning of the code. In fact, being it developed internally, the Newton method implementation allows a deep monitoring on the system convergence (or non-convergence) and thus was useful to keep track of the residuals and test the new implementations of component functions and of the system itself. This solver turned out to be also fast and highly performant in most of the applications tested and analysed, and for this reason, with the proper modification and enhancement, has been used as the main solver for the studied applications. The main drawback of this solver are twofold: (i) it is unbound in the search of a solution, thus it is difficult to recover from values that diverge consistently, and (ii) it is highly sensitive to the initial conditions, thus proper modifications were required, as explained in the next sub-chapter.

Other possible solvers are the ones native to MATLAB. In particular, the *fsolve* function [74] is the recommended one to solve a root-finding problem with a nonlinear system, which is the case of the analyses carried out in TEMP-EVO. It implements different possible algorithms, and for each of them it is possible to pass the information on the Jacobian or let the code compute a numerical one:

- 'trust-region-dogleg'. This is the default algorithm and it is the only one that is specially designed to solve nonlinear equations.
- 'trust-region'. This attempts to minimize the sum of squares of the functions. Can work only with squared problems.
- 'levenberg-marquardt'. More general. This attempts to minimize the sum of squares of the functions. Can work also with non-squared problems.

The *fsolve* solver is able to converge using fewer iterations with respect to the Newton solver, but, unless the initial guesses are well treated, each iteration can be slower than the Newton one.

Another possibility implemented is the usage of native minimisation algorithms, such as patternsearch, surrogateopt, or others. These algorithms are requested to minimise the norm of the vector of the residuals F:

$$\|F\| = \sqrt{\sum_i {r_i}^2} \qquad (46)$$

These algorithms, despite being slower, are more robust and can also take into account other information, such as the minimum and maximum boundaries of the space in which to search for the solution value of each variable.

One of the drawbacks of the complete-system thermodynamic solving logic is that when a system of equations becomes particularly large, implementing highly nonlinear equations, the solvers may not converge, even if a solution exist. As also explained in the chapter on introduction to the computational methods, a way to deal with this difficulty is to manage the initial guess values, of paramount importance to guarantee more stability, by increasing the probability that the initial point is inside a basin of attraction of the desired solution. Another way is the modification of the tool, to implement also a sequential logic, resulting in a so-called semi-parallel method. This would reduce the number of incognitae by solving the “most linear” equations, and also

initialise better the values for the highly nonlinear equations. Despite not being implemented, this can be a next step in the development of the tool.

Another method found, similar in concept, is the ordering of the equations. This allows the tool to automatically ordering the equations so that that the system can be solved in sequence of equations or group of equations, and using the exact result of the previous ones to compute only the still unknown variables.

The next subchapters present the description of the developed solvers and their mathematical background.

### 2.5.4 Modified Newton Solver

As described before, the developed solver applies, in its simplest form, a sightly modified Newton method, in order to find the roots of the system of equations that represent the physical thermodynamics process.

Other similar methods, called quasi-Newton methods, were also initially implemented in the tool to test the convergence of the system, and some of them are presented in [75]. In particular, the Broyden method is a method initially developed to reduce the computation effort of the Jacobian of the system, operating instead with matrix manipulations, and its implementation in the tools has proven to be stable and efficient, but didn't seem to provide many advantages against the normal Newton method.

The system of equations considered in TEMP-EVO is a system of implicit equations, where all the known terms are zero, and all the variables are all the possible parameters of the system. The variables are collected into the generic vector of the variables $\mathbf{x} = (x_1, x_2, \dots, x_k)$. In the following, it is presented the method used in the presence of a squared system, which is obtained, as explained in the previous chapter, with the "reduction" operations (RED) on the general system.

The Newton method basically consists of the sequential resolution of a linear system that approximate the nonlinear one in the point $\mathbf{x}^{(t)}$ at the t-th iteration. It is possible to express the system of the characteristic equations in matrix form, and obtain the root-finding Newton's iterative procedure:

$$\mathbf{x}^{(t)} = \mathbf{x}^{(t-1)} - \mathrm{J}\left(\mathbf{x}^{(t-1)}\right)^{-1}\mathbf{F}(\mathbf{x}^{(t-1)}) \qquad (47)$$

where $t = 1, 2, \dots, n_{iter}$ is the iteration counter of the variable vector $\mathbf{x} \in \mathbb{R}^k$, $\mathbf{F} \in \mathbb{R}^k$ is the vector of the functions (numerically, it is the vector of the residuals of the equations) and $\mathrm{J}(\mathbf{x})^{-1}$ is the inverse of the Jacobian matrix. The iterations stop when the system $\mathbf{F}(\mathbf{x}) = 0$ is solved. Few important concepts are so defined:

1. $\mathbf{F}$ is a function $\mathbb{R}^n \to \mathbb{R}^n$

$$\mathbf{F}(x_1, x_2, \dots, x_k) = \begin{bmatrix} f_1(x_1, x_2, \dots, x_k) \\ f_2(x_1, x_2, \dots, x_k) \\ \vdots \\ f_k(x_1, x_2, \dots, x_k) \end{bmatrix} \qquad (48)$$

where $f_i: \mathbb{R}^k \to \mathbb{R}$ and are the characteristics equations of all the components, plus the closure equations as defined in the previous chapter.

2. The variables vector is $\mathbf{x} \in \mathbb{R}^k$, where $x_i \in \mathbb{R}^k$ e $i = 1, 2, \dots, k$

$$\mathbf{x} = \begin{bmatrix} x_1 \\ x_2 \\ \vdots \\ x_k \end{bmatrix} \qquad (49)$$

3. While the Jacobian (and its inverse) follows the standard definition:

$$J(\mathbf{x})^{-1} = \begin{bmatrix} \frac{\partial f_1(\mathbf{x})}{\partial x_1} & \frac{\partial f_1(\mathbf{x})}{\partial x_2} & \cdots & \frac{\partial f_1(\mathbf{x})}{\partial x_k} \\ \frac{\partial f_2(\mathbf{x})}{\partial x_1} & \frac{\partial f_2(\mathbf{x})}{\partial x_2} & \cdots & \frac{\partial f_2(\mathbf{x})}{\partial x_k} \\ \vdots & \vdots & \ddots & \vdots \\ \frac{\partial f_k(\mathbf{x})}{\partial x_1} & \frac{\partial f_k(\mathbf{x})}{\partial x_2} & \cdots & \frac{\partial f_k(\mathbf{x})}{\partial x_k} \end{bmatrix}^{-1} \qquad (50)$$

Essentially, the Newton method consists of the following steps:

1. Define the vector $\mathbf{x}^{(0)} = (x_1^{(0)}, x_2^{(0)}, \dots, x_k^{(0)})$, which is the initial guess for the variables vector.
2. Compute $J(\mathbf{x}^{(0)})$ and $\mathbf{F}(\mathbf{x}^{(0)})$
3. Compute a vector $\mathbf{s}^{(0)}$, solution of the linear system:

$$J(\mathbf{x}^{(0)})\,\mathbf{s}^{(0)} = -\mathbf{F}(\mathbf{x}^{(0)}) \tag{51}$$

$$\boldsymbol{s}^{(0)} = -J(\mathbf{x}^{(0)})^{-1}\,\mathbf{F}(\mathbf{x}^{(0)}) \tag{52}$$

Thus:

$$\mathbf{s} = \begin{bmatrix} s_1 \\ s_2 \\ \vdots \\ s_k \end{bmatrix} \tag{53}$$

Generalising the expression for the t-th iteration and substituting, it can be obtained:

$$\mathbf{x}^{(\mathrm{t})} = \mathbf{x}^{(\mathrm{t}-1)} - \boldsymbol{s}^{(\mathrm{t}-1)} \tag{54}$$

4. Once solved the step value $\mathbf{s}^{(0)}$, it is possible to compute the guess for the new iteration $\mathbf{x}^{(1)}$.
5. Once computed $\mathbf{x}^{(\mathrm{t}+1)}$, the process is repeated until $\mathbf{x}^{(\mathrm{t})}$ converges to the $\bar{\mathbf{x}}$, solution to the system $\mathbf{F}(\mathbf{x}) = 0$. Once converged to the solution, not only the vector $\mathbf{F}$ becomes null, but also the vector of the differences between two consequent iterations of the variable vector: $\left\|\mathbf{x}^{(\mathrm{k})} - \mathbf{x}^{(\mathrm{k}-1)}\right\| = 0$.

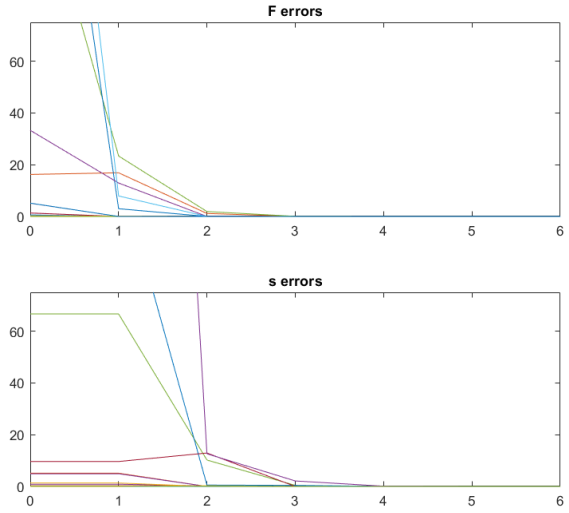


*Figure 25 - Residuals for a simple system (number of iterations on x axis)*

Finally, it is important to highlight that in case of a nonlinear system, the solution is not unique a-priori.

In all the applications analysed with TEMP-EVO, the physical range of the variables and the selection of the degrees of freedom allows for only one feasible solution. Indeed, even though the uniqueness of the solution is difficult if not impossible to demonstrate generally, in the great majority of the cases for the heat and mass balances, and in all cases for the analysed ones, the other possible solutions of the mathematical system representing the energy system involve the break of some physical constraints (such as a pressure ratio below 1, or a mass flow below zero, or a temperature difference not aligned with the heat exchanged, etc.) that the tool implements and that lead to the obtainment of the only physically acceptable solution that can be found, given the definition of: a) the system of equations representing the energy system, b) the values of the parameters chosen by the user for the specific plant analysis, and c) the physical constraints that the involved variables have to respect.

Anyway, a simple Newton method could still diverge or converge to a non-physical solution, thus modifications were necessary to the simplest solver.

One of the main reasons that can lead to divergence for these systems is the usage of a bad guess for the "initial conditions". This has to be managed by the user, which has to select numbers that are consistent with the possible physical range of the modules. The user is also helped by the predefined "fCheck" functions, which modify the initial guesses of the vector of variables to manage the physical constraints inside each component, such as adjust values below a certain limit or respecting reasonable inequalities (one variable greater than another).

Another modification that is a simple and effective way to help the method achieving a global convergence is the usage of a damped Newton method, also generally called successive over-relaxation method, which is presented in detail, among others, in [76] and [77].

The main idea behind is to reduce the step between two iterations of the Newton method, similarly to what is also implemented in the passing-info logic (and in the original W-TEMP code). To do this, a parameter α can be defined and modified during iterations, to ensure that each equation is "moving" towards the solution. This parameter thus relaxes the rate of change of the variable vector, increasing the number of iterations needed to reach the solution, but also preventing the divergence of a specific variable, setting a limit to the variation between one iteration and the next one. The following formulas present the scalar α parameter:

$$\mathbf{x}^{(t)} = \mathbf{x}^{(t-1)} - \alpha \cdot \boldsymbol{s}^{(t-1)} \tag{55}$$

$$\alpha_{min} \leq \alpha \leq 1 \tag{56}$$

It is possible to change the value of this parameter within its aforementioned boundaries, reducing it towards $\alpha_{min}$ if the values of the residuals are diverging, or increasing it towards 1 vice versa, to speed up the computation close to the convergence.

$$if\ \exists\ f_i\ s.t. \left| \left| f_i^{(t)} \right| - \left| f_i^{(t-1)} \right| \right| > 0 \rightarrow\ \alpha = \alpha_{previous}/2 \tag{57}$$

$$otherwise \rightarrow\ \alpha = \alpha_{previous} \cdot 2 \tag{58}$$

Moreover, to avoid exceeding the physical boundaries, limits are also set on the maximum absolute values of the step vector $\boldsymbol{s}$ in the tool.

Another problem that can arise with large systems during iterations is the decay in the rank of the Jacobian matrix. This can be caused, for example, by a value obtained in a point of the Jacobian, which is locally close to zero, in the vicinity of a certain point $\mathbf{x}^*$. When the rank of the Jacobian of the system decays, at least two equations cannot be considered independent again, and the inverse of the Jacobian matrix cannot be computed; this would stop the computation, since it would not be possible to solve the linear system (Eq.(59)) at the t-th iteration, to compute the next step in a reliable way.

$$J(\mathbf{x}^*)\ \mathbf{s}^{(t)} = -\mathbf{F}(\mathbf{x}^*) \tag{59}$$

The *condition number* for inversion (*cond*) of a matrix indicate how much a matrix inverse is sensitive to the changes in the values of the matrix itself, and thus also to their round-off errors. For this reason, this number is a way to evaluate if the rank of the system decayed at the t-th iteration, which would result in a non reliable inverse of the Jacobian matrix, and thus a divergence of the method.

$$cond(J) = \|J\|\|J^{-1}\| \tag{60}$$

When this number becomes large, passing a recommended threshold, the system can be considered to be decayed in rank, and thus the system cannot be solved, since a small variation of the values of the Jacobian matrix would cause a large variation of the values of its inverse. The MATLAB function "cond" [78] is used to determine this parameter, which is used to evaluate a change in the resolution method.

In fact, when the tool faces such a problem, a switch towards a different method, to compute the solution of the linearised system, has been implemented. The method switches to the generalised minimum residual method (GMRES), described by Saad et al. in [79], and implemented in the homonymous native MATLAB function [80]. This was proven to be an efficient algorithm to compute the minimum residuals of a linear system, also with unsymmetric matrices.

In the tool, if the condition number computed for the actual Jacobian is over the threshold, after a preconditioning of the Jacobian itself, the t-th linear system is solved with the usage of the GMRES function instead of the simple Newton method described before. In this way, the tool can "advance", solving the step vector **s** with the minimum residuals of the functions, and to find then a new point $\mathbf{x}^{(t+1)}$. After a few iterations, if the condition number should have been returned to low values, the solution can proceed again with the fast Newton method.

### 2.5.5 Ordering of the equations

When the process analysed is composed by many modules, but more importantly when the system of equations that is derived from it is composed also by highly nonlinear equations, the convergence of the method becomes highly dependent on the initial guess values, and the simple Newton method could not converge. When this happens, the usage of the *fsolve* MATLAB function can compensate for it, but usually in the applications tested also the MATLAB solver was characterised by the same convergence problems. This can happen, for instance, during the sensitivity and optimisation analyses of complex thermodynamic cycles, where the same initial point can sometimes not lead to convergence with different fixed independent parameters (boundary conditions) for the same process layout.

A set of methods to improve the robustness of the tool in these cases that proved to be effective is constituted by the tearing methods, as also suggested in [81]

and in particular the re-ordering of the equations of the system in a sequential way.

The method allows the tool to automatically select the sequence of equations, or block of equations, that need to be solved in sequence in order to solve the entire system, with each block of equations that rely on the results of the previous one. In this way, the system is not solved as a whole anymore, but given the dependencies between the equations in each specific case, the method align them to be able to solve in sequence blocks of highly coupled equations.

It is also important to underline the difference between this method and the idea of solving the components in chain. In fact, the sequence of the equations is not determined by the thermodynamic process layout that needs to be solved, but only by the mathematical dependencies between equations. Thus, this analysis starts with the composition of the entire system of equations for the whole process, and then proceeds to separate the system into blocks of equations that can be solved in series.

In order to implement this idea, it has been necessary to establish a way to determine how the equations are coupled.

Similarly to what happens for the formulation and composition of the Jacobian matrix, each component module also computes an *incidence matrix*, which is a matrix where each row represents a characteristic equation, and each column a variable of the system. Thus, the values of each row are zero if the corresponding variable is not present in the equation, while it is one if the variable is present in the equation. The result is a matrix that has the same structure of the Jacobian matrix, but is made of only ones and zeros, and it does not modify the values depending on the point analysed at the specific iteration. In fact, as said, some values of the Jacobian can approach zero depending on the point considered, and thus an independent composition of the incidence matrix was necessary. When assembling the system, similarly to what happens with the Jacobian, the general incidence matrix of the entire system is assembled appending the single incidence matrices of each component. This matrix is only

computed before the iteration and it does not change during the resolution of the system.

The matrix so formed gives information on the dependencies between each equation and each variable, and is basically a sparse matrix of ones and zeros, that can be managed and analysed through the use of proper mathematical instruments [82]. Figure 26 shows an example of the incidence matrix of the system of equations of a recuperated Brayton cycle. It can be noted the different number of rows and columns, that represent the different number of equations and variables before the so-called reduction (RED) of the system. Depending on the independent variables selected for the system, this $m \times n$ matrix will then be reduced to a $k \times k$ matrix, where $m \leq k \leq n$.

| | 1 | 2 | 3 | 4 | 5 | 6 | 7 | 8 | 9 | 10 | 11 | 12 | 13 | 14 | 15 | 16 | 17 | 18 | 19 | 20 | 21 | 22 | 23 | 24 | 25 | 26 | 27 | 28 | 29 | 30 | 31 | 32 |
|---|---|---|---|---|---|---|---|---|---|---|---|---|---|---|---|---|---|---|---|---|---|---|---|---|---|---|---|---|---|---|---|---|
| 1 | 1 | 0 | 0 | 1 | 0 | 0 | 0 | 0 | 0 | 0 | 0 | 0 | 0 | 0 | 0 | 0 | 0 | 0 | 0 | 0 | 0 | 0 | 0 | 0 | 1 | 0 | 0 | 0 | 0 | 0 | 0 | 0 |
| 2 | 1 | 1 | 0 | 1 | 1 | 0 | 0 | 0 | 0 | 0 | 0 | 0 | 0 | 0 | 0 | 0 | 0 | 0 | 0 | 0 | 0 | 0 | 0 | 0 | 0 | 0 | 0 | 0 | 0 | 0 | 0 | 0 |
| 3 | 0 | 0 | 1 | 0 | 0 | 1 | 0 | 0 | 0 | 0 | 0 | 0 | 0 | 0 | 0 | 0 | 0 | 0 | 0 | 0 | 0 | 0 | 0 | 0 | 0 | 0 | 0 | 0 | 0 | 0 | 0 | 0 |
| 4 | 0 | 0 | 0 | 0 | 0 | 0 | 1 | 0 | 0 | 1 | 0 | 0 | 0 | 0 | 0 | 0 | 0 | 0 | 0 | 0 | 0 | 0 | 0 | 0 | 0 | 0 | 0 | 0 | 0 | 0 | 0 | 0 |
| 5 | 0 | 0 | 0 | 0 | 0 | 0 | 0 | 1 | 1 | 0 | 1 | 0 | 0 | 0 | 0 | 0 | 0 | 0 | 0 | 0 | 0 | 0 | 0 | 0 | 0 | 1 | 0 | 0 | 0 | 0 | 0 | 0 |
| 6 | 0 | 0 | 0 | 0 | 0 | 0 | 0 | 0 | 1 | 0 | 0 | 1 | 0 | 0 | 0 | 0 | 0 | 0 | 0 | 0 | 0 | 0 | 0 | 0 | 0 | 0 | 0 | 0 | 0 | 0 | 0 | 0 |
| 7 | 0 | 0 | 0 | 0 | 0 | 0 | 0 | 0 | 0 | 1 | 0 | 0 | 1 | 0 | 0 | 0 | 0 | 0 | 0 | 0 | 0 | 0 | 0 | 0 | 0 | 0 | 1 | 0 | 0 | 0 | 0 | 0 |
| 8 | 0 | 0 | 0 | 0 | 0 | 0 | 0 | 0 | 0 | 1 | 1 | 0 | 1 | 1 | 0 | 0 | 0 | 0 | 0 | 0 | 0 | 0 | 0 | 0 | 0 | 0 | 0 | 0 | 0 | 0 | 0 | 0 |
| 9 | 1 | 0 | 0 | 0 | 0 | 0 | 0 | 0 | 0 | 0 | 0 | 0 | 0 | 0 | 0 | 1 | 0 | 0 | 0 | 0 | 0 | 0 | 0 | 0 | 0 | 0 | 0 | 0 | 0 | 0 | 0 | 0 |
| 10 | 0 | 1 | 0 | 0 | 0 | 0 | 0 | 0 | 0 | 0 | 0 | 0 | 0 | 0 | 0 | 0 | 1 | 1 | 0 | 0 | 0 | 0 | 0 | 0 | 0 | 0 | 0 | 1 | 0 | 0 | 0 | 0 |
| 11 | 0 | 0 | 1 | 0 | 0 | 0 | 0 | 0 | 0 | 0 | 0 | 0 | 0 | 0 | 0 | 0 | 0 | 1 | 0 | 0 | 0 | 0 | 0 | 0 | 0 | 0 | 0 | 0 | 0 | 0 | 0 | 0 |
| 12 | 0 | 0 | 0 | 0 | 0 | 0 | 0 | 0 | 0 | 0 | 0 | 0 | 1 | 0 | 0 | 1 | 0 | 0 | 0 | 0 | 0 | 0 | 0 | 0 | 0 | 0 | 0 | 0 | 0 | 0 | 0 | 0 |
| 13 | 0 | 0 | 0 | 1 | 0 | 0 | 1 | 0 | 0 | 0 | 0 | 0 | 0 | 0 | 0 | 0 | 0 | 0 | 0 | 0 | 0 | 0 | 0 | 0 | 0 | 0 | 0 | 0 | 0 | 0 | 0 | 0 |
| 14 | 0 | 0 | 0 | 1 | 1 | 1 | 0 | 0 | 0 | 0 | 0 | 0 | 1 | 1 | 1 | 0 | 1 | 0 | 0 | 0 | 0 | 0 | 0 | 0 | 0 | 0 | 0 | 0 | 1 | 0 | 0 | 0 |
| 15 | 0 | 0 | 0 | 1 | 1 | 1 | 0 | 1 | 0 | 0 | 0 | 0 | 1 | 1 | 1 | 0 | 0 | 0 | 0 | 0 | 0 | 0 | 0 | 0 | 0 | 0 | 0 | 0 | 1 | 0 | 0 | 0 |
| 16 | 0 | 0 | 0 | 0 | 0 | 0 | 0 | 0 | 0 | 0 | 0 | 0 | 0 | 0 | 1 | 0 | 0 | 1 | 0 | 0 | 0 | 0 | 0 | 0 | 0 | 0 | 0 | 0 | 0 | 0 | 0 | 0 |
| 17 | 0 | 0 | 0 | 0 | 0 | 1 | 0 | 0 | 1 | 0 | 0 | 0 | 0 | 0 | 0 | 0 | 0 | 0 | 0 | 0 | 0 | 0 | 0 | 0 | 0 | 0 | 0 | 0 | 0 | 0 | 0 | 0 |
| 18 | 0 | 0 | 0 | 0 | 0 | 0 | 0 | 0 | 0 | 0 | 0 | 0 | 0 | 0 | 0 | 0 | 0 | 0 | 1 | 0 | 0 | 1 | 0 | 0 | 0 | 0 | 0 | 0 | 0 | 0 | 0 | 0 |
| 19 | 0 | 0 | 0 | 0 | 0 | 0 | 0 | 0 | 0 | 0 | 0 | 0 | 0 | 0 | 0 | 0 | 0 | 0 | 0 | 1 | 1 | 0 | 1 | 0 | 0 | 0 | 0 | 0 | 0 | 1 | 0 | 0 |
| 20 | 0 | 0 | 0 | 0 | 0 | 0 | 0 | 0 | 0 | 0 | 0 | 0 | 0 | 0 | 0 | 0 | 0 | 0 | 0 | 0 | 1 | 0 | 0 | 1 | 0 | 0 | 0 | 0 | 0 | 0 | 0 | 0 |
| 21 | 0 | 0 | 0 | 0 | 0 | 0 | 0 | 1 | 1 | 0 | 1 | 1 | 0 | 0 | 0 | 0 | 0 | 0 | 0 | 0 | 1 | 1 | 0 | 1 | 1 | 0 | 0 | 0 | 0 | 0 | 0 | 0 |
| 22 | 0 | 0 | 0 | 0 | 0 | 0 | 0 | 0 | 0 | 1 | 1 | 0 | 0 | 0 | 0 | 0 | 0 | 0 | 1 | 1 | 0 | 0 | 0 | 0 | 0 | 0 | 0 | 0 | 0 | 0 | 1 | 0 |
| 23 | 0 | 0 | 0 | 0 | 0 | 0 | 1 | 1 | 0 | 0 | 0 | 0 | 0 | 0 | 0 | 0 | 0 | 0 | 0 | 0 | 0 | 1 | 1 | 0 | 0 | 0 | 0 | 0 | 0 | 0 | 0 | 1 |

*Figure 26 -Example of the incidence matrix of a recuperated Brayton cycle*

In particular, a parallelism with the graph theory can be made to analyse the dependencies between the equations, but to do that the incidence matrix has to be treated first. At this point it is also important to underline the difference between the incidence matrix and the adjacency matrix, typical of the graphs, that have not to be confused. Using the specific case as an example, while the incidence matrix shows the connection between the equations and the variables

of the system, the adjacency matrix of a graph shows the connection between the same elements of the graph, and thus for example would show the connections between equations, or vice versa the connections between variables. For the application to the tool, it was not of interest to understand the connections between the variables, so which one influences which other, but more importantly the connections between the equations, to establish an order of resolution of them.

In order to establish an order of resolution of the equations it is possible to perform a permutation of the incidence matrix, to obtain a matrix that has a lower triangular block form, which means that it is not purely a lower triangular, but it has on its diagonal a series of blocks of number, as shown in Figure 27 in the case of a bordered block lower triangular matrix; this example figure is taken from Baharev et al. [83], where a new robust approach to solve sparse systems of nonlinear equations is developed.

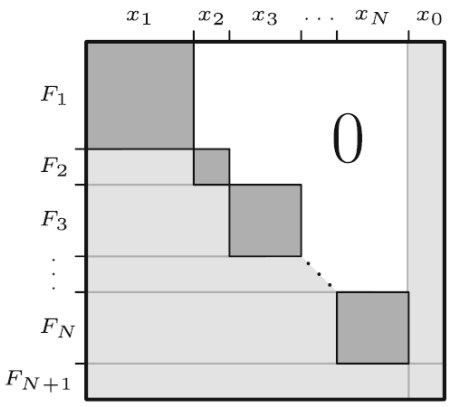


*Figure 27 - Example of bordered block lower triangular matrix* [83]

To perform a similar approach in the TEMP-EVO tool, it has been used the Dulmage-Mendelsohn (DM) permutation [84], implemented in the native MATLAB function "dmperm" [85], which allows, after few modifications (as also shown in [86]), to obtain the block lower triangular (BLT) form of the incidence matrix. An example is provided in Figure 28, where the DM permutation was performed on the reduced (RED) version of the matrix shown in Figure 26. In

this simple case, both due to the simple structure of the cycle and more importantly due to the selection of well-posed boundary conditions, the system can be structured in many uncoupled equations that can be solved in sequence; in fact, it can be seen that the diagonal of the permuted matrix consist of single values, thus $1 \times 1$ blocks, with the only exception of the rows 21 and 22 of the specific example, in which a block is clearly visible.

| | 1 | 2 | 3 | 4 | 5 | 6 | 7 | 8 | 9 | 10 | 11 | 12 | 13 | 14 | 15 | 16 | 17 | 18 | 19 | 20 | 21 | 22 | 23 |
|---|---|---|---|---|---|---|---|---|---|---|---|---|---|---|---|---|---|---|---|---|---|---|---|
| 1 | 1 | 0 | 0 | 0 | 0 | 0 | 0 | 0 | 0 | 0 | 0 | 0 | 0 | 0 | 0 | 0 | 0 | 0 | 0 | 0 | 0 | 0 | 0 |
| 2 | 1 | 1 | 0 | 0 | 0 | 0 | 0 | 0 | 0 | 0 | 0 | 0 | 0 | 0 | 0 | 0 | 0 | 0 | 0 | 0 | 0 | 0 | 0 |
| 3 | 0 | 1 | 1 | 0 | 0 | 0 | 0 | 0 | 0 | 0 | 0 | 0 | 0 | 0 | 0 | 0 | 0 | 0 | 0 | 0 | 0 | 0 | 0 |
| 4 | 0 | 1 | 0 | 1 | 0 | 0 | 0 | 0 | 0 | 0 | 0 | 0 | 0 | 0 | 0 | 0 | 0 | 0 | 0 | 0 | 0 | 0 | 0 |
| 5 | 0 | 0 | 0 | 0 | 1 | 0 | 0 | 0 | 0 | 0 | 0 | 0 | 0 | 0 | 0 | 0 | 0 | 0 | 0 | 0 | 0 | 0 | 0 |
| 6 | 0 | 0 | 0 | 0 | 0 | 1 | 0 | 0 | 0 | 0 | 0 | 0 | 0 | 0 | 0 | 0 | 0 | 0 | 0 | 0 | 0 | 0 | 0 |
| 7 | 0 | 0 | 0 | 0 | 0 | 1 | 1 | 0 | 0 | 0 | 0 | 0 | 0 | 0 | 0 | 0 | 0 | 0 | 0 | 0 | 0 | 0 | 0 |
| 8 | 0 | 0 | 0 | 0 | 0 | 0 | 1 | 1 | 0 | 0 | 0 | 0 | 0 | 0 | 0 | 0 | 0 | 0 | 0 | 0 | 0 | 0 | 0 |
| 9 | 0 | 0 | 0 | 0 | 0 | 0 | 0 | 0 | 1 | 0 | 0 | 0 | 0 | 0 | 0 | 0 | 0 | 0 | 0 | 0 | 0 | 0 | 0 |
| 10 | 0 | 0 | 0 | 0 | 0 | 0 | 0 | 0 | 1 | 1 | 0 | 0 | 0 | 0 | 0 | 0 | 0 | 0 | 0 | 0 | 0 | 0 | 0 |
| 11 | 0 | 1 | 0 | 1 | 1 | 0 | 1 | 1 | 0 | 1 | 1 | 0 | 0 | 0 | 0 | 0 | 0 | 0 | 0 | 0 | 0 | 0 | 0 |
| 12 | 0 | 0 | 0 | 0 | 1 | 0 | 0 | 0 | 0 | 0 | 0 | 1 | 0 | 0 | 0 | 0 | 0 | 0 | 0 | 0 | 0 | 0 | 0 |
| 13 | 0 | 0 | 0 | 0 | 0 | 0 | 0 | 0 | 0 | 0 | 1 | 1 | 1 | 0 | 0 | 0 | 0 | 0 | 0 | 0 | 0 | 0 | 0 |
| 14 | 0 | 0 | 0 | 0 | 0 | 0 | 0 | 0 | 0 | 0 | 0 | 1 | 0 | 1 | 0 | 0 | 0 | 0 | 0 | 0 | 0 | 0 | 0 |
| 15 | 0 | 0 | 0 | 0 | 0 | 0 | 1 | 0 | 0 | 0 | 0 | 0 | 0 | 0 | 1 | 0 | 0 | 0 | 0 | 0 | 0 | 0 | 0 |
| 16 | 0 | 1 | 0 | 1 | 1 | 0 | 1 | 1 | 0 | 1 | 0 | 0 | 0 | 0 | 0 | 1 | 0 | 0 | 0 | 0 | 0 | 0 | 0 |
| 17 | 0 | 0 | 0 | 0 | 0 | 0 | 0 | 0 | 1 | 0 | 0 | 0 | 0 | 0 | 0 | 1 | 1 | 0 | 0 | 0 | 0 | 0 | 0 |
| 18 | 0 | 0 | 0 | 0 | 0 | 0 | 0 | 0 | 0 | 0 | 0 | 0 | 0 | 0 | 0 | 0 | 0 | 1 | 0 | 0 | 0 | 0 | 0 |
| 19 | 0 | 0 | 0 | 0 | 0 | 0 | 0 | 0 | 0 | 0 | 0 | 0 | 0 | 0 | 0 | 0 | 0 | 1 | 1 | 0 | 0 | 0 | 0 |
| 20 | 1 | 0 | 0 | 0 | 0 | 0 | 0 | 0 | 0 | 0 | 1 | 0 | 0 | 0 | 0 | 0 | 0 | 0 | 0 | 1 | 0 | 0 | 0 |
| 21 | 0 | 0 | 0 | 0 | 0 | 0 | 0 | 0 | 0 | 0 | 0 | 0 | 0 | 0 | 0 | 0 | 0 | 0 | 0 | 0 | 1 | 1 | 0 |
| 22 | 0 | 0 | 0 | 0 | 0 | 0 | 0 | 0 | 0 | 0 | 1 | 1 | 0 | 1 | 0 | 0 | 0 | 0 | 1 | 1 | 1 | 1 | 0 |
| 23 | 0 | 0 | 0 | 0 | 0 | 0 | 0 | 0 | 0 | 0 | 0 | 0 | 0 | 0 | 0 | 0 | 0 | 0 | 1 | 1 | 1 | 0 | 1 |

*Figure 28 – Permutation of the Reduced Incidence Matrix into BLT form*

Now, if an ordering algorithm is performed on the permuted matrix, it is possible to find the relations between the equations of the system. The algorithm selected is the Tarjan algorithm [87]. The implementation was performed by modifying the version of the algorithm present in the MATLAB file exchange [88]. This algorithm allows to find the strongly connected components (SCC) of a directed graph, by grouping all the connected nodes that are also coupled into a so-called connectivity level, and producing a spanning tree of the digraph, highlighting the dependencies between the nodes [82]. Thus, for the specific application to TEMP-EVO, it is possible to identify the graph of the connections between the equations (which are the nodes of the graph in this case). A similar procedure

could be used also to identify the connections between the variables, but is of less interest for the resolution of the system.

Transferring the relations found in this way back to the original system, it is possible to draw the graph of the connected equations, and an example, on the same system as the previous figures, is provided in Figure 29. In this case, from left to right, it is possible to see which equations can be computed using the results of the previous ones. For example, the equations 14 and 15 are reliant on a large number of other equations, and they are in this case, energy exchange equations implemented in heat exchangers. It is also possible to notice that equations 20 and 21 are coupled (they correspond to the number 21 and 22 of the permuted matrix), since they depend one on the other, and thus their resolution has to be made at the same time.

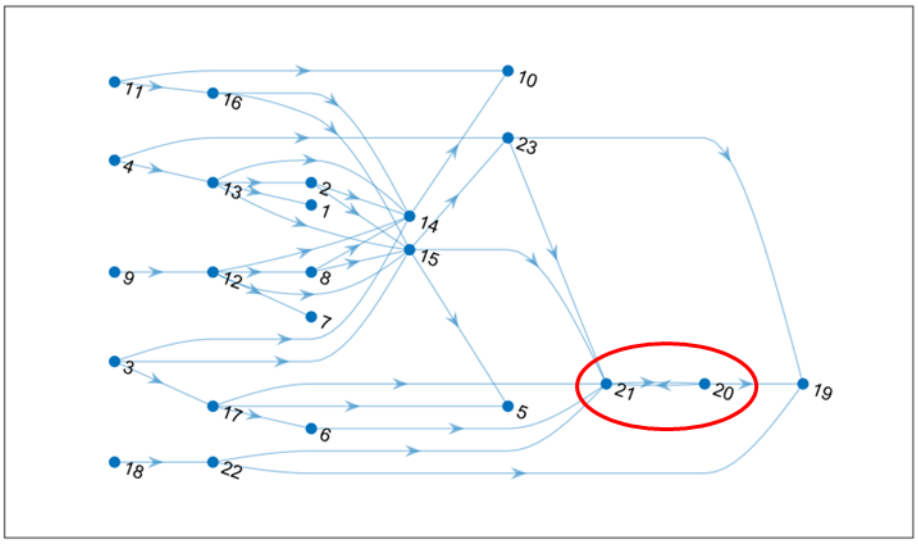


*Figure 29 - Graph of the dependencies of the equations of the system, with highlight of the block*

Once the strongly connected components are found, this information is used to order the system and separate the equations into a sequence of successive equations blocks. To do that, the permutations that was found for the DM-permutated incidence matrix is applied to the vector of variables **x**, the vector of functions (residuals) **F**, and to the Jacobian of the system.

The permuted arrays are called ordered (ORD) in the tool, and later is selected only a portion of them (a procedure called CUT) in order to consider only a system which is a small portion of the complete one, and which is solved typically in less than 5 iterations, or depending on the number of coupled equations. The results of a smaller system (in the previous example, only one or two equations) are then used in the computation of the successive small system, since having the previous variables already solved they can be considered as parameters. At the end of the process, all the equations are then solved and thus the solution is found.

In this way, it has been possible to increase the robustness of the *complete-system* logic to improve the reliability of it while performing large system computations, including optimisation.

## 2.6 Efficiency-size correlations

The most correct way to estimate the efficiency of a machine would be the computation of at least its mean line gas path and applying the main loss correlations, but this method would need several design parameters that are not strictly related to the thermodynamics of a cycle, and would lead to a computation too complex to be included in the plant iteration process.

Thus, there are two ways to overcome this difficulty: first option, to allow the user to set a pre-defined value of machine efficiency, which might be particularly useful in case consistent comparison among different cycle layouts is addressed; secondo option, to implement a pre-defined map of the efficiency of machines, to be used by the component functions as a simple characteristic equation.

In order to develop a sufficiently reliable correlation, without the need of many design details, which could also impact on the non-linearity of the correlation itself, the simplest map possible has been implemented, correlating the performance of the machines to the size of the equipment. The outcomes of such a work are also presented in [89].

This approach has been developed only for the machinery typically studied for sCO2 cycles, and the correlations are based on literature data or obtained from original equipment manufacturers. In particular, thanks to the collaboration with Baker-Hughes and Franco Tosi Meccanica within the European Project SOLARSCO2OL, it has been possible to include more data into the correlation curves.

The parameter of interest is the isentropic efficiency of the machine, which has a strong impact on the performance of the thermodynamic cycle. A simplification was also necessary given the available data from literature; in fact, the isentropic efficiency is either found, or interpreted as the total to static efficiency presented in the relative source from the literature.

The data thus obtained, a total of 12 points for axial turbines and 6 points for radial compressors, were then compared with each other and different regression curves were tested.

A logarithmic law was found to well capture the relation between such two parameters. On the other side, given the nature of these curves, they cannot be used as a detailed forecast of the efficiency of machines to be designed in specific operating points, but more as a way to estimate the influence of component size on the general performance of the cycle of interest, and to allow quantitatively-founded scale-up analyses.

Usually, turbomachinery tends to be more efficient while increasing in size. This is due to many reasons, mainly because bigger dimensions lead to higher technological precision and, percentage-wise, smaller clearances and surface drag.

Data collected for the turbine analysis are presented in Table 1, while data on the compressor machines are not presented, due to confidentiality constraints within the aforementioned EU project.

*Table 1 - Data used to compute the turbine performance curve (nominal conditions)*

| Source | Turbine Power [MW] | Isentropic Eff. [%] |
|---|---|---|
| Franco Tosi Meccanica S.p.A. [61] | 1.96 | 86.5 |
| Shi et al. [90] | 10.37 | 86.6 |
| Kalra et al. (SunShot) [91] | 14 | 85 |
| Glos et al. 50 MW [92] | 51 | 87.5 |
| Bidkar et al. [93] | 70 | 90.3 |
| Glos et al. 150 MW [92] | 147 | 92 |
| McDowell et al. [94] | 220 | 90.1 |
| Bidkar et al. 450 MWe (LPT) [93] | 260 | 91.6 |
| Bidkar et al. 450 MWe (HPT) [93] | 360 | 90.6 |
| Le Moullec [31] | 1677 | 93 |

The least squares method was applied to the data points with different equation models, and the best fit was achieved using a logarithmic model. Values of the correlation coefficients are reported in Table 2.

$$\eta = a + b \cdot \ln\left(P_{turbomachinery}[MW]\right) \quad (61)$$

*Table 2 - Regression analysis (*=confidential values)*

| | Axial Turbine | Radial Compressor |
|---|---|---|
| No. of data points | 10+2* | 2+4* |
| a | 83.81925874 | 71.055034 |
| b | 1.236712856 | 3.7144955 |

| | | |
|---|---|---|
| $R^2$ | 0.771100773 | 0.974312 |

Most of the selected literature data refer to design studies, in which different loss correlations were used, and not all the values were experimentally validated. Despite this, the obtained correlations match sufficiently well with the available data. Further studies could improve the correlation through the implementation of dependencies from other key thermophysical or technical parameters.

The following figures shows the graphs of the correlations for centrifugal compressors and the axial turbines.

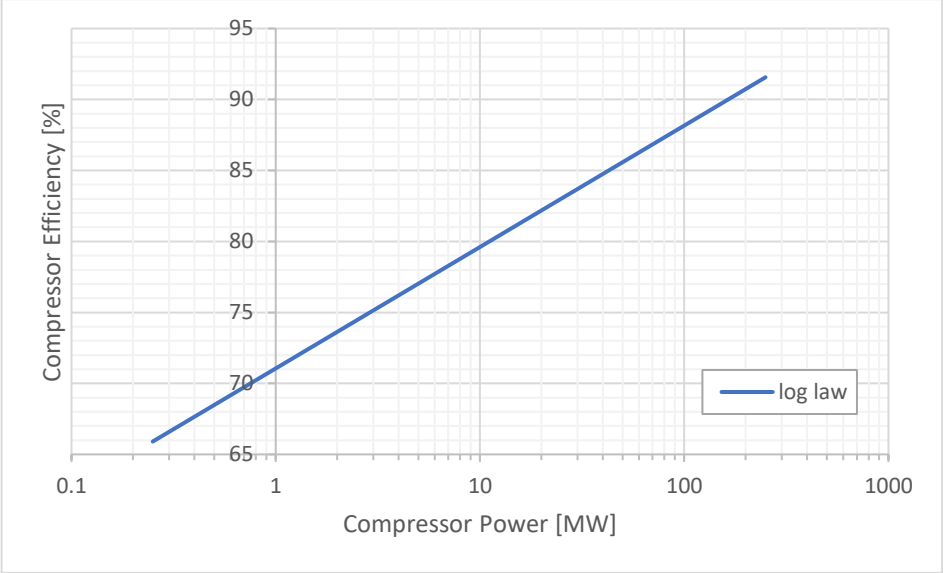


*Figure 30 – sCO2 radial compressors size-efficiency map*

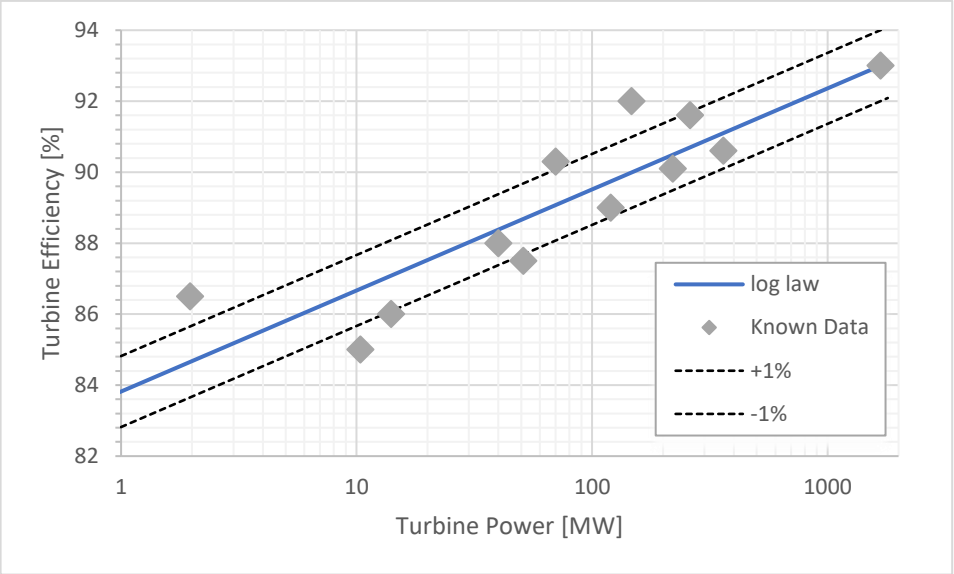


*Figure 31 - sCO2 axial turbines size-efficiency map*

## 2.7 General Concepts of Economic Analysis in TEMP-EVO

Following the logic structure of the TEMP-EVO code illustrated in Figure 9, here the analyses following the thermodynamic resolution of the desired cycle are reported. Once the properties of all the components and all the thermodynamic points of the process are obtained, these can be used to perform, in sequence, (i) the geometrical computation of the heat exchangers, (ii) the cost estimation of the main components, and (iii) the investment analysis over a pre-defined lifetime.

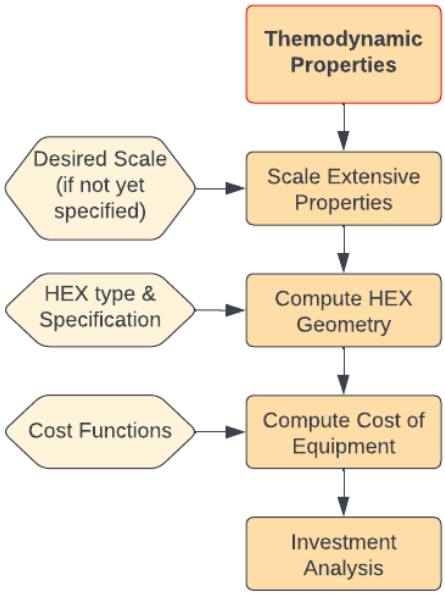


*Figure 32 - Structure of the economic part of the tool*

The geometrical computation of the heat exchangers has not been included in the thermodynamic resolution, so that it could be possible to solve the thermodynamic problem with less constraints on the actual pressure losses and heat transfer effectiveness inside these components, and later use a more detailed analysis to verify the results and estimate the necessary dimensions.

Not all the analyses of the economic part has to be performed, and the user could decide to terminate the analysis, for example, at the geometrical evaluation of the heat exchangers, simply by not launching the relative scripts of the successive analyses.

Moreover, the results obtained at the end of each step of the economic analysis can also be used as objectives for optimisation or sensitivity analysis, that obviously include also the re-computation of the thermodynamic part at each iteration. In case of an optimisation analysis, any possible MATLAB native algorithm can be used, but, in particular, the tool implements those showing the best computational performance, such the native functions “surrogateopt”, that create a surrogate surface during the computations, and “patternsearch”, both

taking advantage of gradient-free optimisation methods to find the global optimum of the cost function.

## 2.8 Geometry Analysis

During the thermodynamic resolution of the cycle the exchangers are simulated as a countercurrent heat exchange and only the thermodynamic parameters are calculated. Subsequently, the details of the heat exchanger geometry are calculated, having set the type of heat exchanger and some specifications as input, and receiving information on flow rates and temperatures from the thermodynamic calculation. In this way, the transmittance and the value of the number of transport units (NTU) are calculated, used to compute the value of the surface required to achieve the desired heat transfer. The reference correlations used are reported in the following.

In the heat and mass balance (thermodynamic calculation) the heat exchangers are simply solved with 0D or quasi-1D equations, while once the inlets and outlets are solved, the geometric analysis can solve the internal distribution of temperatures and other properties, referring to a countercurrent heat exchanger divided into subsections. Otherwise, it is also possible to compute the geometric parameters considering the complete heat exchanger with no thermophysical property of the fluid varying inside, or with mean values, and in this way estimate different equipment typologies.

In the case of studies on supercritical carbon dioxide (or other working fluids with high real-gas behaviour in the operational range), given the large variations in thermophysical properties of real fluids near the critical point, and in particular of specific heat, it is essential to have the possibility of dividing the heat exchangers into sections to evaluate the real temperature distribution and the required heat transfer surface. In fact, while in the thermodynamic analysis compliance a check on the second principle of thermodynamics is sufficient, e.g. the non-inversion of temperatures, in the geometric calculation function this

aspect is essential for a correct calculation of the value of the heat exchanger surface.

For this reason, the option to select the number of sections in which to calculate the heat exchangers is implemented, and usually a division into at least 20 sections is suggested in the literature [95]]: the numerical tests confirmed to be a sufficient approximation. Thus, a division of an heat exchanger is performed starting from the known values at the inlets and outlets; then it is possible to divide the total heat exchanged in the chosen number of subsections of this countercurrent heat exchanger, and linearise the temperature distribution in each subsection, and for each of them compute the thermal exchange parameters. Otherwise, different configurations can be studied without considering the internal distribution.

The ε-NTU method is used to compute the product of the transmittance and the heat transfer surface UA, also called "thermodynamic size"; this parameter is computed either in each subdivision of the heat exchanger, or as the mean value for the whole heat exchanger, and it is then used, together with the estimations of the transmittance U values, in order to compute the value of the heat transfer surface A of each heat exchanger.

In practice, the geometric resolution for the heat exchangers is made so that the tool needs in inputs also the heat exchanger type (usually a shell and tube or a printed-circuit) and the design parameters for the tube diameter and a velocity inside the tubes, at least as first guess values, and the computation returns the temperature distribution and the values of heat transfer surface A, as well as the "thermodynamic size" UA of the heat exchanger.

The user has to initially estimate the value of the diameters of the tubes inside the heat exchangers, as well as the velocity inside the tubes.

The heat exchanged $Q$ is divided into a number of cells (N_cells), used to compute a distribution of the properties along the length, thus having N_cells+1

boundaries of cells and N_cells+1 property values, considering also the inlets and outlets. If the number of cells is sufficient, the linearised properties are approximated with a negligible error.

Into each cell, properties are considered constant (e.g: the specific heat Cp is taken as mean of the boundaries of the cell) and each cell is considered as a small HEX where the heat transfer coefficient and the surface are computed.

Then, the ε-NTU method is used [96]. Given the mass flows and the temperatures at the boundaries of each cell, and the constant properties computed as mean of the boundaries, the effectiveness of the cell is computed. From that, the corresponding number of transfer units (NTU) is computed.

In each cell also the values of the convective heat transfer coefficient $h$ is computed, and then the transmittance U is calculated.

$$A = \frac{UA}{U} \tag{62}$$

with

$$UA = HCR_{min} \cdot NTU \tag{63}$$

Where the $HCR_{min}$ is the minimum heat capacity rate between the two fluids, defined as it follows for each cell (or as mean values for a single-cell HEX):

$$HCR_{min} = min(HCR_{hot}, HCR_{hot}) \tag{64}$$

$$HCR_{hot} = \dot{m}_{hot} \cdot C_{p_{hot}} \tag{65}$$

$$HCR_{cold} = \dot{m}_{cold} \cdot C_{p_{cold}} \tag{66}$$

The NTU can be found using correlations that depend on the type of heat exchanger considered, and that implement the effectiveness of the heat exchanger $\varepsilon$, and the ratio between the two heat capacities, named heat capacity rate ratio (HCRR), and defined as it follows:

$$HCRR = \frac{min(HCR_{hot}, HCR_{hot})}{max(HCR_{hot}, HCR_{hot})} \tag{67}$$

For the transmittance the following simplified formula has been used:

$$U = \frac{1}{\frac{1}{h_{int}} + \frac{1}{h_{ext}}} \tag{68}$$

### 2.8.1 Heat transfer coefficient correlations

This chapter illustrates some of the empirical correlations used to compute the heat transfer coefficients inside the heat exchangers.

To compute the heat transfer coefficients and the temperature distribution, a traditional approach has been followed, estimating the flow convective coefficients for the two fluids, using the Nusselt number $Nu$ derived from empirical correlations:

$$Nu = \frac{h \cdot D}{k_{fluid}} \tag{69}$$

where $h$ is the convective heat transfer coefficient, which is the variable of interest, $D$ is the characteristic length on which the number is computed, in these cases the diameter of the tube, and $k_{fluid}$ is the thermal conductivity of the fluid.

The computation of the external convective coefficient for the shell and tube type is usually considered for single phase flows and for the majority of the heat exchangers has been used the following correlation for the Nusselt number [97], valid for $Re \cdot Pr > 0.2$ :

$$Nu = 0.3 + \frac{0.62 \cdot Re^{\frac{1}{2}} \cdot Pr^{\frac{1}{3}}}{\left(1 + \left(\frac{0.4}{Pr}\right)^{\frac{2}{3}}\right)^{\frac{1}{4}}} \cdot \left(1 + \left(\frac{Re}{282000}\right)^{\frac{5}{8}}\right)^{\frac{4}{5}} \tag{70}$$

For the estimation of the convective coefficient internal to the tubes for single phase flow, the correlations for laminar flow and the one suggested by Gnielinski [98] have been used to compute the Nusselt number.

If $Re < 2100, Pr > 0.7$ :

$$Nu = 4.36 \tag{71}$$

If $Re > 2500, Pr > 0.5$ :

$$Nu = \frac{\frac{f}{8} \cdot (Re - 1000) \cdot Pr}{1 + 12.7 \cdot \left(\frac{f}{8}\right)^{\frac{1}{2}} \cdot \left(Pr^{\frac{2}{3}} - 1\right)} \tag{72}$$

$$f = (0.79 \cdot \log(Re) - 1.64)^{-2} \tag{73}$$

In the case of two-phase flow inside tubes, the following correlations for the convective coefficients have been used. The first one is the approach used by Kandlikar [99] and it is used for evaporation.

$$h_{conv} = \left(h_{conv\_1}, h_{conv\_2}\right) \tag{74}$$

$$\frac{h_{conv1}}{h_{sp}} = 0.6683 \cdot Co^{-0.2} + 1058 \cdot Bo^{0.7} \tag{75}$$

$$\frac{h_{conv2}}{h_{sp}} = 1.136 \cdot Co^{-0.9} + 667.2 \cdot Bo^{0.7} \tag{76}$$

where $h_{sp}$ is obtained from a modified Dittus-Boelter correlation, the convection number Co and the Boiling number Bo:

$$Nu = 0.023 \cdot Re_{mod}^{0.8} \cdot Pr^{0.4} \tag{77}$$

$$Re_{mod} = Re \cdot (1 - x) \tag{78}$$

$$Co = \left(\frac{1 - x}{x}\right)^{0.8} \cdot \left(\frac{\rho_v}{\rho_l}\right)^{0.5} \tag{79}$$

$$Bo = \frac{Q''}{u \cdot \rho \cdot h_{fg}} \tag{80}$$

The second approach is instead used for condensation inside the tubes, and is derived from Chato [100]:

$$h_{conv} = 0.555 \cdot \left( \frac{g \cdot \rho_l \cdot (\rho_l - \rho_v) \cdot k_l^3 \cdot h'_{fg}}{\mu_l \cdot (T - T_{tube}) \cdot D_{int}} \right)^{\frac{1}{4}} \quad (81)$$

$$h'_{fg} = h_{fg} + \frac{3}{8} \cdot c_{p,l} \cdot (T - T_{tube}) \quad (82)$$

In the specific case of estimation of printed-circuit heat exchanger (PCHE), typically studied for sCO2 applications, one of the correlations suggested by Jiang et al. [101] has been implemented:

$$Nu = 0.0176 \cdot Re^{0.809} \cdot Pr^{\frac{1}{3}} \quad (83)$$

## 2.9 Cost Evaluation

Once the geometrical features of the heat exchangers have been determined, the next step to carry out a thermo-economic analysis is to evaluate the purchase cost of the main components necessary to create the desired process. To do this, cost correlations for the components were used, chosen from among those available in literature, and therefore implemented as calculation functions. As a general principle, the correlations for turbomachines are based, as a scaling parameter, on the power of the machines themselves, while the correlations for heat exchangers are based either on the heat transfer surface A, or on the "thermodynamic size" UA. These correlations usually have a range of validity, and if the size parameter selected to evaluate the cost of the equipment exceeds the limits, the cost is computed but the user is warned about the possible non-validity of the correlations utilised.

For what concerns the study of more traditional technology, such as gas turbines, and steam or organic fluid cycles, the more general functions contained

in the book "Analysis, Synthesis and Design of Chemical Processes" by Turton et al. were used [102]. Instead, for the supercritical $CO_2$, the cost functions of the components were selected from the work by Weiland et al. [103], where some correlations were developed to estimate the cost of this non-off-the-shelf equipment. In case of future applications in different fields, the modularity of the approach will allow the user to introduce the desired cost estimating functions for the each application.

In general, the first and simplest way to compute the cost of a component is to scale the cost from a known equipment of the same type, based on a characteristic parameter (such as the power of a machine), used as size (or scale) parameter $SP$. In this case, the following proportion can be used:

$$Cost_{equipment} = Cost_{reference} \cdot \left(\frac{SP_{equipment}}{SP_{reference}}\right)^{n} \qquad (84)$$

where n is an exponent that depends mainly on the equipment type and on the working fluid. A general value that can be used to perform a rough estimation of the cost of an equipment can be made using $n \in (0.6; 0.7)$ [102] [104]. This simple equation is instead better used together with other correlations that compute the cost of equipment in a more specialised way, and it can be used to scale the range of validity of these correlations.

In the book by Turton et al., a general approach is used, called module costing technique and firstly developed by Guthrie [105], and summarised here. The cost of the equipment if formed by the base cost $C_0$ of the equipment, computed on a size parameter $SP$, which depends on the equipment type:

$$\mathrm{Log}(C_0) = k_1 + k_2 \cdot \mathrm{Log}(SP) + k_3 \cdot (\mathrm{Log}(SP))^2 \qquad (85)$$

which is then modified with different factors that take into account the pressure levels, the material, and other costs associated with the realisation of the bare module of each component.

$$Cost = C_0 \cdot (B_1 + B_2 \cdot F_M \cdot F_p) \quad (86)$$

$$Log(F_p) = c_1 + c_2 \cdot Log(p) + c_3 \cdot (Log(p))^2 \quad (87)$$

where $F_p$ is the pressure factor, depending on the pressure level $p$, while $F_M$ depends on the material selected, and $B_1$ and $B_2$ are coefficient typical of each equipment type.

For the sCO2 applications, the correlations used are reported in the following. As said, the cost is based on a size parameter $SP$ which depends on the equipment selected, on the specific coefficient reported in Table 3, and on a scaling factor based on the temperature (in °C) $f_T$, which tries to take into account the usual need for high performance materials above a certain temperature threshold.

$$Cost = a \cdot SP^b \cdot f_T \quad (88)$$

$$f_T = 1 + c \cdot (T_{max} - 550) + d \cdot (T_{max} - 550)^2 \quad (89)$$

*Table 3 - Coefficients used in the correlations for the sCO2 components [Weiland]*

| | **a** | **b** | **c** | **d** | **SP** |
|---|---|---|---|---|---|
| **Compressor IG Type** | 1230000 | 0.3992 | 0 | 0 | $P_{compr}$ [MW] |
| **Compressor Barrel Type** | 6220000 | 0.1114 | 0 | 0 | $V_{in}$ [m3/s] |
| **Axial Turbine** | 182600 | 0.5561 | 0 | 1.106E-4 | $P_{turb}$ [MW] |
| **Radial Turbine** | 406200 | 0.8 | 0 | 1.137E-5 | $P_{turb}$ [MW] |

| | | | | | |
|---|---|---|---|---|---|
| **Recuperator** | 49.45 | 0.7544 | 0.02141 | 0 | UA [W/K] |
| **Air Cooler** | 32.88 | 0.75 | 0 | 0 | UA [W/K] |
| **Gearbox** | 177200 | 0.2434 | 0 | 0 | $P_{turb}$ [MW] |
| **Generator** | 108900 | 0.5463 | 0 | 0 | $P_{elect}$ [MW] |

Finally, all costs obtained from such cost functions need to be actualised to the year in which the calculation is made, and this can be done using a cost index; in the tool, the CEPCI, the Chemical Engineering Plant Cost Index [106], was selected. This allows to use cost correlations developed in different years and to actualise them to the present (or desired) year. The index follows a simple proportion:

$$Cost_{yearB} = Cost_{yearA} \cdot \frac{idx_{yearB}}{idx_{yearA}} \qquad (90)$$

The yearly-average values of the CEPCI for the last 40 years are reported in Table 4 and in Figure 33. The recent rise in raw materials, interlinked with the Covid-19 pandemic, is well reflected in the very high values of the 2021 and 2022 years (the 2023 not being yet published at the time of writing).

*Table 4 - Yearly average value for the CEPCI Index in the last 40 years* [107] [106]

| **Year** | **CEPCI** | **Year** | **CEPCI** | **Year** | **CEPCI** | **Year** | **CEPCI** |
|---|---|---|---|---|---|---|---|
| 2022 | 816 | 2012 | 584.6 | 2002 | 395.6 | 1992 | 358.2 |
| 2021 | 708.8 | 2011 | 585.7 | 2001 | 394.3 | 1991 | 361.3 |
| 2020 | 596.2 | 2010 | 550.8 | 2000 | 394.1 | 1990 | 357.6 |

| | | | | | | | |
|---|---|---|---|---|---|---|---|
| 2019 | 607.5 | 2009 | 521.9 | 1999 | 390.6 | 1989 | 355.4 |
| 2018 | 603.1 | 2008 | 575.4 | 1998 | 389.5 | 1988 | 342.5 |
| 2017 | 567.5 | 2007 | 525.4 | 1997 | 386.5 | 1987 | 323.8 |
| 2016 | 541.7 | 2006 | 499.6 | 1996 | 381.7 | 1986 | 318.4 |
| 2015 | 556.8 | 2005 | 468.2 | 1995 | 381.1 | 1985 | 325.3 |
| 2014 | 576.1 | 2004 | 444.2 | 1994 | 368.1 | 1984 | 322.7 |
| 2013 | 567.3 | 2003 | 402 | 1993 | 359.2 | 1983 | 317 |

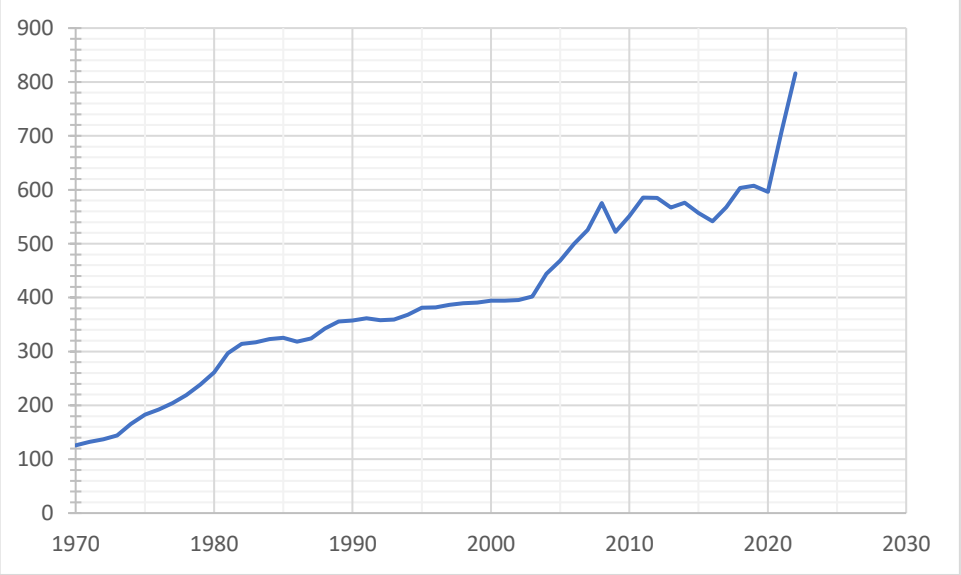


*Figure 33 - Yearly average value for the CEPCI Index through the years (see Table 4)*

## 2.10 Investment Analysis

From the evaluation of the cost of the main components of a plant, it is then possible to proceed in the computation of different parameters that allow the user to evaluate the plant or even compare different solutions, taking into account the investments necessary in the plant and the expected revenues during its lifetime.

Thus, an investment analysis was set up to evaluate some parameters such as the levelized cost of electricity (LCOE) or the payback period (PBP), to allow the user to evaluate the desired process and its variation on a thermo-economic point of view.

The economic aspects of the desired plant can be studied with two approaches in the tool. A simple analysis is possible, carried out by estimating the CAPEX (capital expenditure) and the OPEX (operational expenditure) starting from the total cost of the cycle components (Ctot or PEC - Purchase Equipment Cost). Otherwise, a more complex analysis can also be performed, which takes multiple factors into account, and leads to the calculation of the Total Revenue Requirement (TRR). This second analysis is suggested for more traditional plants, since it requires the introduction of many parameters that are usually difficult to estimate for new technologies.

In the first case, in the followings are reported some of the formulas used to calculate the main parameters of the investment analysis, such as, for instance, the LCOE or the IRR (Internal Rate of Return).

$$LCOE = \frac{CAPEX + \sum_{n=1}^{N} \frac{OPEX_n}{(1+r)^n}}{AEY \cdot N} \tag{91}$$

$$AEY = Pow \cdot UF \cdot 8760 \tag{92}$$

$$OPEX_n = Pow \cdot \left(opex_{sp} \cdot (1+\mathrm{e})^n\right) \tag{93}$$

$$CAPEX = PEC \cdot (1 + c_{inst}) \tag{94}$$

$$-CAPEX + \sum_{n=1}^{N} \frac{Rev_n - OPEX_n}{(1+IRR)^n} = 0 \tag{95}$$

$$Rev_n = Pow \cdot (8760 \cdot \mathrm{U}F \cdot \lambda_e (1 - dr)^n) \qquad (96)$$

where $n$ is the subscript relative to a single year, $N$ is the total number of years used in the analysis, usually equal to the lifetime ($LT$) of the plant. $AEY$ is the annual energy yield, which is computed based on the nominal power ($Pow$) of the plant, and its utilisation factor ($UF$). The annual operational expenditure is computed based on a specific value, $opex_{sp}$, measured in [€/$kW_{el}$], and on an escalation rate $e$. In a similar way, the capital expenditure is computed from the $PEC$ with the utilisation of an installation cost factor $c_{inst}$. The real discount rate is taken into account and is indicated with $r$. Finally, the annual revenues of the plant ($Rev_n$) are computed through a fixed electricity price $\lambda_e$, and a plant degradation rate $dr$.

### 2.10.1 The Total Revenue Requirement Method

In general, the revenue requirement method is used to determine the total revenue that must be collected to cover the costs associated with a project or a regulated utility. Thus, in the context of power production plants, this method is applied to ensure that the utility can recover its costs and earn a fair return. The revenue requirement is based on the costs of service, including operating expenses, as well as the cost of capital invested to provide the service. It is typically determined based on the costs incurred during a test year, which is expected to be representative of future costs; for this reason, in the tool this method is suggested to be utilised for more traditional technologies. The revenue requirement is an important aspect of rate regulation for utilities, as it ensures the financial viability of the operations while providing a fair return for investors. The calculation of the revenue requirement involves various components such as rate base, cost of capital, operating expenses, and income tax. The analysis implemented in the tool is based on what is presented in the book “Thermal Design and Optimization” by Bejan et al. [104].

Thus, in the case of using this investment analysis, it is structured so as to obtain the Total Revenue Requirement (TRR) value for each j-th year, defined by Eq.:

$$TRR_j = TCR_j + ROI_{j,ce} + ROI_{j,ps} + ROI_{j,d} + ITX_j + OTXI_j + FC_j + OMC_j \qquad (97)$$

As said, the TRR is in fact the revenue that must be earned in a given year through the sale of all products, to compensate the company that manages the system for all the expenses incurred in the same year and to guarantee a solid economic operation of the plant; in the plants analysed with the TEMP-EVO tool this is usually the produced electricity, but other products could be included, such as district heating, etc.

The main term is the annual portion of the Total Capital Recovery (TCR), which is the net investment that must be recovered during the economic life of the plant, and it is calculated starting from direct, indirect and related costs. The cost of components represents a part of the direct costs, and all others can be calculated through estimates or by imposing a reasonable percentage of the component purchase costs (PEC).

More in detail, the $TCR$ can be expressed as a combination of the annual book depreciation $BD_j$, plus some parameters due to taxes and to the return on the common equities. The book depreciation itself is a distribution of the Total Depreciable Investment ($TDI$) over the economic life of the plant (Book Life $BL$).

$$TCR_j = BD_j + DITX_j + RCE_{AFUDC,j} \qquad (98)$$

$$BD_j = \frac{TDI}{BL} \qquad (99)$$

$$TDI = TCI - LAND - WorkingCapital - Other\_nondepreciable \qquad (100)$$

The $TDI$ is a part of the Total Capital Investment (TCI), which is computed mainly from direct and indirect costs, that can be all estimated from the purchase equipment cost (PEC), as shown in Figure 34.

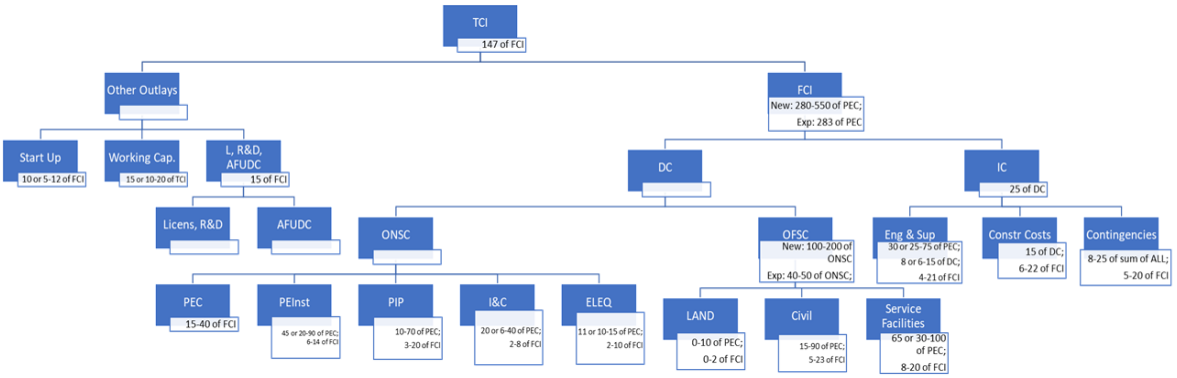


*Figure 34 - Computation of the Total Capital Investment*

In the following the other parameters relative to the formulation of the annual *TRR* are now illustrated.

The ROI (Return on Investment) are instead all the passive charges on the total capital investment not yet covered, and are divided into common equities, preferred stocks and debts, each with its own cost of capital. Alternatively they can be calculated based on an averaged cost, the WACC (weighted average cost of capital).

$$WACC = r_{Debt} \cdot \frac{Debt}{Debt + Equity} + r_{Equity} \cdot \frac{Equity}{Debt + Equity} \tag{101}$$

Finally, ITX and OTXI are composed of taxes and insurance, while the last two terms represent the operating costs, i.e. the cost of fuel (FC - Fuel Cost), if present, and the general operating and maintenance costs (O&M Costs).

Subsequent to the TRR analysis, based on the results obtained it is possible to finally obtain the relative LCOE, PBP, IRR values, useful for evaluating the desired plant and comparing different solutions.

# 3 Applications of TEMP-EVO

In the present chapter some of the applications are shown in which the TEMP-EVO tool has been used to assess or optimise the design performance of different layouts.

Different cycle layouts, mainly evolving sCO2 but also steam and organic fluids, were implemented with the approach explained in the previous chapter, and different solutions were achieved comparing both thermodynamic and also thermoeconomic performances. In these cases, following what said in the previous chapter, all of the cycles have in common to elaborate a working fluid along a closed path, therefore being named closed cycle, without any change in composition.

The chapter is structured into three main parts.

At first, a simple analysis on the influence of pressure levels on the main sCO2 possible cycles is performed, keeping the focus of the analysis on applications of this to CSP system, but also simulating only the part relative to the power block.

In the second part, a comparative analysis between sCO2, steam, and organic Rankine cycles has been made, with a focus on the application to a waste heat recovery system.

Finally, a study is shown presenting a pumped thermal energy storage system, evolving sCO2, and integrated with a thermal source coming from waste heat. this system showed high results in terms of key thermodynamic parameters, mainly the round trip efficiency of this thermomechanical battery.

## 3.1 Simple sCO2 Cycle for CSP applications

The first application here presented regards a study on the influence of the pressure levels on the performance and costs of the sCO2 cycles for CSP applications. For this reason, throughout the analysis a constant value was

considered for the maximum temperature of the cycle, equal to the maximum temperature achievable by commercial binary molten salts, 580°C.

Another relevant aspect of this initial analysis was the high efficiencies considered for the turbomachinery, which positively impacted the results. In the previous chapter correlations were described between size and efficiency of these components, but it was not used here, where fixed assumptions were rather employed. The main results obtained indicate that for the simple cycle the reduction in pressure levels doesn't hugely affects the efficiency values, and slightly reduce the cost of the plants thanks to pressure reduction, also shifting the operating points towards more gas-like behaviour of the fluid. On the other hand, for the most efficient cycle the pressure reduction is not justified and leads to a significant drop in the efficiency of the cycle. This is mainly due to the intrinsic behaviour of the recompressed cycle, conceived to work close to supercritical conditions with huge variations in the thermophysical properties of the fluid. For these reasons, the sCO2 solutions here presented can be considered of interest only for demonstration tests, but not for upscaled or commercial applications.

### 3.1.1 sCO2 cycle layouts

This analysis focused on three typical cycle configurations for $CO_2$, either at supercritical or transcritical pressures, outlined hereby.

The Recuperated Cycle is shown in Figure 35. It consists of a compressor, a molten salts heater, a turbine, an air cooler and a recuperator, in its simplest representation. It is assumed that hot molten salts are provided by the CSP field.

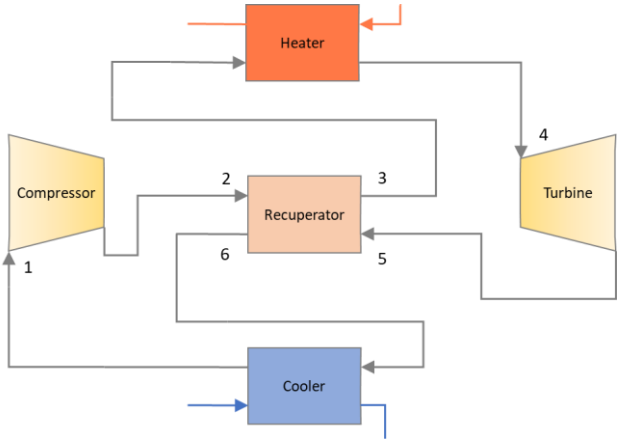


*Figure 35 - The Recuperated Cycle*

The plant configuration of the Intercooled Cycle is shown in Figure 36. It consists of a main compressor, a molten salts heater, a turbine, a main cooler, another compressor (called first compressor or IC compressor) positioned between the two coolers, a second cooler (called intercooler or IC cooler), positioned between the two compressors, and a recuperator.

To define the cycle operating conditions, in this case, a parameter is needed to state how the total pressure ratio is distributed among the two compressors. So the pressure ratio split parameter is introduced ($\xi_{PR}$), and it is used in the model to calculate the pressure ratio across the first (IC) compressor with respect to the total pressure ratio of the cycle ($\beta_{tot}$).

$$\beta_{IC} = (\beta_{tot})^{\xi_{PR}} \qquad (102)$$

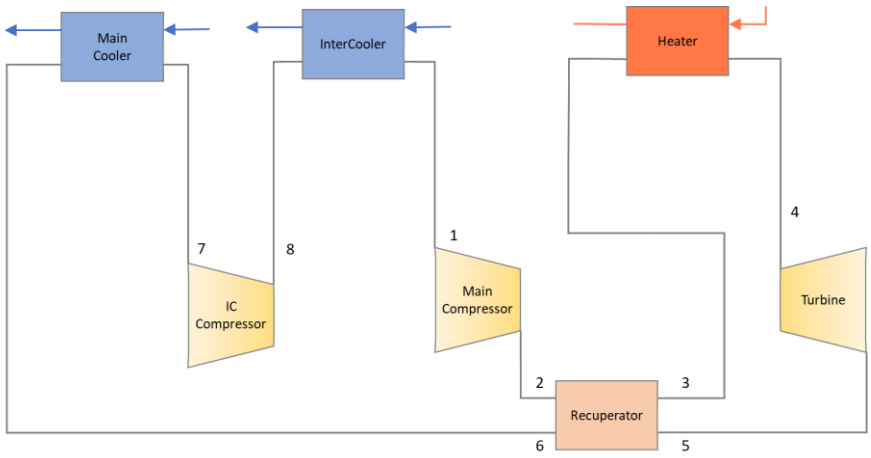


*Figure 36 - The Intercooled Cycle*

The plant configuration of the Recompressed Cycle is shown in Figure 37. It consists of a main compressor, a low temperature recuperator (LTR), second compressor (called recompressor or split compressor or bypass compressor), a high temperature recuperator (HTR), a molten salts heater, a turbine, and a air cooler. To define the cycle configuration a parameter is needed to state how much of the total mass is split and directed to the split compressor. So the mass split parameter is introduced ($\xi_{SPLIT}$), and it is used in the code to calculate the mass in the recompressor.

$$\dot{m}_{recompressor} = \xi_{SPLIT} \cdot \dot{m}_{cooler} \qquad (103)$$

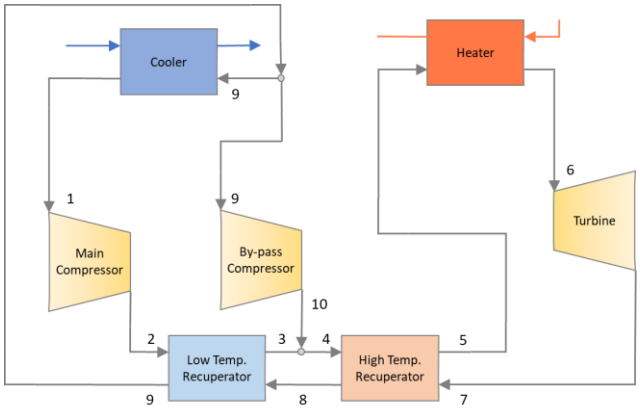


*Figure 37 - The Recompressed Cycle*

Since the main focus of this analysis is on the techno-economic impact of maximum pressure reduction, the maximum temperature of the $CO_2$ cycle is kept constant, and calculations of the molten salts heater and air coolers follow. For this reason, heater and cooler were not sized using effectiveness, but their physical and thermal properties were set as reported in Table 5. A minimum temperature difference of 15°C between salts and sCO2 has been set for the molten salt heater.

*Table 5 - Cycle and component assumptions (machinery efficiencies are kept constant)*

| **Parameter** | **Value** | **Unit** |
|---|---|---|
| Maximum pressure P_max | 135; 180; 215; 250 | bar |
| Compressor efficiency | 88 | % |
| Pressure ratio split $\xi_{PR}$ | 0 – 50 | % |
| Mass split $\xi_{SPLIT}$ | 0 – 40 | % |
| Pressure losses in HEX | 2 | % |
| Thermal losses in HEX | 0 | % |
| Maximum cycle temp. | 565 | °C |
| Temp. MS heater inlet | 580 | °C |
| ΔT MS heater outlet | 15 | °C |
| MS specific heat | 1541 | J/kgK |
| Turbine efficiency | 90 | % |
| Turbine outlet pressure | variable | |
| Compressor Inlet temp. | 35 | °C |
| Inlet cooling air temp. | 25 | °C |
| Outlet cooling air temp. | 40 | °C |

| | | |
|---|---|---|
| Recuperator eff. ε | 90 | % |
| Thermal power output | 10 | MW |

### 3.1.2 Results

At first, a thermodynamic analyses has been performed for all cycle layouts previously described for four different maximum pressure levels (maximum pressure occurs at compressor outlet, due to pressure losses in heat exchangers): 250bar, 215 bar, 180bar and 135bar. The maximum temperature, which is the turbine inlet temperature, is fixed in all cases to 565 °C. Performance results are reported in the following as multi-variate sensitivity analysis, which allows to clearly indicate both the local of peak performance as well as the impact of the relevant parameters.

#### *3.1.2.1 Recuperated Cycle*

In a recuperated cycle, having fixed the maximum temperature and pressure, the only free parameter remains the minimum pressure, at the turbine outlet.

Given the simple cycle layout of this case, only the efficiency curve is reported in Figure 38. The peak efficiency moves backward reducing the maximum pressure, also at values below the critical pressure (P_crit = 73.8bar). It should be noted that for each step of reduction of maximum pressure, the peak efficiency is reduced of 1 percentage point, with the 250bar case showing the reference case at almost 35% thermal efficiency. Since the minimum cycle temperature is fixed at 35°C, the compressor intake moves away from the critical point, thus increasing the compression work but also the turbine work, and above all allowing a better heat recuperation, which leads to a quite good efficiency.

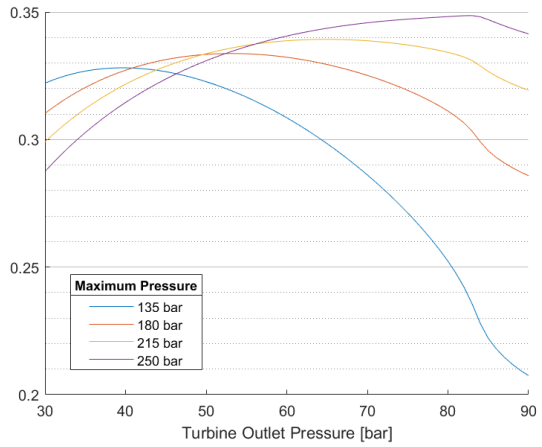


*Figure 38 - Thermal efficiency for Recuperated cycles at different levels of maximum pressure*

### *3.1.2.2 Intercooled Cycle*

In case the compressor is split into two parts with an intercooler in the middle, the additional degree of freedom represented by the split of total pressure ratio needs to be considered, originating the contours diagrams of the following figures. Referring to the highest pressure, 250bar, it is clear that a local of maximum efficiency is present, exceeding 36%; therefore, more than 1 percentage point is gained against the reference recuperated cycle.

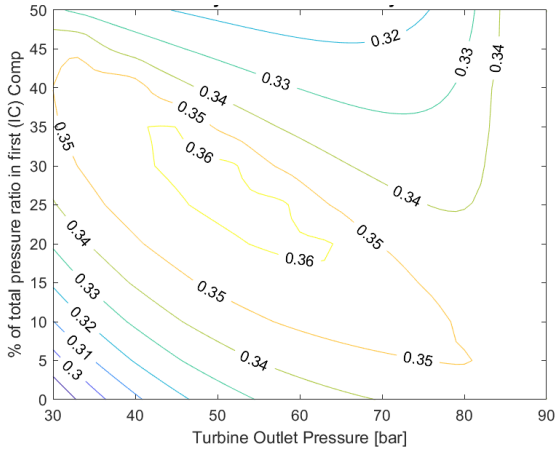


*Figure 39 - Thermal efficiency of Intercooled cycles at maximum pressure of 250 bar*

Going at lower maximum pressure the peak efficiency gradually moves towards lower minimum cycle pressures, and the pressure ratio is gradually more balanced between the two compressors; the second one, however, is always subject to a higher pressure ratio. This is because moving towards lower pressures maintaining the minimum temperature constant means moving away from the critical point, and so the peak efficiency moves towards a more balanced distribution of the pressure ratio between the two compressors.

Similarly to the recuperated case, also here approx. 1 percentage point in peak efficiency is lost per each step of reduction of maximum pressure from 250bar down to 135bar.

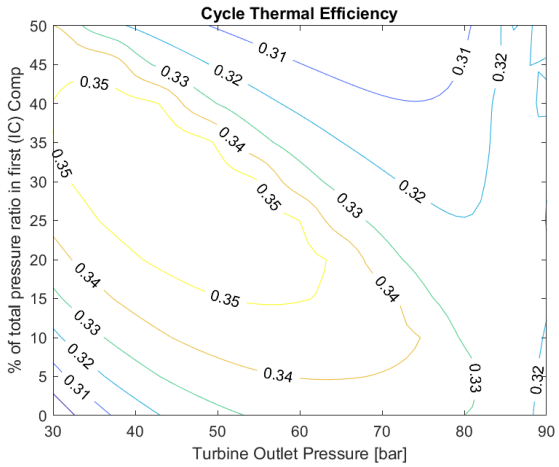


*Figure 40 - Thermal efficiency of Intercooled cycle at maximum pressure of 215 bar*

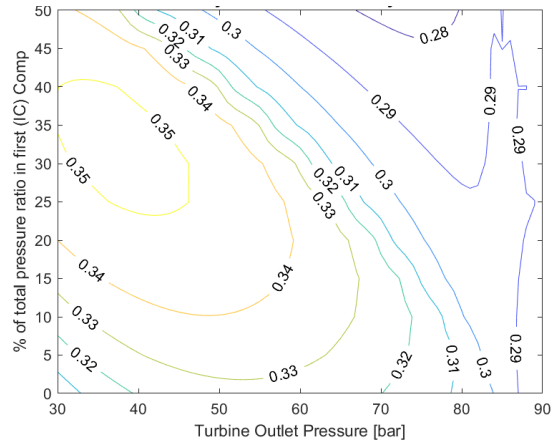


*Figure 41 - Thermal efficiency of Intercooled cycle at maximum pressure of 180 bar*

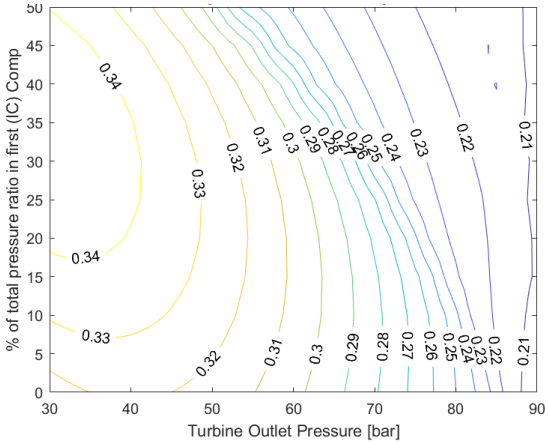


*Figure 42 - Thermal efficiency of Intercooled cycle at maximum pressure of 135 bar*

Focusing on the intermediate case of P_max = 180bar, the following Figure 9 reports the required $CO_2$ mass flow rate at compressor exit to obtain 10MW net power output. As expected, the closer the operating point is to the peak efficiency region, the lower the mass flow rate required. However, it should be noted that still within the 35% efficiency region, an area exists where mass flow can vary as much as from 90kg/s to 100kg/s: this is important for a multi-objective optimization of the plant, where efficiency is only one of the elements, and, for instance, volumetric flow available at turbine inlet is another relevant aspect, particularly for demo or pilot installations.

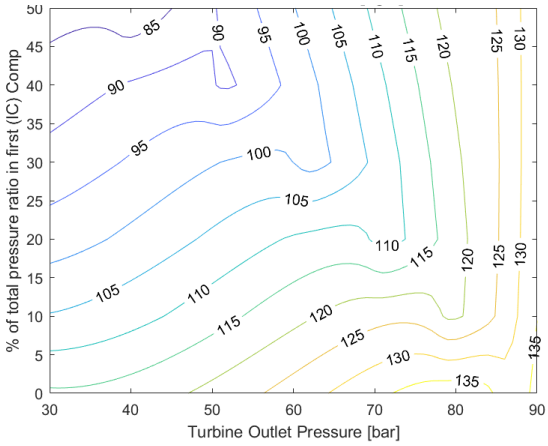


*Figure 43 - Mass flow rate of Intercooled cycle at maximum pressure of 180 bar*

Finally, the following Figure 10 reports the recuperator UA, calculated by dividing the recuperator in different sections to consider the variation of the fluid properties inside the heat exchanger, as explained in a previous paragraph.

In this case it is of utmost importance observing that the area close to the peak efficiency (180bar case) is also where the recuperator presents the lowest "thermodynamic size" UA (W/K), which means highest compactness and, potentially, lowest cost: therefore, this is one of the few cases where top performance can coincide with minimum capital cost.

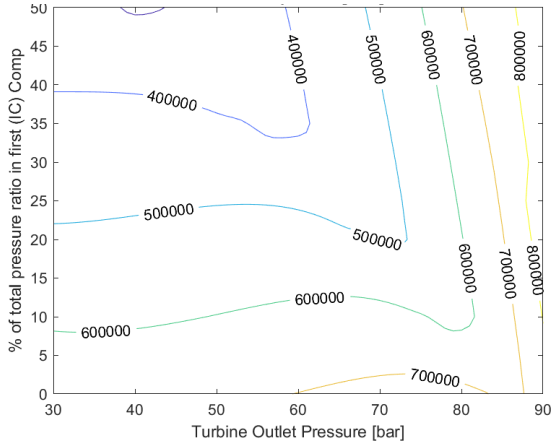


*Figure 44 - Recuperator UA of Intercooled cycle at maximum pressure of 180 bar*

### *3.1.2.3 Recompressed Cycle*

It is recognized that the recompressed cycle shows the top performance among sCO2 cycles for CSP application. Within the assumptions of this analysis for cycle performance estimation, the peak efficiency of almost 42% is achieved for the 250bar maximum pressure case within an area of mass flow split of approximately 30% and a turbine outlet pressure of 90 bar, corresponding to a minimum pressure near to 85 bar, higher than the critical pressure; this is due to the fact that, because of the minimum temperature considered constant, increasing the minimum pressure leads the compressor inlet point move towards a higher density region, and until the pressure ratio reduction does not impact heavily on the expansion, this leads to lower compressor work and

consequently to higher efficiency. In this case, sensitivity against the maximum pressure is higher than previous cycles, loosing approximately 3 percentage point per each step in reduction of the maximum pressure.

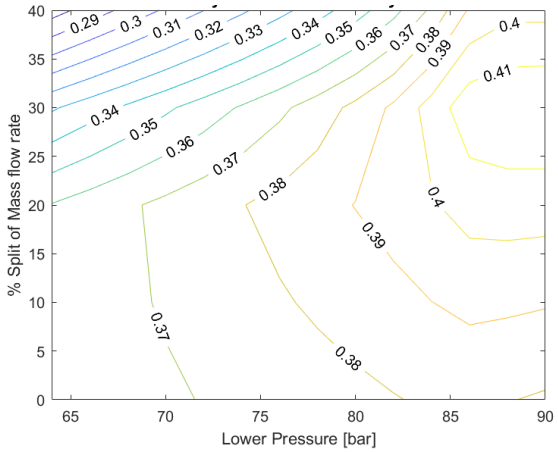


*Figure 45 - Thermal efficiency of Recompressed cycle at maximum pressure of 250 bar*

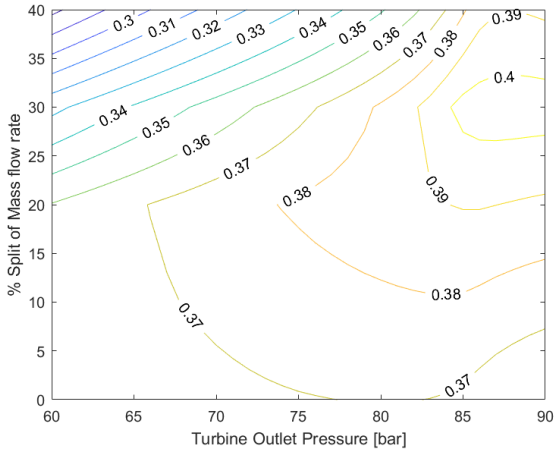


*Figure 46 - Thermal efficiency of Recompressed cycle at maximum pressure of 215 bar*

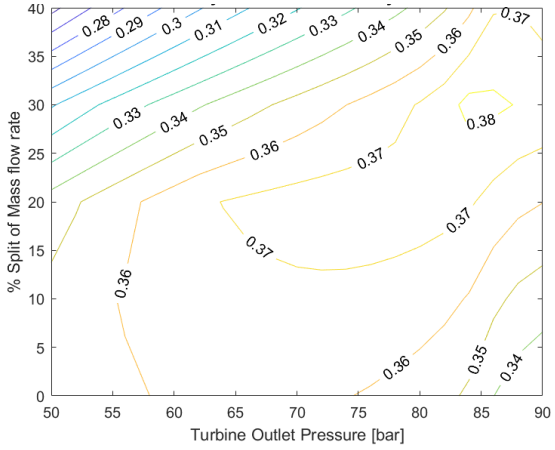


*Figure 47 - Thermal efficiency of Recompressed cycle at maximum pressure of 180 bar*

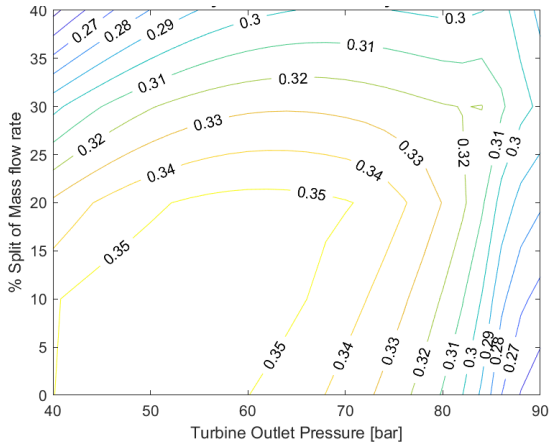


*Figure 48 - Thermal efficiency of Recompressed cycle at maximum pressure of 135 bar*

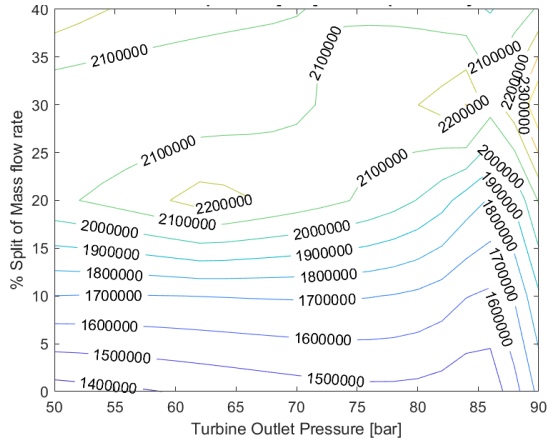


*Figure 49 - Total recuperator UA for LTR and HTR of Recompressed cycle at maximum pressure of 180 bar*

In Figure 49 the total UA for the recuperator is reported: as expected, the recompression cycle requires high surface values, that translates into bulky equipment, compared to the simple recuperated case.

#### *3.1.2.4 Combined Performance Analysis*

Here a performance analysis is presented to compare the different cycle configurations in the four selected values of maximum pressure. For each of those, it has been selected the turbine outlet pressure that shows the peak efficiency. In the following tables, maximum efficiency for each cycle configuration and corresponding maximum pressure (Table 6) are reported, including the values of lower pressure that lead to the best efficiency values (Table 7).

*Table 6 - Maximum efficiency of each cycle*

| Maximum pressure | Recuperated | Intercooled | Recompressed |
|---|---|---|---|
| 135 bar | 32.81% | 34.79% | 35.81% |
| 180 bar | 33.37% | 35.24% | 38.30% |
| 215 bar | 33.93% | 35.71% | 40.52% |
| 250 bar | 34.86% | 36.28% | 41.96% |

*Table 7 - Turbine outlet pressure for maximum efficiency cycles*

| Maximum pressure | Recuperated | Intercooled | Recompressed |
|---|---|---|---|
| 135 bar | 40 bar | 30 bar | 54 bar |
| 180 bar | 53 bar | 39 bar | 84 bar |
| 215 bar | 65 bar | 45 bar | 87 bar |
| 250 bar | 83 bar | 55 bar | 90 bar |

In the following figures, as an example, the T-s diagrams of the three cycle configurations at maximum efficiency points are presented, for maximum pressure set at 180bar. By observing the relative magnitude of the cycle areas, it can be qualitatively inferred the highest specific work of the Intercooled cycle, against the lowest specific work of the Recompressed cycle. But more importantly, it can be seen the difference between the simpler cycles, that move towards gas-like behaviour, and the recompressed one, whose compressor inlet is positioned close to the critical point.

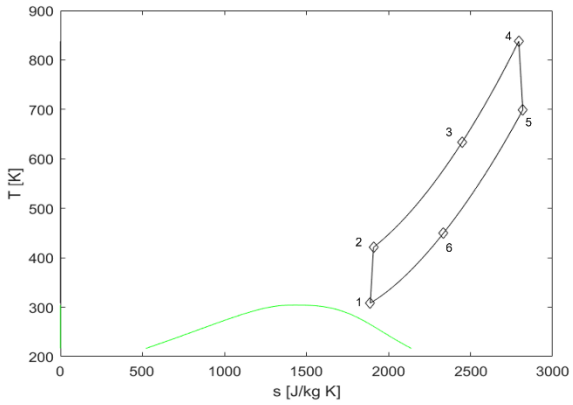


*Figure 50 - T-s diagram for Recuperated Cycle at maximum pressure of 180 bar*

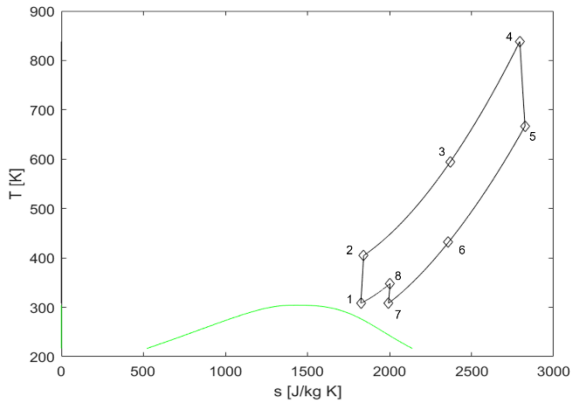


*Figure 51 - T-s diagram for Intercooled Cycle at maximum pressure of 180 bar*

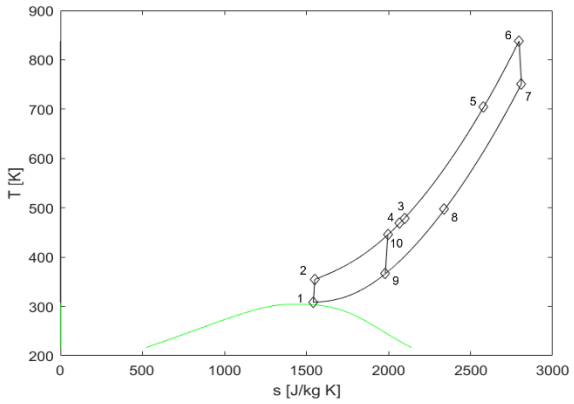


*Figure 52 - T-s diagram for Recompressed Cycle at maximum pressure of 180 bar*

The maximum efficiency for different cycle configurations versus maximum pressure is shown in Figure 53, where it can be clearly seen the large variation in efficiency for the recompressed cycle. This is because the recompressed cycle fits well low compression work configurations and high heat recuperation: when the maximum pressure is reduced, the best low pressure doesn't move as significantly as the other cycles, and the consequent reduction in pressure ratio largely reduces the turbine expansion work, and so the efficiency.

It can also be noted that the Intercooled cycle is the least sensitive to maximum pressure variation, because compression work is minimised thanks to the intercooler, regardless of the proximity to the critical point.

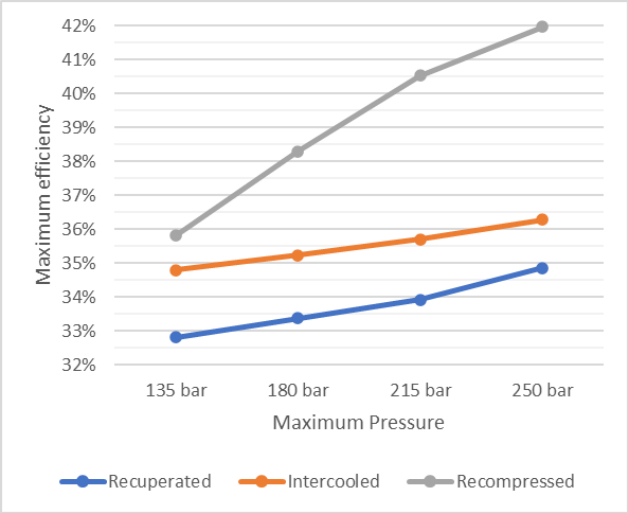


*Figure 53 - Maximum efficiency vs maximum pressure for the three cycle configurations*

The following figure shows the total UA for the recuperator only, not considering the heater and cooler sizes, which, for constant electrical power output, are just a function of the electrical efficiency, being smaller for the more efficient configurations.

For the recuperator, the minimum size is achieved by the Intercooled cycle, thanks to the lower temperature at the compressed $CO_2$ delivery, which allows higher temperature difference across this component. On the other side, the very large surface of the Recompressed cycle is clearly highlighted: this is a consequence of assumptions, in particular the constant effectiveness assumption for all heat exchangers. In fact, the Recompressed Cycle requires a higher heat recovery, and therefore it has a smaller temperature difference, which necessarily results in a higher UA size.

In general, the impact of the pressure increase on recuperator size (i.e. UA) is positive: the higher the pressure, the more compact recuperator is possible, as shown in Figure 54.

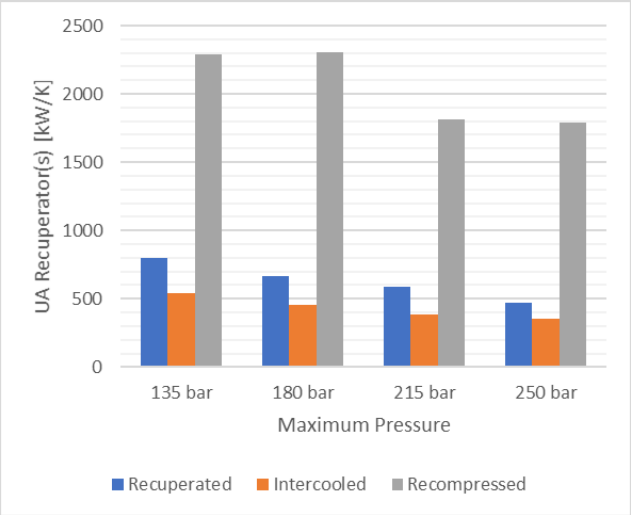


*Figure 54 - UA of the Recuperator(or sum of the UA of the Recuperators in each cycle) for different cycle configurations and maximum pressures, at the maximum efficiency point for each combination*

The following Figure 55 shows the overall compression power, which increases by reducing the maximum pressure, as far as the minimum pressure reduces with respect to the critical pressure. In particular, it can be seen that the compressor work in the Recuperated cycle is the highest, despite of the presence of two compressors in the other two cycles, which clearly allows minimization of overall compression work.

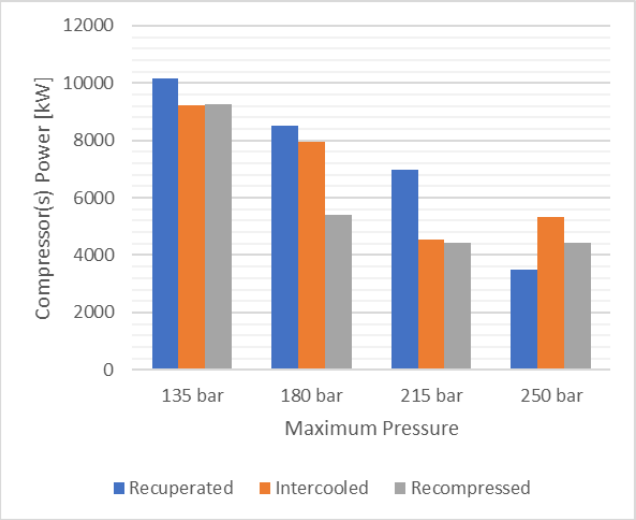


*Figure 55 - Compressor(s) power for different cycle configurations and maximum pressures, with maximum efficiency point for each combination*

### *3.1.2.5 Economic Comparison*

In this section the economic results are presented.

In Figure 56 the specific total cost obtained is presented as main result from this investigation; these costs are relative to main components of the power loop only. First of all, for all cycles considered, it demonstrates the benefit of reducing the maximum operating pressure: the decrease in specific cost has similar trend for all the cycle configurations with monotone behaviour, with exception for the recompressed cycle, which shows an optimum. It can be inferred that Recuperated cycle is the least cost attractive configuration, showing specific cost up to 50% more that the other options, mainly because of the large size of components and large $CO_2$ mass flow rate, dictated by the relatively lower efficiency. On the other hand, Intercooled and Recompressed cycles are quite aligned and, in general, show interesting cost figures. Despite these costs are obtained with lumped correlations and so useful mainly for an "internal" comparison, namely among the different cycle layouts and parameters analysed, they are in line with those obtained in other studies.

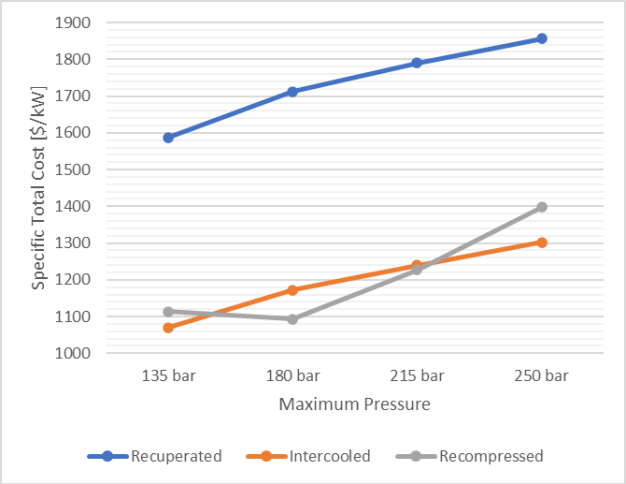


*Figure 56 - Specific total cost ($/kW) for different cycle configurations and maximum pressures, with maximum efficiency point for each combination*

Figure 57 shows a quite stable value of the cost of the recuperator, even taking into account the reduction factor for the operating pressures. This is because for this cycle is mandatory having high component size to achieve the target power with a high efficiency. However, it is clear that pressure reduction well benefits the cooler and heat capital costs: the three heat exchanger cost reduction with pressure reduction drives the total cycle cost reduction. So, it is confirmed that heat exchangers are key to optimise the capital cost features of supercritical $CO_2$ cycles.

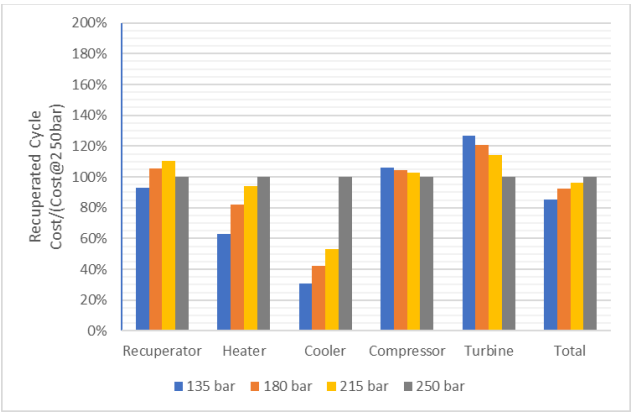


*Figure 57 - Normalized costs for Recuperated cycle at the best efficiency point*

On the other hand, for Intercooled and Recompressed cycles the recuperator follows a similar monotone cost reduction with pressure reduction, which also drives the total cost reduction, with exception of the recompressed cycle which, for the lowest pressure case, is affected by the significant increase of compressor train: in fact, as far as the turbine outlet pressure is far from the critical pressure, the Recompressed scheme loses its attractiveness, and the compressors become large in size (and required work).

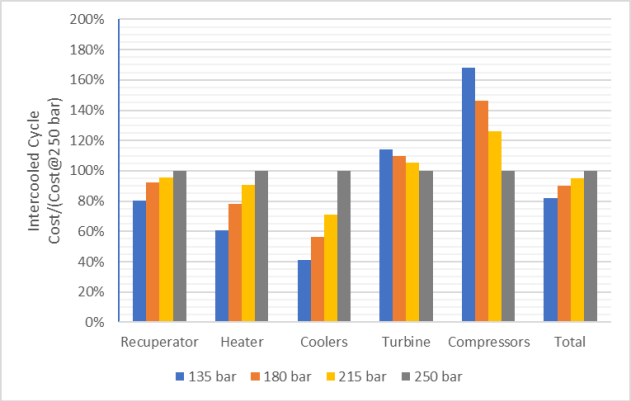


*Figure 58 - Normalized costs for Intercooled cycle at the best efficiency point*

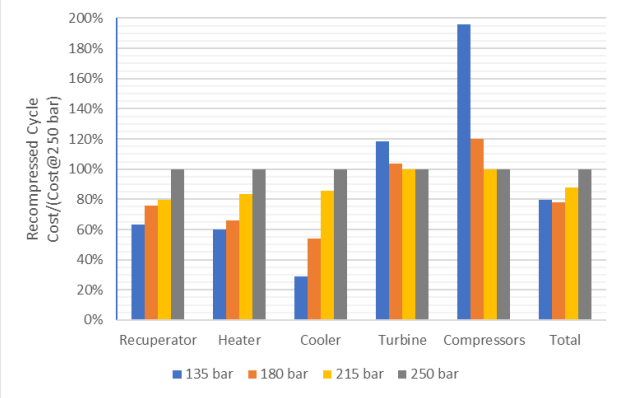


*Figure 59 - Normalized costs for Recompressed cycle at the best efficiency point*

### *3.1.2.6 Critical Analysis on the Recuperator effectiveness*

In this paragraph a fundamental analysis of the recuperator effectiveness for the recuperated and recompressed cycle layouts is carried out. It has been

observed that, assuming the same effectiveness for each recuperator (i.e. 90% according to Table 5), the resulting total heat transfer coefficient UA, which is proportional to the heat exchanger surface, is significantly increased for the recompressed case: in the peak efficiency points when the maximum pressure is equal to 250bar (35% and 41% for the recuperated and recompressed layouts, respectively), the UA is equal to 467604 W/K for the recuperated cycle and to 1793248 W/K for the recompressed case (Figure 54). Therefore, despite this is due to the specific configuration of the recompressed cycle that allows a more efficient recuperation from turbine outlet, it seems that the two layouts have not been compared with fair and equal conditions.

Referring to the Recuperated cycle, if we split such a single recuperator into two parts, for instance with 50% thermal load each, we obtain two series recuperators with an effectiveness of 67% the LTR and 68% the HTR. This is clearly contrasting against the 90% effectiveness for the recuperator as a whole. This is due to the definition of effectiveness, i.e. the actual heat transferred over the "ideal" heat transferred in case of infinite-surface heat exchanger.

From this simple example, it is clear that assuming the same effectiveness for one single recuperator, as in the Recuperated cycle, and for each split recuperator, such as the LTR and HTR in the recompressed cycle, brings to non-comparable results, because the size of the heat exchanger equipment is significantly different, favouring the Recompressed cycle.

To try a different comparison, therefore, it is proposed here to maintain the same total heat transfer coefficient UA for both the Recuperated cycle and the Recompressed cycle. By keeping as reference the Recompressed cycle total UA equal to 1793248 W/K, at the best efficiency point and maximum pressure equal to 250 bar, which corresponds to LTR and HTR effectiveness of 90% each, we obtain a "technically equivalent" recuperator for the recuperated cycle, which would have an effectiveness equal to 99.4%. Such an equivalent Recuperated cycle has now a recuperator heat exchanger which has the same size (i.e. UA) of the Recompressed cycle. Such equivalent Recuperated cycle is now showing, in

the 250 bar case, a peak efficiency of near 40%, surprisingly very close to the Recompressed case.

On the other hand, by looking closely at the recuperator operating conditions, while the minimum temperature differences of the Recompressed cycle are 21°C for the HTR and 12°C for LTR, in the equivalent Recuperated cycle a minimum temperature difference of 2°C is now reached, at the cold section: this is a very low value, difficult to reach in practise, but dictated by the very high equivalent effectiveness.

In conclusion the difference in UA should not be ignored and the assumption of constant effectiveness for a single recuperator, like in the Recuperated cycle, or a split recuperator, like in the Recompressed cycle, needs to be carefully evaluated.

## 3.2 Comparison of sCO2, ORC, and Steam cycles for WHR applications

Another analysis performed with the use of the TEMP-EVO tool is presented in the following, and regards the comparison of usage of sCO2, steam, and organic fluids, for application to waste heat recovery. In the following, four of the analysed cycles are reported, which showed the most interesting performance; in particular, these cycles are studied to fit the recuperation from a sensible thermal source, such as a stream of flue gases from a gas turbine.

The sCO2 cycles showed comparable results with the top performing cycle analysed, the steam cycle with two levels of pressure. Moreover, the successive economic analysis showed a slightly better results of the main investment parameters. Despite the economic analyses are always influenced by the specific assumptions made, this analysis shows anyway that the sCO2 can achieve results comparable with those typical of more traditional technologies.

### 3.2.1 Layouts Considered and Assumptions

For the comparison, four different plant configurations (illustrated in Figure 60) were considered, one for steam, one for organic fluid, and two for $CO_2$:

- Steam Rankine cycle with two pressure levels ("Steam 2L"): the more traditional cycle typically used for WHR applications with plant size comparable to those analysed; it is composed of two pumps, two turbines ("Turb"), two economizers ("Eco"), two evaporators ("Eva"), two superheaters ("SH"), all divided between a low-pressure line ("LP" ) and one high ("HP"), and a condenser ("Cond");
- Regenerated ORC ("ORC Rec"): a Rankine cycle regenerated with organic fluid, state of the art for this type of application; reference was made to the "ORegen" system [108] developed by General Electric (GE Oil & Gas), which uses cyclopentane as a working fluid and is commonly used as a GT bottoming cycle; it is composed of a pump, a turbine, a recuperator ("Recup"), the condenser and the HRSG, consisting of an economizer, an evaporator and a superheater;
- Supercritical $CO_2$ regenerated Brayton cycle ("s$CO_2$ Rec"): the simplest and consequently the cheapest $CO_2$ cycle, but also the one offering the worst performance; it consists of a compressor ("Comp"), a turbine and three exchangers, cooler, heater, and recuperator;
- Supercritical $CO_2$ Brayton dual split dual expansion cycle ("s$CO_2$ 2split2exp"): a more complex cycle proposed by Kimzey et al. [109] and subsequently reworked by Cho et al. [110]; it allows $CO_2$ systems to be competitive in terms of power output, as it is a good compromise between the optimization of heat recovery from the upper source and the thermodynamic efficiency of the cycle itself; it is composed of two turbines, two heaters and two recuperators, divided between a high-temperature line ("HT") and a low-temperature line ("LT"), and of a compressor and a cooler.

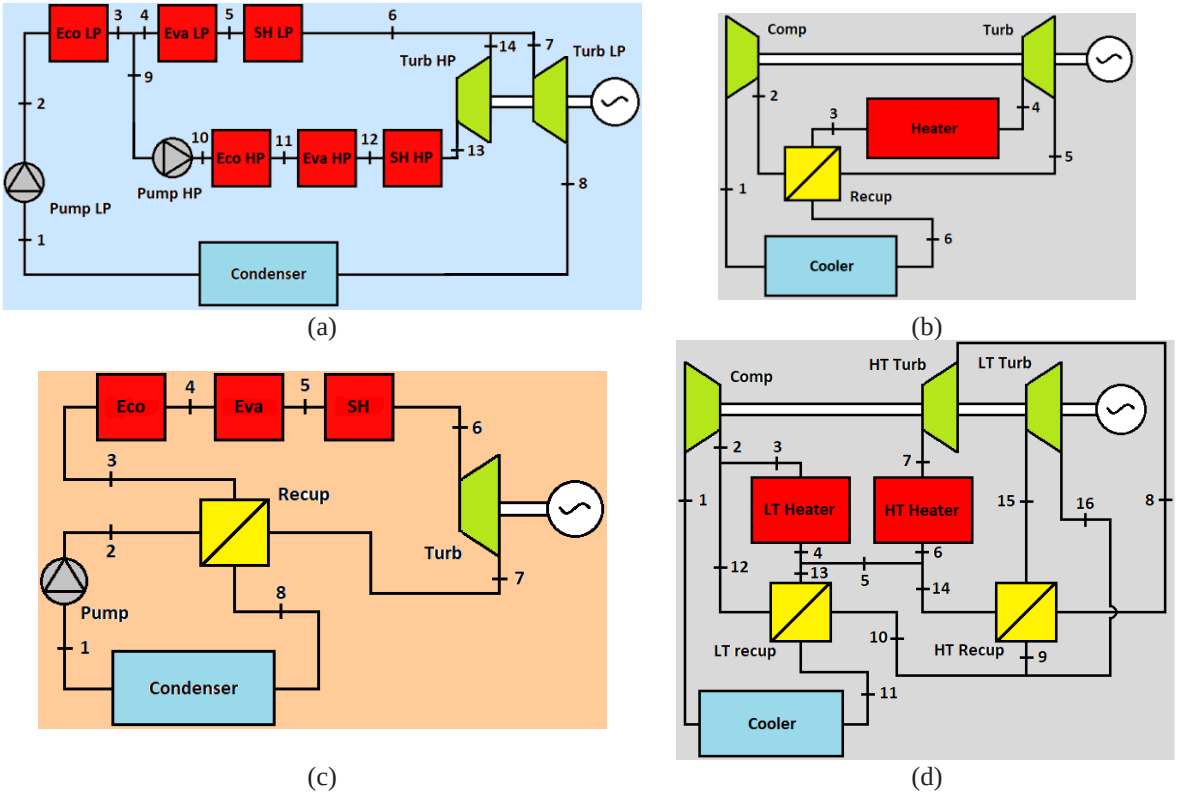


*Figure 60 - Analysed cycle layouts: a) Steam 2L, b) sCO2 Rec, c) ORC Rec, d) sCO2 2split2exp*

### *3.2.1.1 Thermodynamic Assumptions*

Model assumptions are reported in the following tables. The plant size is impacting the mechanical and electrical efficiencies and turbomachinery efficiencies, which also depend on the evolving fluid.

Table 8 shows the values of the general assumptions. The heat source, both at high and low temperatures, is always approximated by a mass flow rate of air at ambient pressure, whose value determines the two different plant size ranges.

*Table 8 - General assumptions*

| | ***Small Size*** | ***Medium Size*** |
|---|---|---|
| $\eta_{el}$ | 95 % | 97 % |

| | | |
|---|---|---|
| $\eta_{mec}$ | 95 % | 97 % |
| $\dot{m}_{in,HS}$ | 40 kg/s | 145 kg/s |
| $\Delta T_{appr}$ | > 10 °C | |
| $T_{in,CS}$ | 25 °C | |
| $\Delta T_{pp,cond/cooler}$ | 5 °C | |

*Table 9 - Steam cycle decision variables and specific assumptions*

| ***Steam*** | | |
|---|---|---|
| **Decision variables and optimization bounds** | | |
| $T_{out,SH\ LP}$ | 120 °C | 200–300 °C |
| $p_{in,turb\ LP}$ | 1 bar | 10 bar |
| $p_{in,turb\ HP}$ | 10 bar | 100 bar |
| $\Delta T_{appr}$ | 10 °C | 110 °C |
| $\dot{m}_9/\dot{m}_3$ | 0.3 | 1 |
| **Assumptions** | | |
| | ***Small Size*** | ***Medium Size*** |
| $\eta_{turb\_LP/HP}$ | 85 % | 90 % |
| $T_{in,turb}$ | < 600 °C | |
| $x_{out,turb\_LP}$ | > 0.9 | |
| $\eta_{pump\_LP/HP}$ | 75 % | 80 % |
| $p_{in,pump\_LP}$ | 0.08 bar | |
| $\Delta p/p_{in,cond}$ | 5 % | |
| $\Delta T_{subc}$ | 5 °C | |

| | |
|---|---|
| $\Delta p/p_{in,eco\_LP}$ | 15 % |
| $\Delta p/p_{in,eco\_HP}$ | 10 % |
| $\Delta p/p_{in,eva\_LP/HP}$ | 5 % |
| $\Delta T_{pp,eva\_LP}$ | 10 °C |
| $\Delta p/p_{in,SH\_LP/HP}$ | 5 % |

Regarding the two-level pressure steam cycle, the pressure at the condenser has been assumed constant since the thermodynamic efficiency increases as its value decreases, but it is limited below by the ambient temperature. Therefore we assumed a pressure equal to 0.08 bar, which corresponds to a saturation temperature of 41.54 °C and which allows excellent performance and acceptable dimensions of the condenser. The inlet pressures to the two turbines, on the other hand, were left as decision variables to be optimized, in the same way as the two superheaters outlet temperatures and the flow fractions to the two branches leaving the splitter. Furthermore, the turbine inlet temperature is bounded below 600 °C due to technological and economic constraints related to the materials.

*Table 10 - ORC decision variables and specific assumptions*

| ***Cyclopentane*** | | |
|---|---|---|
| **Decision variables and optimization bounds** | | |
| $T_{out,SH} \equiv T_{in,turb}$ | 232 °C | 277 °C |
| **Assumptions** | | |
| | ***Small Size*** | ***Medium Size*** |
| $\eta_{turb}$ | 85 % | 90 % |
| $p_{in,turb}$ | 40 bar | |

| | | |
|---|---|---|
| $\eta_{pump}$ | 60 % | 65 % |
| $p_{in,pump}$ | 0.6–1.013 bar | |
| $\Delta p/p_{in,cond}$ | 5 % | |
| $\Delta T_{subc}$ | 5 °C | |
| $\Delta p/p_{in,eco}$ | 10 % | |
| $\Delta T_{pp,eco}$ | 10 °C | |
| $\Delta p/p_{in,eva}$ | 5 % | |
| $\Delta p/p_{in,SH}$ | 5 % | |
| $\varepsilon_{rec}$ | 0.8 / 0.9 | |
| $\Delta p/p_{in,rec,h/c}$ | 1 % | |

*Table 11 - sCO2 cycles decision variables and specific assumptions*

| ***sCO2*** | | |
|---|---|---|
| **Decision variables and optimization bounds** | | |
| $p_{in,turb}$ | 180 bar | 300 bar |
| $p_{in,comp}$ | 75 bar | 90 bar |
| $\Delta T_{appr}$ | 10 °C | 250 °C |
| $T_{out,heater\ LT}$ | 100 °C | 200–300 °C |
| $\dot{m}_{12}/\dot{m}_2$ | 0.5 | 0.9 |
| $\dot{m}_{14}/\dot{m}_5$ | 0.1 | 0.6 |
| **Assumptions** | | |
| | ***Small Size*** | ***Medium Size*** |
| $\eta_{turb}$ | 88 % | 93 % |

| | | |
|---|---|---|
| $T_{in,turb}$ | unbounded above | |
| $\eta_{comp}$ | 67 % | 80 % |
| $\Delta p/p_{in,cooler}$ | 2 % | |
| $T_{out,cooler}$ | 35 °C | |
| $\Delta p/p_{in,heater}$ | 1 % | |
| $\Delta T_{pp,heater}$ | 10 °C | |
| $\varepsilon_{rec}$ | 0.8 / 0.9 | |
| $\Delta p/p_{in,rec,h/c}$ | 1 % | |

The ORC uses cyclopentane as a working fluid, which has a critical temperature of 238.57 °C and critical pressure of 45.712 bar. The choice of fluid affects the lower and upper limits of operating temperature and pressure:

- the superheater outlet temperature, the only decision variable of the cycle, is constrained below by the saturation temperature at the turbine inlet pressure, assumed constant and equal to the maximum value to be safe under the critical pressure, and above by technical limits imposed by CoolProp, in fact cyclopentane can be considered thermally stable at temperatures below 300 °C [111];
- the pressure at the condenser is assumed equal to 0.6 bar, which imposes a temperature of about 35 °C, however a second case with the condenser at ambient pressure, as the Oregen system works in this way [108], has been considered.

Furthermore, since there is a recuperator, the cycle was analysed with two different values of the component effectiveness, in order to evaluate the impact of this parameter on the behaviour of the system in terms of performance and costs.

Since the two $CO_2$ cycles make use of the same technology, the same assumptions were made for the respective components. Both cycles process fluid under supercritical conditions, therefore pressure and temperature are important parameters and it must be ensured that their values are always above the critical ones. Consequently, the temperature at the outlet of the cooler was assumed to be constant and equal to 35 °C, on the other hand, the inlet pressure to the compressor was selected among the decision variables, but its value is bounded below at 75 bar.

The turbine inlet pressure is also a decision variable to which, however, a lower constraint has not been placed, but a higher one given by technological limits.

In the "sCO2 2split2exp" cycle, since it is more complex, there are several decision variables, including the temperature difference at the approach between the hot source and $CO_2$, the latter in common with the "sCO2 rec" cycle, the LT heater outlet temperature and the flow fractions coming out of the two splitters.

As for the ORC, two cases of recuperator effectiveness were evaluated.

#### *3.2.1.2 Geometric and economic assumptions*

In order to use the cost functions related to heat exchangers and then carry out the economic analysis, it is necessary to calculate the exchange surface and the *UA* product of the heat exchangers themselves. For this purpose, a simplified geometric model has been developed, which requires some assumptions on the type and size of heat exchangers used in the various plants.

To maintain the generality of the analysis, the same types of heat exchangers were selected and the same assumptions were made, kept constant for all the temperatures of the hot source, for the corresponding components in the different configurations:

- The condenser of the steam cycle and the ORCs and the cooler of the supercritical $CO_2$ cycles have been modelled according to a cross-flow finned tube heat exchanger;
- The steam generator (consisting of economizer, evaporator, and superheater depending on the configuration of the cycle) and the supercritical $CO_2$ cycle heater were modelled as a cross-flow finned tube exchanger;
- The recuperator for ORC has been modelled as a Shell & Tube heat exchanger in which the coldest fluid circulates in the tubes while the hottest one circulates outside of them;
- The recuperator for supercritical $CO_2$ has been modelled according to a printed circuit heat exchanger (PCHE), specific for this type of application.

*Table 12 - Geometric assumptions*

| | **ORC Recup** | **Heater, Eco, Eva, SH** | **Cooler, Cond** | **PCHE** |
|---|---|---|---|---|
| $u_h$ | 3.5 m/s | 10 m/s | 1.5 m/s | 3.5 m/s |
| $u_c$ | 3.5 m/s | 1.65 m/s | 10 m/s | 3.5 m/s |
| $D_{int/ch}$ | 12 mm | 34 mm | 12 mm | 2 mm |
| $D_{ext}$ | 15.9 mm | 38 mm | 15.9 mm | \ |
| $t_{fin}$ | \ | 0.8 mm | | \ |
| $h_{fin}$ | \ | 20 mm | | \ |
| $N_{fin}$ | \ | 295 | | \ |
| $k_{fin}$ | \ | 50 W/mK | | \ |

| | | | |
|---|---|---|---|
| $\boldsymbol{a}$ | \ | \ | Low angle (5°–25°) |
| $\boldsymbol{R_p}$ | \ | \ | 2 |

The dimensional parameters of the tubes and fins and the operational ones, such as the velocity of the fluids involved, were obtained from relevant scientific literature [101] [112] [113] [114].

For what concerns the economic analysis, the purchase equipment cost is only influenced by the size of the components themselves, in terms of power, area, or other parameters according to the type of component and the relative size parameter, as specified in the functions used.

However, a more detailed bottom-up investment analysis needs a series of further assumptions (more linked to constructions, permits, balance of plant, etc.), and those can heavily influence the final results. For this reason, the assumptions made are listed in Table 13, together with the references used either to select the same value or to assume a reasonable one. Among all, it is worth to highlight the assumption of the same *specific opex* value for all the technologies investigated; even though it is foreseen a lower value of OPEX for sCO2 applications, at this stage it was selected the same value for all, and further analyses will be needed on this topic.

*Table 13 - Economic assumptions*

| **Name** | **Symbol** | **Value** | **UoM** | **Ref.** |
|---|---|---|---|---|
| Plant Lifetime | N | 20 | Years | [26] [115] [116] |
| Utilization Factor | UF | 50 | % | [26] [115] [116] |
| Real Discount Rate | R | 5 | % | [26] [115] |

| | | | | |
|---|---|---|---|---|
| Electricity Price | $\lambda_e$ | 0.06 | €/kWh | [26] [115] |
| Plant degradation rate | Dr | 1 | % | [115] |
| Specific opex | $opex_{sp}$ | 30 | €/kWe | [115] [116] |
| Escalation rate | E | 3 | % | [115] [116] |
| Installation Cost factor | $c_{inst}$ | 30 | % | [115] |

### 3.2.2 Results

The results of the techno-economic analysis are divided into three parts:

- a first part for thermodynamic optimization aiming at the maximization of the net electrical power produced, since the plants were designed for WHR application, with constant hot exhausts source (different exhausts temperatures have been considered as discrete parameter);
- a second part in which techno-economic features are evaluated;
- a third part in which economic optimization was performed aiming at minimizing specific capital cost (€/kW) of the plants.

Indeed, the solutions achieved through thermodynamic optimization generally have disproportionate capital costs, which make them impracticable, while minimization of the specific cost can find trade-off solutions between costs and performance, highlighting the most realistic options for sCO2 early implementations.

#### *3.2.2.1 Thermodynamic optimization*

The cycles analysed were optimized by maximizing the net electrical power for the two different cases of plant size as a function of the hot source initial

temperature, which varies between 300 and 700 °C, as already explained. In all cases, however, the hot source mass flow is kept constant for the respective plant size ranges. Since this is a performance optimization, for this section the main parameters of interest are the electrical power, the thermodynamic efficiency, and the heat recovery efficiency.

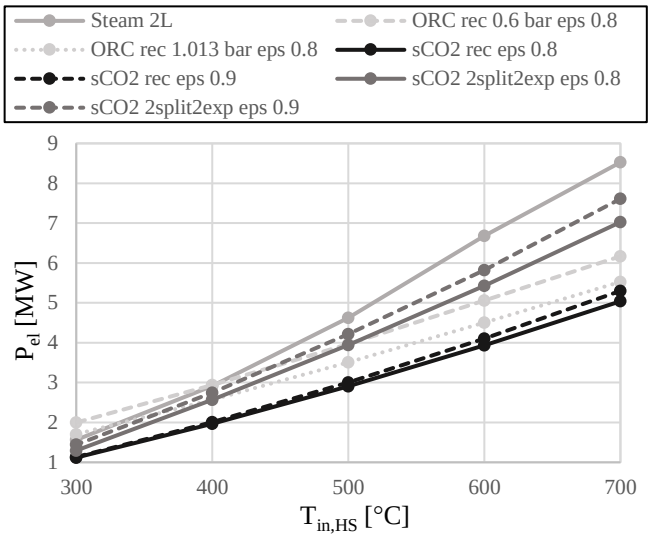


*Figure 61 - Electric power vs waste heat source temperature for small size plants*

The heat recovery efficiency is defined as the ratio between the heat actually extracted and that potentially available, calculated by taking the source from the initial temperature to the ambient one, considered equal to 25 °C.

$$\eta_{cycle} = \frac{P_{el}}{Q_{in}} \qquad (15)$$

$$\eta_{rec} = \frac{Q_{in}}{Q_{pot}} \qquad (16)$$

Figure 61 shows the trend of the electrical power for each cycle studied as a function of the hot source initial temperature for small size plants.

- For $T_{in,HS} \geq 500$ °C the steam cycle has clearly better performance than all the other cycles, as it combines good heat recovery from the source and good thermodynamic efficiency.

- For $T_{in,HS} \leq 400$ °C the regenerated ORC prevails, in particular the one with the pump inlet pressure equal to 0.6 bar, since both the thermodynamic efficiency and the heat recovery are not affected much by the temperature variation, as illustrated in the graphs of Figure 62.

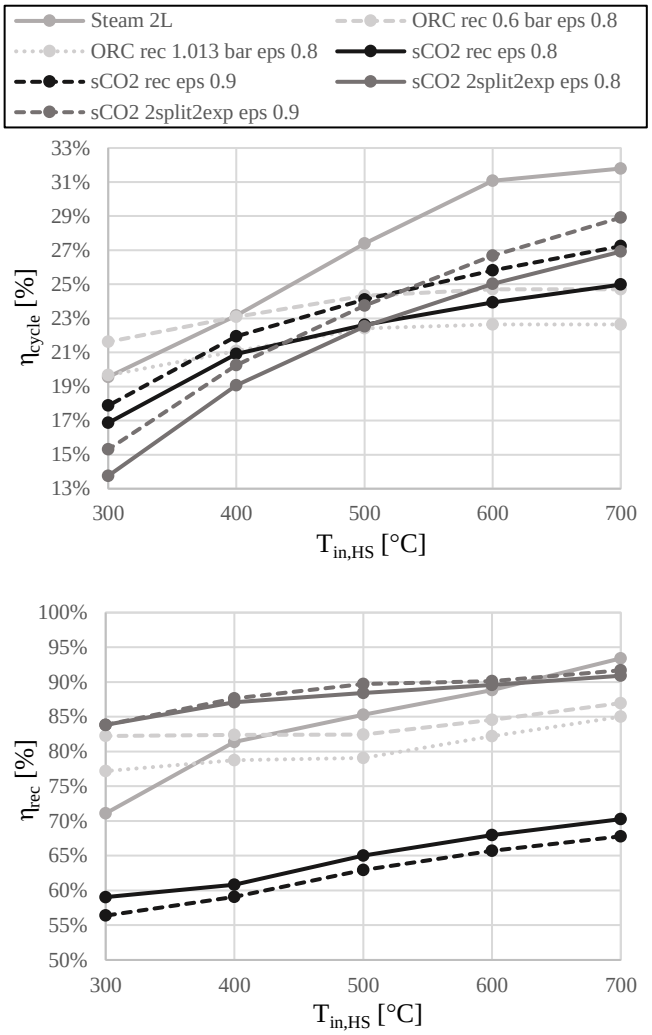


*Figure 62 - Cycle efficiency (above) and heat recovery efficiency (below) vs hot source temperature for small size plants*

The sCO2 dual split dual expansion cycle is not competitive, especially at high temperatures, because, although it always allows excellent heat recovery from thermal waste, with the efficiency of the turbomachinery adopted for small sizes, it has a low cycle efficiency compared to the steam cycle. As regards the sCO2 regenerated cycle, it is unable to recover heat from the source optimally and

shows much lower heat recovery efficiency than the other configurations, which does not compensate with the cycle efficiency as it has values comparable to those of the other technologies. The increase in the effectiveness of the recuperator, where appears, allows a slight performance improvement.

In the case of medium-size plants, the results for sCO2 cycles become more interesting, as shown in Figure 63.

- At 300°C ORCs are still advantageous, in particular for pump inlet pressure equal to 0.6 bar.
- At 400 and 500°C, the sCO2 dual split dual expansion cycle offers better performance than the other cycles, slightly compared to steam.
- For temperatures of 600 and 700 °C, the steam cycle with two pressure levels prevails.

For medium-size plants, therefore for higher turbomachinery efficiencies, the dual split dual expansion supercritical $CO_2$ cycle is always competitive in terms of power produced with the steam cycle; in this case, in addition to having excellent heat recovery efficiencies such as for smaller sizes, it also shows excellent thermodynamic efficiency.

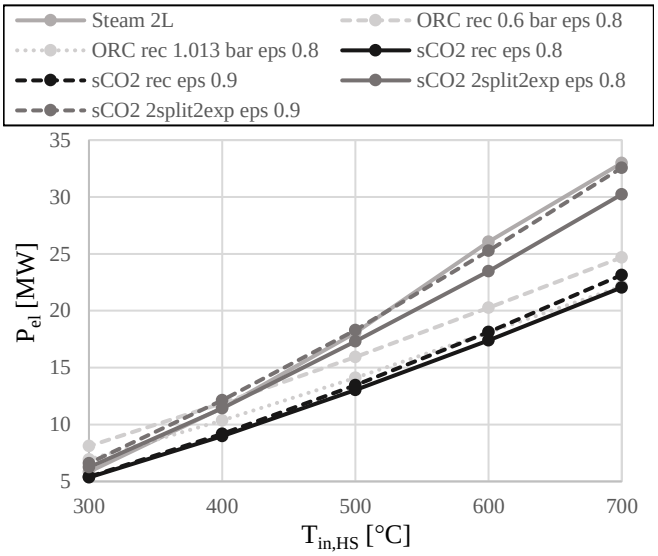


*Figure 63 - Electric power vs waste heat source temperature for medium size plants*

Figure 64 shows how for high temperatures (> 500 °C) the more complex cycles offer better efficiencies and also in terms of thermodynamic efficiency the sCO2 dual split dual expansion cycle is always competitive with the steam one, especially for temperatures higher than 600 °C, where it achieves a higher value because no upper limit has been set on the $CO_2$ temperature (while limiting the steam temperature to 600°C, as previously explained). On the contrary, for temperatures below 400 °C, the simplest cycles, ORC and regenerated $CO_2$, show the best efficiencies, in fact for such a temperature range the plant complexity is not justified and the exergy losses, for instance, due to the mixing, are larger than the benefits that solutions like “Steam 2L” and "sCO2-2split2exp" cycles bring. However, the sCO2 regenerated cycle clearly remains the solution with the worst performance, together with the ORCs for high temperatures (> 500 °C), since this configuration does not fit well into heat recovery, as suggested by the low values of heat recovery efficiency reached.

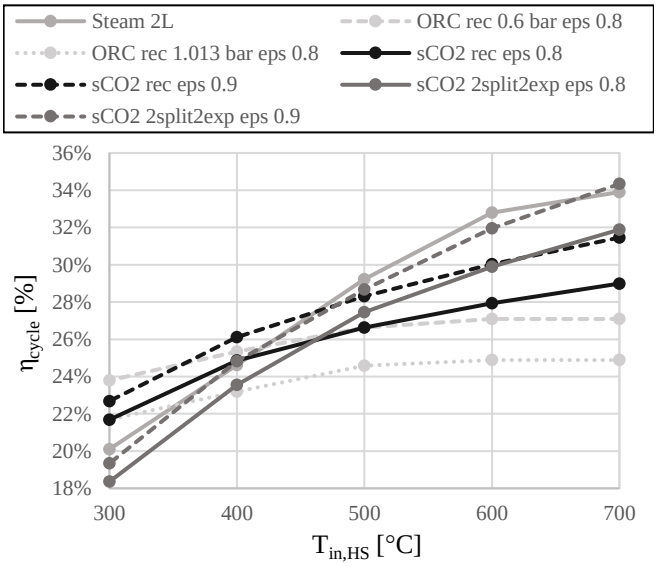

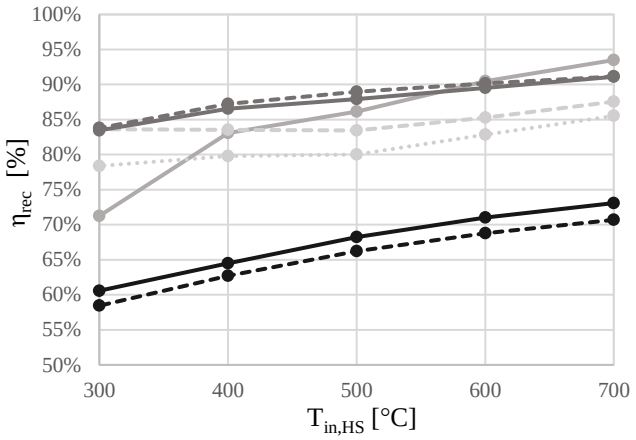


*Figure 64 - Cycle efficiency (above) and heat recovery efficiency (below) vs hot source temperature for medium size plants*

#### *3.2.2.2 Economic analysis of the optimum thermodynamic solutions*

Once the thermodynamic results were defined, the overall cost of plant components of each cycle in each condition studied was calculated using the economic model and the geometric assumptions. It should be reminded that this is a partial economic analysis based on cost functions for plant equipment, without including other capital costs such as civil works, piping, instrumentation and controls, engineering and licensing, working capital, etc. This brings to an underestimation of the absolute overall capital cost (such additional capital items can be typically estimated through percentages of the equipment cost). However, this allows a reliable comparison among the different cycle technologies presented, even if a detailed bottom-up investment and cost analysis is not yet considered.

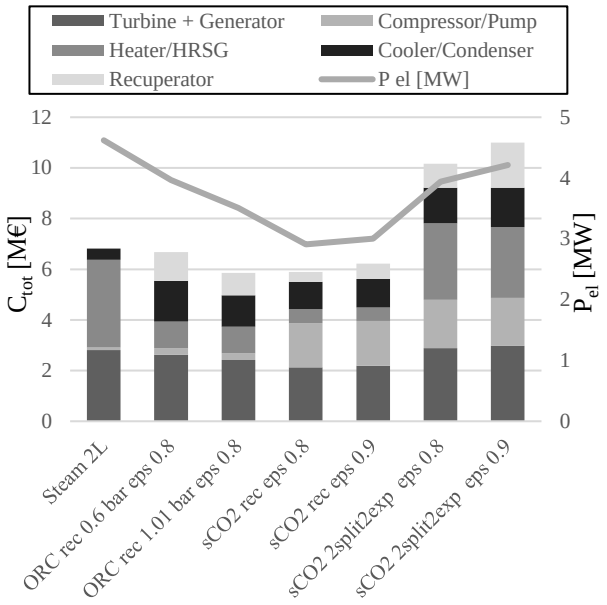


*Figure 65 - Components costs and electric power for hot source temperature of 500 °C and small size plants*

Figure 65 shows the plant costs in the case of hot source initial temperature equal to 500 °C (this case is also representative of the other temperature cases analysed); from the chart some general considerations are deduced, which are also found for larger plant sizes.

- The cost of the pump is negligible in the steam cycle and the ORCs, since the power required by this component is minimal, while the cost of the compressor in the sCO2 cycles is comparable with that of the turbine.
- The cost of the cooler/condenser is comparable for all cycles except for the steam cycle, for which the cost is lower because there is a phase change and compared to ORCs there is no need to cool the fluid in the gaseous phase down to conditions of dry saturated vapor since at the end of the expansion it is already in a biphasic condition.
- Between the two ORCs, there is a difference proportional to the electrical power produced, the lower the pressure at the condenser, the better the performance and the greater the sizes of the components and consequently their price.

- The increase in the effectiveness of the recuperator from 0.8 to 0.9 in sCO2 cycles causes an increase in the cost of the component itself, as its performance improves.

Now considering the case of medium-size plants, whose economic model differs from the previous one only for the $CO_2$ turbine model: an axial rather than a radial turbine has been adopted. This variation allows the costs distribution of supercritical $CO_2$ cycles to differ from the previous case: compared to Figure 65, in fact in Figure 66 there is a lower relevance of the cost of turbomachinery than that of heat exchangers and the cost of the turbine for $CO_2$ is very low compared to that of steam or organic fluid power plants.

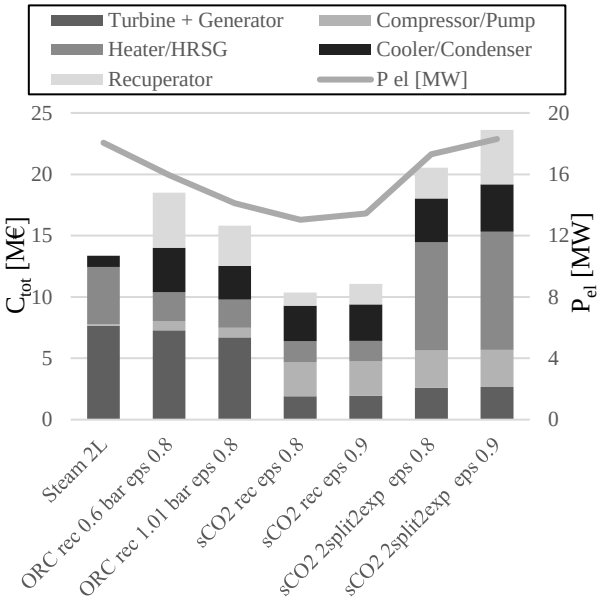


*Figure 66 - Components costs and electric power for hot source temperature of 500 °C and medium-size plants*

Overall, the sCO2 regenerated cycle is the least expensive solution, but also the one that offers the worst performance, while the "sCO2-2split2exp" cycle represents the most expensive solution despite not having the best performance since the price of heat exchangers is very high and assumes approximately 70-80% of the total cost of the system.

A particularly interesting parameter of evaluation and comparison is the value of the specific capital cost, as it provides a more general indication of the competitiveness of each plant from an economic point of view.

As shown in Figure 67, both in the case of small size and medium-size plants, for all system configurations the specific capital cost decreases as the electrical power produced increases; for economies of scale, the more it is produced, the less the unit of power produced costs. Furthermore, it must be considered that the increase in electrical power corresponds to the increase in the hot source initial temperature, and for low temperatures the cycle efficiencies are lower, with a consequent increase in the specific capital cost.

In particular for the sCO2 regenerated cycle and ORC, as the source temperature decreases, the optimized value of $\Delta T_{appr}$ decreases, which determines an increase in the *UA* factor and, for the same *U*, involves greater exchange surfaces and consequently also higher costs; this partly justifies the greater slope of the trend of the specific capital cost at low electric power for these cycles.

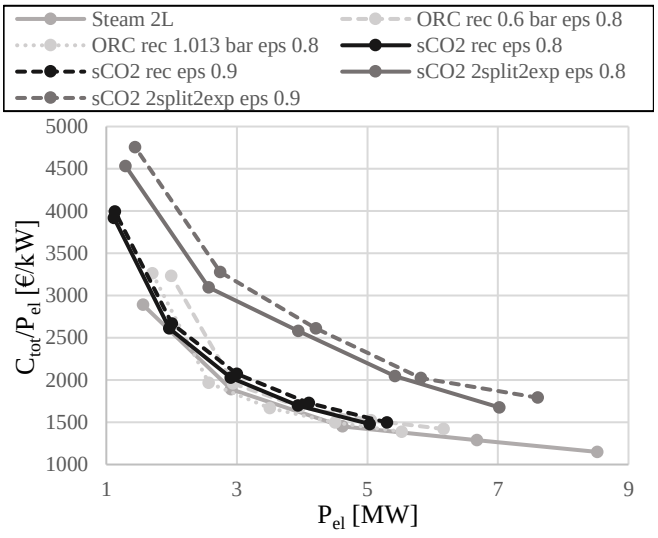

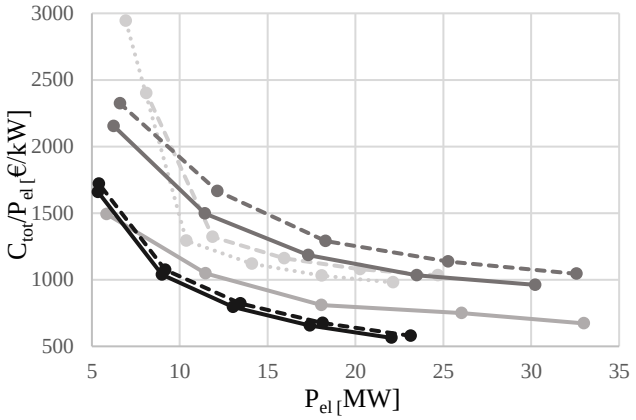


*Figure 67 - Specific capital cost vs electric power for small size (above) and medium-size (below) plants (dots represents solutions at 300°C, 400°C, 500°C, 600°C, and 700°C)*

Compared to the analysis on small size plants, in which the specific capital cost is comparable for all cycles except for the "sCO2-2split2exp" one, in the case of medium size there is a distinction of the value of this parameter for all types of power plants. In fact, the sCO2 regenerated cycle presents the best results for specific cost, while the dual split dual expansion shows the worst. As regards the steam cycle, it is competitive both in terms of electrical power and costs; ORCs, on the other hand, have high costs with no benefits in performance that justify them, if not for low temperatures ($T_{in,HS}$ = 300–400 °C).

Following the evaluation of the specific cost of the equipment, a more comprehensive analysis has been made, considering both an increase of the capital expenditure to take into account the installation costs, and the presence of operational expenditures.

For all the cycles the same assumptions are made, as listed in Tab. 7, deeming different values to be not correctly stateable at this stage, and possibly resulting in unfair comparisons.

In Figure 68, the results of LCOE and IRR for the medium size plants are presented.

Given the methodology adopted, the main driver of the analysis remains the capital equipment cost, thus Figure 68 presents a behaviour analogous to Figure 67. The simple recuperated sCO2 cycle is confirmed to be the most convenient solution, despite the lower electrical power.

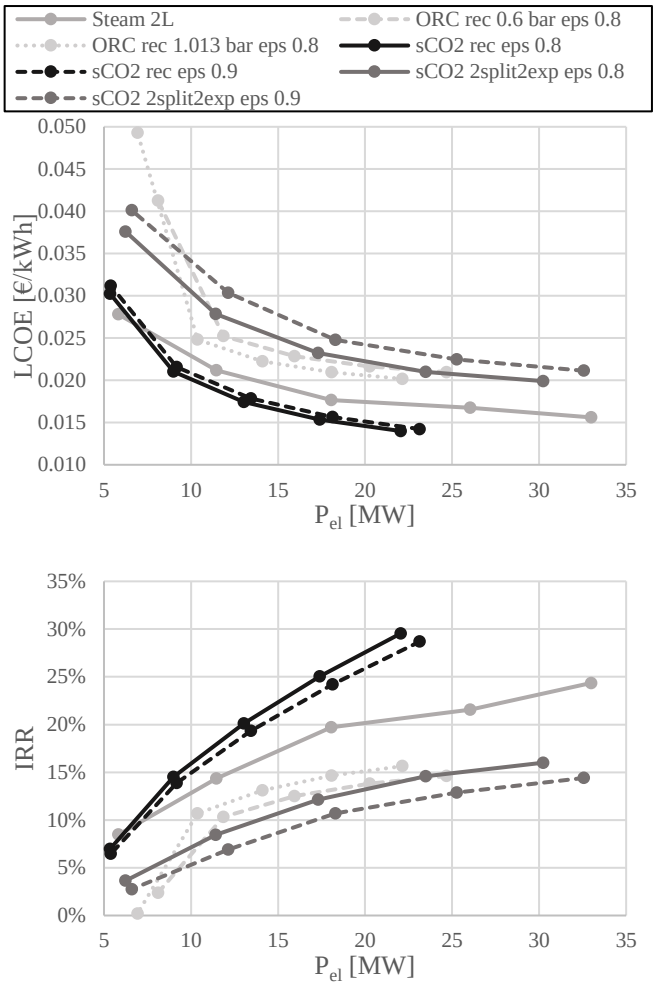


*Figure 68 - LCOE (above) and IRR (below) vs electric power for medium-size plants (dots represents solutions at 300°C, 400°C, 500°C, 600°C, and 700°C)*

### *3.2.2.3 Economic optimization*

The analysis with economic optimization concerned only the case of medium-size plants, as it presents the most interesting results for $CO_2$, and consisted of a sensitivity analysis with optimization of the specific capital cost as $\Delta T_{appr}$

varies; this was carried out for different temperatures of the thermal waste between 300 and 700 °C. For the simulations, the assumptions and decision variables already presented for thermodynamic optimization were maintained. The range of interest in which the $\Delta T_{appr}$ was varied depends on the system configuration and the initial temperature of the hot source, and was obtained in such a way that it was possible to determine an absolute minimum of the specific capital cost.

In general, by increasing the temperature difference at the approach in the heater or the HRSG, the *UA* factor decreases and, with the same *U* (i.e. the same fluid and the same geometric conditions) the exchange surface too, with a consequent drop in the price of the component itself. At the same time, however, the turbine inlet temperature decreases and causes a worsening of the cycle efficiency and therefore of the performance. Generally, the optimal value of $\Delta T_{appr}$ increases with the hot source temperature since, as it increases, it is possible to detach more from it without losing too much in performance and favouring a reduction in costs.

Following the sensitivity analysis, for each temperature of the waste heat source and for each power plant configuration, the optimized solution with the absolute minimum value of the specific capital cost was selected, in order to construct a graph of the same type as that of Figure 67, obtained through thermodynamic optimization, and to make the results of the different cycles more simply comparable.

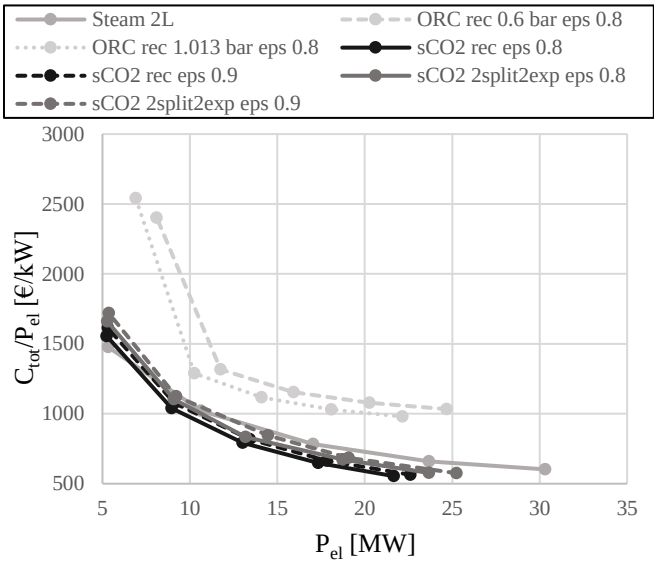


*Figure 69 - Specific capital cost vs electric power for medium size plants, economic optimization (dots represents solutions at 300°C, 400°C, 500°C, 600°C, and 700°C)*

The first result that can be observed from Figure 69 is the competitiveness in terms of the specific capital cost of all the cycles except for the ORCs, which have higher costs. Analysing in detail, as the power increases, supercritical $CO_2$ cycles are slightly more advantageous than the steam one, this has already been found in the thermodynamic optimization for the sCO2 regenerated cycle, but in this case it is also valid for the dual split dual expansion cycle. In fact, the "sCO2-2split2exp" cycle has the greatest capacity for variation in the value of the specific capital cost compared to the thermodynamic optimum: for recuperator effectiveness equal to 0.8 the specific capital cost curve shifts downwards by about 400 €/kW, while for $\varepsilon_{rec} = 0.9$ by about 500 €/kW. Therefore, through economic optimization, the dual split dual expansion cycle tends to simplify and reach the values of the recuperated one.

Furthermore, comparing Figure 69 with the analogous Figure 67, there is no evident variation of results for the ORCs and the sCO2 regenerated cycle, so the thermodynamic optimum corresponds approximately to the economic optimum. For the steam cycle and the dual split dual expansion cycle, on the other hand,

there is a more or less marked reduction both in terms of electric power and the specific capital cost.

If we exclude the ORCs, which in this case do not have a competitive specific capital cost, the choice of the best cycle configuration to be adopted at different temperatures depends on the investors' interest. In fact for $T_{in,HS}$ > 400 °C ($P_{el}$ > 9 MW), if the aim is to have a compact plant and limit capital costs, the best solution is represented by the simplicity of the supercritical $CO_2$ regenerated cycle, while if it is to produce more electric power, (keeping relatively low costs) then it is represented by the steam cycle with two pressure levels; the "sCO2-2split2exp" cycle fits in between the two solutions. Instead, for $T_{in,HS}$ = 300 °C ($P_{el} \approx 5$ MW) the steam cycle turns out to be optimal compared to the sCO2 ones both from a thermodynamic and economic point of view.

For what concerns the investment analysis shown in Figure 70, it can be seen that the economic optimization benefits both the more complex sCO2 cycle and the steam one, compared to Figure 68. Both the solutions with supercritical carbon dioxide seem more profitable than the competitors, even though the difference with steam performances are diminished in both the LCOE and IRR; compared to Figure 68. This behaviour suggests that more complex sCO2 layouts have a wide range of possible optimal solutions depending on the applications and the investor priorities. Moreover, this also suggests that a more detailed analysis and optimization of the investment can lead to results not achievable with simple thermodynamic analysis, and that further work is needed on this topic.

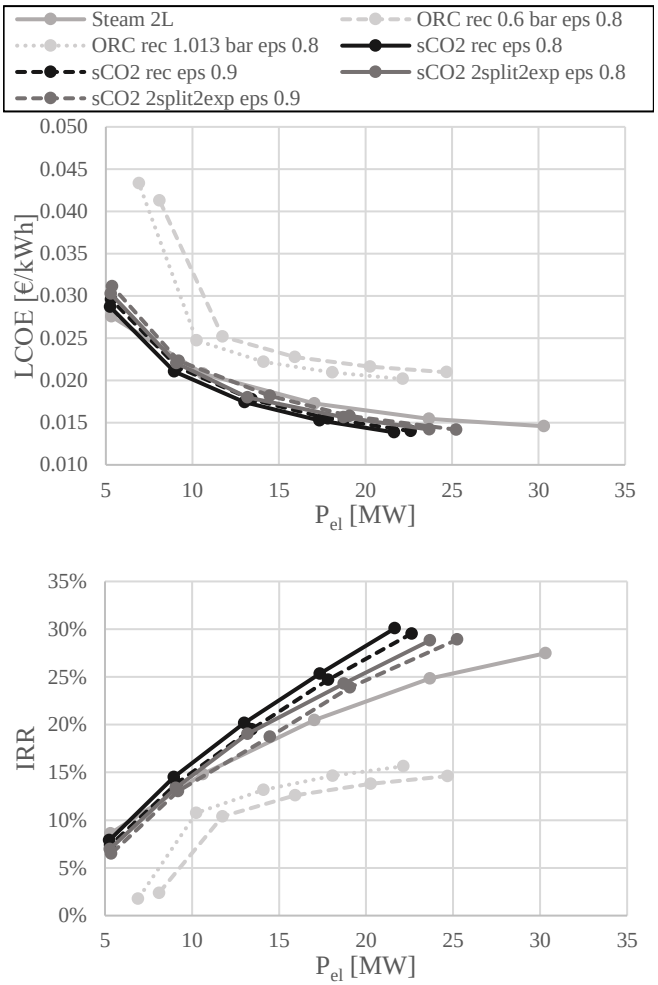


*Figure 70 - LCOE (above) and IRR (below) vs electric power for medium-size plants, economic optimization (dots represents solutions at 300°C, 400°C, 500°C, 600°C, and 700°C)*

## 3.3 A PTES layout for industrial WHR integration

Here an analysis made with the TEMP-EVO tool is presented to perform an evaluation of a thermomechanical battery system denominated Pumped Thermal Energy Storage (PTES). This consists of a system composed of an heat pump (or charging cycle, CC) and a power cycle (or discharging cycle, DC), coupled through the use of Thermal Energy Storages (TES), and it is used to store electricity in form of heat.

The system analysed have sCO2 as working fluid, and it is studied to be integrated to an available waste heat source at low temperature (in this case it is considered coming from the effluents of a cement production plant). For this reason, it is called a Thermally-Integrated-PTES (TI-PTES), and this integration allows the system both to achieve theoretically also values of the round trip efficiency higher than 100%, taking advantage of this free non-electric energy source, as well as to valorise industrial waste heat, making the industries more grid-flexible, and capable of storing electrical energy possibly produced mainly through non-dispatchable energy sources, such as most of the renewable energy sources.

The TEMP-EVO tool was used to simulate some different configurations, and some of the results are reported in the followings.

At first, the main performance indicators used in the analysis are presented, followed by the analysed layouts that compose the PTES battery. Then, the main influence of the pressure and temperature levels is showed, followed by the results of a preliminary cost analysis.

### 3.3.1 Key parameters definition

Since the system here presented is indeed a battery, used to store electrical energy, the PTES main performance indicator is considered to be the electrical round-trip efficiency (RTE); this means, accounting only for the electrical energy flows E or power P, both during discharge cycle DC and charge cycle CC, and $\Delta t$ is the charging and discharging time.

$$RTE_{el} = \frac{E_{DC}}{E_{CC}} = \frac{P_{DC} \cdot \Delta t_{DC}}{P_{CC} \cdot \Delta t_{CC}} = \eta \cdot \dot{Q}_{HT_{DC}} \cdot \frac{COP}{\dot{Q}_{HT_{CC}}} \cdot \frac{\Delta t_{DC}}{\Delta t_{CC}} = \eta \cdot COP \qquad (104)$$

$$if: \qquad Q_{stored} = \dot{Q}_{HT_{DC}} \cdot \Delta t_{DC} = \dot{Q}_{HT_{CC}} \cdot \Delta t_{CC} \qquad (105)$$

$$\eta = {P_{DC}}/{\dot{Q}_{HT_{DC}}} \quad (106)$$

$$COP = {\dot{Q}_{HT_{CC}}}/{P_{CC}} \quad (107)$$

If the two cycles are designed with the same storage capacity and same operating time and, consequently, the same mass flow rate of the thermal energy storage (TES) fluid, the electrical round trip efficiency (RTE) can be determined based on the total electrical power consumed and produced by the two cycles, rather than relying on total electrical energy values. Otherwise, by only imposing the same storage capacity and neglecting the losses in the storage system, it is possible to express the electrical RTE as the product between the performance of the two separate cycles, as indicated in the previous equations.

Despite the RTE value represents the performance of the system on the point of view of it being an electrical battery, this value cannot represent the inherent thermodynamic efficiency of a power-to-heat-to-power system if a freely available heat input (like solar or waste heat) is included in the cycle, boosting the RTE itself.

In such a case, exergy can be considered as a consolidated framework for properly accounting for additional energy inputs.

So, when an external additional thermal source or fuel mass flow is provided, it should be properly accounted for in the denominator of RTE through its exergy content. Therefore, the exergy-based RTE formulation, applicable also to hybrid storage systems such as the one considered in this analysis, is:

$$RTE_{ex} = |Ex_{W_{out}}| \,/\, (Ex_{W_{in}} + Ex_{Q_{in}}) \quad (108)$$

Notably, only thermal inputs are considered in the above equation, excluding the possibility of useful thermal outputs, which should be placed in the numerator.

$RTE_{ex}$ can be therefore used for PTES assessment with supplementary thermal input (i.e., accounting for electrical and thermal exergy flows). Considering the

actual power flows ($P$) and the actual waste heat flows ($Q$) at their entropy-average temperature $T_{avg}$ (indeed, an explicit logarithm temperature expression could be derived by the analytical integration of $Ex_{Q_{in}}$ when specific heat can be considered constant), the following expressions are used in the following analysis:

$$RTE_{ex} = \frac{P_{DC}}{P_{CC} + Q_{WH} \cdot \left(1 - \frac{T_0}{T_{avg}}\right)} \tag{109}$$

$$T_{avg} = \frac{\int_{in}^{out} Tds}{s_{out} - s_{in}} \cong \frac{h_{out} - h_{in}}{s_{out} - s_{in}}; \quad if\ p \cong const. \tag{110}$$

To calculate the exergy round-trip efficiency ($RTE_{ex}$), the actual waste heat (WH) input to the cycle must be considered. As the heat exchange does not occur at a constant temperature, the corresponding entropy-averaged temperature is computed.

### 3.3.2 Proposed Plant Layouts

In the following, the layouts of the cycles composing the PTES are presented.

Figure 71 illustrates the charging (heat pump) cycle which depicts the utilization of heat from the waste heat (WH) source of the cement plant through a heat pump to raise its temperature. The heat is subsequently stored in a commercial molten salt thermal energy storage (TES) system, specifically using HITEC molten salt [117]. The arrows on the heat exchangers indicate the direction of heat transfer. Heat is extracted from the heat exchanger (WH HEX) and transferred to the thermal energy storage heat exchanger (TES HEX) where it is stored in the TES.

During TES charging, the high-temperature effluents from the cement processes are released into the ambient surroundings at significantly lower temperatures, namely in the 150–80 °C range, depending on the operating conditions of the heat pump, thus contributing to process energy efficiency.

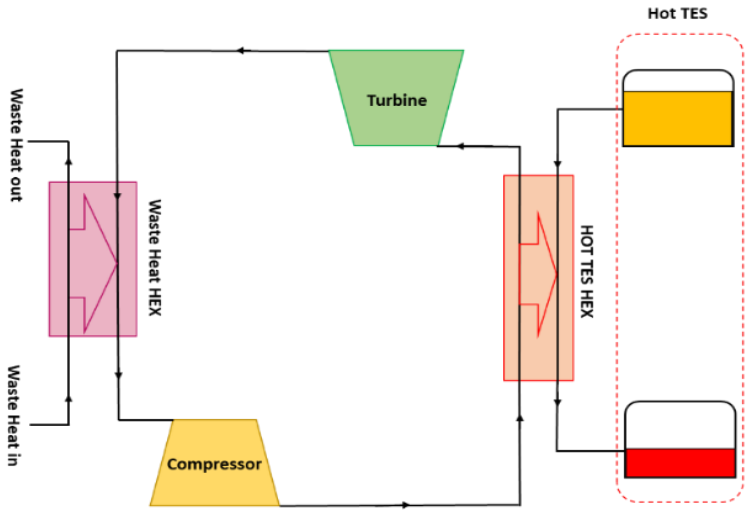


*Figure 71 - Charging cycle configuration*

The charging cycle is followed by a discharging cycle. Figure 72 presents two different configurations of the discharging cycle that will be examined to identify the most suitable configurations for this case study. In the first configuration, a simple sCO2 discharging cycle is depicted where the heat stored in the thermal energy storage (TES) is utilized. The sCO2 working fluid is compressed and heated up by the TES heat exchanger (TES HEX). It then enters the sCO2 turbine where it expands and releases the remaining heat in the cooling HEX, closing the cycle. Notably, the cooling HEX in the discharging process operates at a significantly lower temperature than the waste heat (WH) temperature. Such a feature significantly reduces the work required by the compressor, even when employing the same pressure ratios.

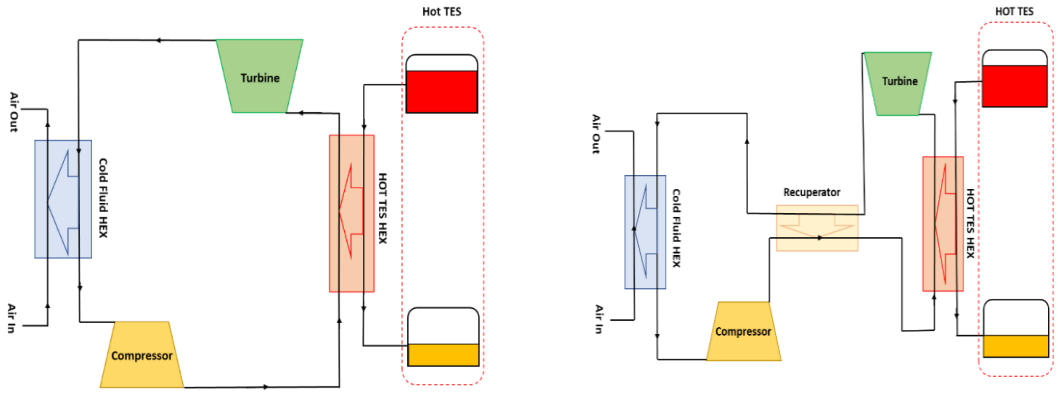

**(a)** **(b)**

*Figure 72 - Discharging cycle configurations: (a) simple discharge cycle and (b) recuperated discharging cycle.*

Targeting discharging cycle efficiency maximization, a recuperated $sCO_2$ cycle was also considered and analyzed. Thanks to the recuperator, the heat is utilized immediately after the compressor, resulting in improved efficiency of the discharging cycle. The configurations of the discharging cycle were thoroughly examined to identify the optimal performance in terms of the electrical round trip efficiency (RTE).

### 3.3.3 Assumptions

Since the proposed PTES systems consist of two distinct and independent cycles, one for charging and one for discharging (not considering reversible machines), the simulation approach proposed by TEMP-EVO distinctly separates the computation of the two cycles, which are inter-related by imposing the equivalence of the TES temperatures and the amount of energy and mass stored in it.

In practice, the code initially computes the discharging cycle and utilizes the results to initialize the computation of the charging cycle. Specifically, since the discharge layout may involve a recuperated cycle, the minimum temperature of the TES depends on the inlet temperature of the hot heat exchanger (HEX) in the discharging cycle, which, in turn, relies on the effectiveness of the recuperator.

For this specific study, the modeling approach involved separate calculations of the charging and discharging cycles. This was performed to conduct sensitivity analyses on specific parameters identified as highly relevant for each cycle layout, like minimum and maximum pressures and the TES material temperature (highest temperature of the cycle).

Considering the available waste heat (WH) temperature at 330°C [118], different commercial TES materials were studied in the range between 400 °C and 600 °C as the maximum temperature. Table 2 reports the main assumptions for the charging and discharging cycles, while Table 3 presents the properties of the TES materials investigated [118].

*Table 14 - Thermodynamic assumptions*

| **Assumptions** | **Value** | **UoM** |
|---|---|---|
| TES max temperature | Between 400 and 600 | °C |
| Recuperator effectiveness | 60; 80 | % |
| Isentropic efficiency turbomachinery | 80 | % |
| Thermal losses of the TES | 1 | % |
| Electrical efficiency | 98 | % |
| Mechanical efficiency | 98 | % |
| Pressure loss in heat exchanger | 2 | % |
| Min ΔT in heat exchanger | 10 | K |
| Compressor inlet temperature | 35 | °C |
| Ambient temperature $T_0$ | 25 | °C |
| Air temperature cooler exit | 45 | °C |
| Waste heat temperature | 330 | °C |
| Waste heat mass flow rate | 38.6 | kg/s |

*Table 15 - TES Material properties* [118].

| TES Material | Max $T_{TES}$ [°C] | Density [kg/m³] | Specific Heat [kJ/kgK] | Th. Conductivity [W/mK] | Heat Transfer Fluid | Min Temp. [°C] | Cost |
|---|---|---|---|---|---|---|---|
| Syltherm | 400 | 548 | 2.26 | 0.064 | Oil | −40 | 4 $/kg |
| Yara Salt | 450 | 1913 | 1.43 | 0.52 | Salt | 220 | 1.5 $/kg |
| HitecXL | 500 | 1877 | 1.43 | 0.52 | Salt | 220 | 1.6 $/kg |
| Solar salt | 550 | 1740 | 1.54 | 0.5 | Salt | 250 | 1.3 $/kg |
| Concrete\air | 600 | 1008 | 1.10 | 1.9 | Air | 25 | 0.04 $/kg |

The temperature and pressure levels for the discharging phase were carefully selected to optimize cycle performance. Subsequently, a corresponding charging cycle was thoroughly examined and chosen. This was made possible by considering the complete decoupling of the charging and discharging cycles, in contrast to a standalone PTES system, owing to the integration with high-temperature waste heat (WH).

In the subsequent paragraphs, performance sensitivity analyses of both the charging and discharging cycles are presented. The aim is to ensure the compatibility and alignment between the two cycles, starting from the discharging phase.

### 3.3.4 Analysis of the Impact of Different Operating Parameters on WH-Driven PTES Cycle Performance

#### *3.3.4.1 Operating Pressure of Charging and Discharging Cycles*

The PTES system has been studied starting from an analysis of the discharging cycle with a maximum pressure limit of 250 bar and a TES with a temperature of 450 °C (HITEC XL as the TES media). This value was determined considering technological factors to ensure manageable compression ratios and the use of pressurized HEXs among other considerations. Additionally, in accordance with the assumptions made, a maximum $CO_2$ temperature of 440 °C and a typical compressor inlet temperature of 35 °C were selected to ensure stable compressor operation.

The objective of the analysis was to identify the conditions that would maximize the electrical round trip efficiency (RTE) by aligning the discharging cycle with the charging cycle. Results showed that the recuperated discharging cycle maximizes efficiency with the best results observed in the range of the 80 to 85 bar minimum pressure. While the cycle efficiency increases with higher recuperator effectiveness, this parameter has a minimal impact on the total power extracted from the TES source given a constant total mass.

To capture the behaviour of the recuperated layout, two values of recuperator effectiveness (60% and 80%) were analysed. From these values, an optimal minimum pressure of 83 bar was selected (Figure 73), ensuring a maximum power output while also guaranteeing proper compressor operation.

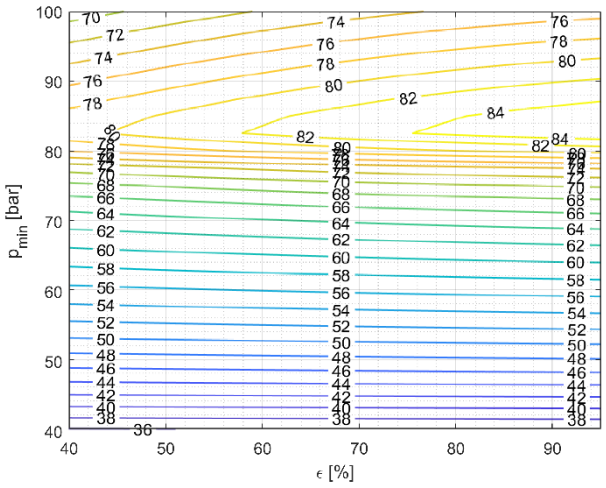


*Figure 73 - Total net power achievable by a recuperated cycle for a 1 kg/s mass flow rate of molten salts; the x-axis is the effectiveness of the recuperator.*

During the charging phase, a common performance parameter to monitor is the compressor outlet temperature and related cycle maximum pressure (compressor outlet). While considering the values of other temperatures, only those equal to or higher than 460 °C were taken into account based on the initial assumptions related to the chosen MS TES storage media. In the following Figure 74 and Figure 75, the minimum temperature line is depicted in red, separating the unacceptable values (above) from the valid values (below). The upper region, unacceptable, represents a zone with a pressure ratio that is too close to 1 or even lower, which is unrealistic.

It is evident that the initial assumptions regarding temperature strongly impact the behaviour of the charging cycle heat pump, necessitating a sensitivity analysis with different temperature values. Furthermore, this behaviour is closely tied to the assumptions made about machinery efficiency, which affects the performance of the heat pump cycle.

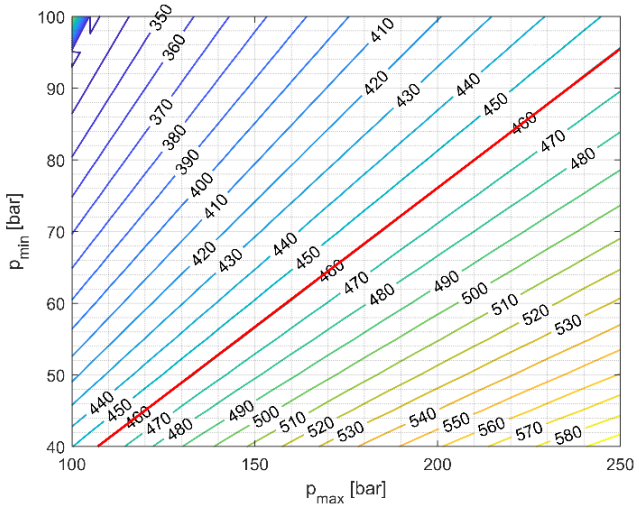


*Figure 74 - sCO2 Maximum temperature in the charging cycle. The minimum allowable value is 460 °C (acceptable area is below the red line).*

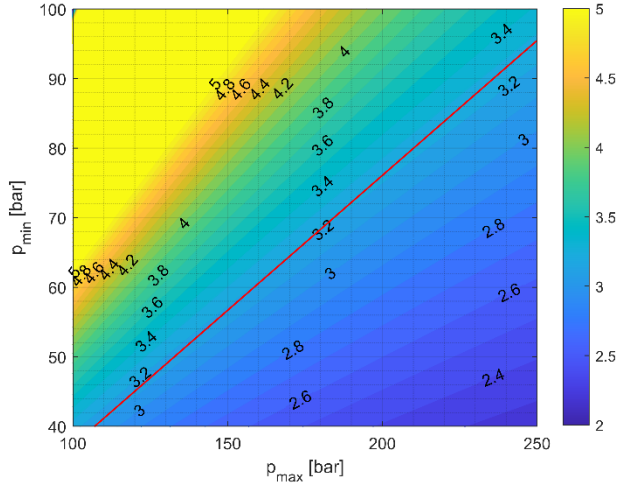


*Figure 75 - COP of the charging cycle with a minimum temperature of the TES equal to 222 °C, as calculated for a recuperated discharging cycle with recuperator effectiveness at 80% (acceptable area is below the red line).*

Figure 76 depicts the trend of HP net power consumption, it is notable that the power values align closely with the temperature values, similar to the behaviour observed for COP. For instance, a temperature value near 460 °C (the lowest acceptable sCO2 temperature) corresponds to a pressure ratio of approximately 2.6, resulting in a COP ranging from 3.7 to 3.9.

This observation is interesting for two reasons. Firstly, from a thermodynamic standpoint, one might expect a higher pressure to be preferred, while a thermo-economic perspective favours lower pressures, particularly for the charging cycle. Secondly, operating at lower pressures can amplify the influence of variations in the thermophysical properties of sCO2, especially its specific heat near the critical point. This could potentially lead to the heat exchangers encountering an internal pinch point at a temperature difference lower than the assumed values at the extremes. Consequently, a more detailed analysis of the heat exchangers would be required, at least 1D, potentially involving the introduction of multiple heat exchanger and TES units that handle different mass flows. Such an approach would allow better matching of the variation in $CO_2$ heat capacity rate and mitigate the impact of the specific heat variation.

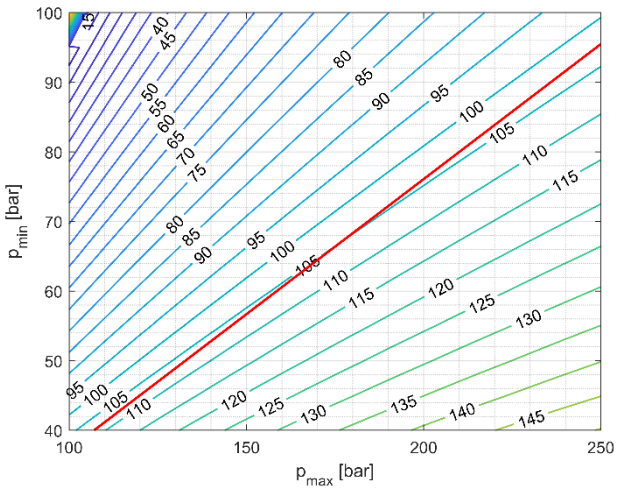


*Figure 76 - Net power absorbed in the charging cycle with a minimum temperature of the TES equal to 222 °C, as calculated for a recuperated discharging cycle with recuperator effectiveness at 80% (acceptable area is below the red line).*

All the previous analyses performed on the discharging and corresponding charging cycles brought the identification of the optimal operating points for the higher RTE P2H2P cycle (Figure 77). These operating points were determined based on the initial assumptions presented in [119] and the goal of maximizing

the apparent electrical RTE, without taking into account the amount of waste heat (WH) that could be utilized.

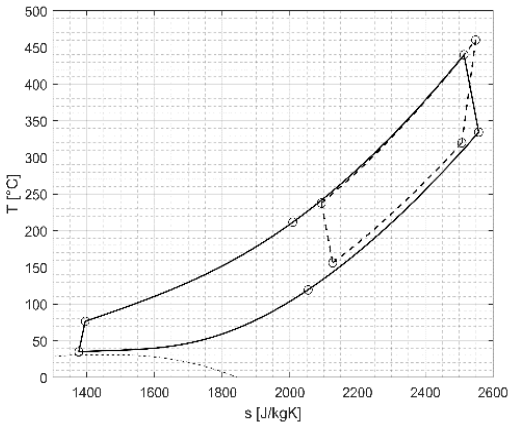


*Figure 77 - T-s diagrams for the proposed most effective P2H2P cycle assuming a recuperated discharging cycle (recuperator effectiveness 80%) and $T_{TES}$ = 450 °C.*

Table 5 displays the optimal operating parameters identified for the cycle presented in Figure 77, including the minimum pressures and TES temperature values. It was found that the optimal maximum pressure for both the charging and discharging phases is 250 bar, which is the highest allowable pressure. Results showed in [119] confirm that integrating waste heat (WH) into a PTES allows for achieving higher electrical RTE values compared to a standalone PTES configuration, as expected. However, it should be noted that this comes at the expense of utilizing the freely available heat source, and therefore, the exergetic RTE provides a more comprehensive estimation of the overall energy utilization in the process. Among the investigated solutions in [119], the highly recuperated configuration demonstrates the highest exergetic RTE although its WH input utilization is relatively low

*Table 16 - Main thermodynamic features for the best operating conditions of a PTES cycle with a recuperated discharging cycle with a TES material maximum temperature of 450 °C and recuperator effectiveness of 80%.*

| CC $p_{min}$ | DC $p_{min}$ | TES $T_{min}$ | CC COP | DC Efficiency | DC Net Power | CC Net Power | RTE electrical | RTE exergetic |
|---|---|---|---|---|---|---|---|---|
| 95.5 bar | 83 bar | 222 °C | 3.24 | 22.9% | 2.18 MW | 2.98 MW | 73.3% | 38.8% |

### *3.3.4.2 Impact of TES Temperature*

In this subchapter the impact of TES temperatures on the proposed PTES cycle performance is analysed.

The high pressure side of both the CC and DC are fixed at suitable values where the commercially available heat exchangers can be exploited; consequently, high pressure sides up to 300 bar were considered. Indeed, this was needed to account for the increasing maximum temperature of the TES; having the temperature of waste heat fixed, the maximum temperature that can be achieved by the charging cycle (CC) indeed relies only on pressure ratio. Therefore, fixing the upper side pressure makes much more sense than fixing the lower side pressure for the CC in order to not obtain too great a value of pressures on the high pressure side for certain thermal storage materials.

In the case of DC, the high pressure side as well as the low pressure side is fixed, which is possible in this case because the recuperator as well as the storage temperature can be set defining the recuperated amount of heat, thus acting on the recuperator effectiveness, rather than on the pressure ratio. The lower temperatures of the TES attained through modelling of the DC then sets the

pressure ratios of the CC. The DC lower pressure at the inlet of the compressor has been kept at 85 bar.

As CC and DC are independent in terms of operation, the high pressure side of the DC (300 bar) has been purposely kept only slightly above the high pressure side (280 bar) of the CC so to utilize the same heat exchanger during charging and discharging and save capital cost. The cold compressor considered in the DC uses much less power than the hot compressor in the CC for similar pressure ratios. As a result of the independence of CC and DC cycles, two benefits can be highlighted: (i) the CC turbine can expand far from the critical point, having higher work values, and (ii) it is possible to decouple the expansion ratio of the discharging turbine from the that of the charging cycle, allowing to select the best operating points for low-pressure side of the discharge cycle, increasing the overall system performance.

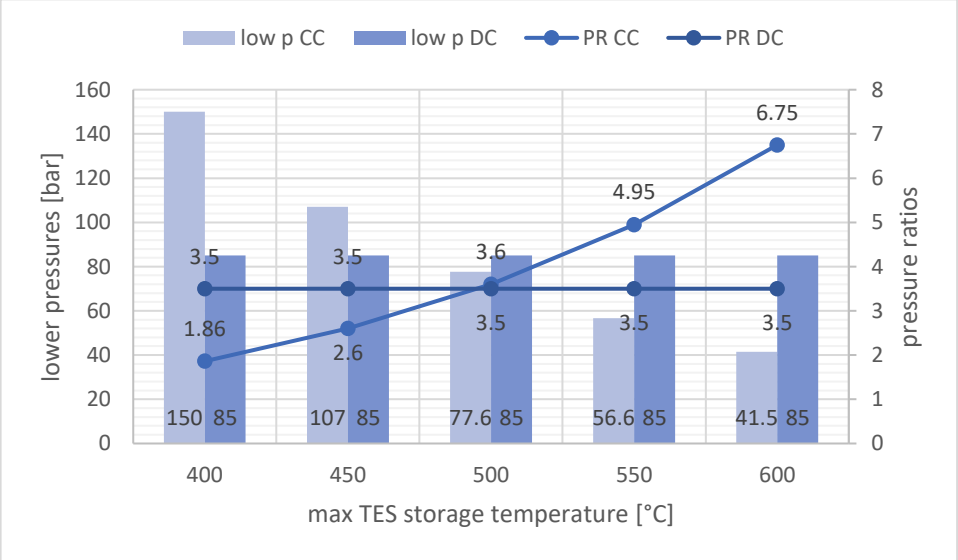


*Figure 78 - Pressure ratio and lower pressure side trends of different PTES systems with different TES materials.*

The pressure ratio of the DC is 3.5 for all the cases of TES. The higher pressure is fixed at 300 bar, assuming design technical extreme constrains, whereas the lower pressure is fixed at 85 bar, which has been known to show the highest performance, as mentioned before. Figure 78 shows the pressure characteristics

for different maximum temperatures reached for the respective TES, showing the lower pressures as well as the pressure ratios.

The lower pressure side of the CC varies from 1.86 to 6.75 for 400 to 600 °C, respectively. The pressure ratios of the CCs for solar salt (550 °C) and concrete (600 °C) are probably too high to be elaborated by a single compressor unit. Therefore, for practical purposes, multiple compressors should be considered to reach these pressure ratios with intercooling to obtain a better isentropic efficiency.

Although this study assumes a single compressor efficiency to evaluate all the cycles, in a multiple compressor scenario the integrated isentropic efficiency of the two compressor units would be less than the single compressor unit. Therefore, the required temperatures of 550 °C and 600 °C may be reached for lower pressure ratios than as mentioned in this study (in case a constant polytropic efficiency, this difference would not be present).

The pressure ratios for charging and discharging are more or less similar for HITEC XL (500 °C): nevertheless, the DC is operates with a maximum pressure of 300 bar whereas CC operates with a maximum pressure of 280 bar. Even though the pressure ratios are almost similar for this case and DC has to reach a higher pressure, the power intake by the CC compressor is 16.1 MW while the DC cycle compressor takes only 4.1 MW (for 10 MW net power in charging and discharging) which is four times less than the CC one. Even considering WH valorisation in the CC, the compressor in the charging cycle has to operate away from the critical point of $CO_2$. Operating into the supercritical gaseous region, the work of the compressor increases due to the diverging isobaric lines, whereas near the critical point, the iso-baric lines are less diverging and as the DC compressor has to operate near the critical point, it takes less power. The compressor power consumption depends, therefore, not only on the pressure ratios but also on the operating pressures and temperatures: the DC compressor operating temperature is significantly lower than CC, which decreases the power consumption significantly for the former. This fact has been exploited in

this study by keeping the higher operating pressure of the DC (300 bar) greater than the CC (280 bar) to obtain a larger expansion ratio at the expense of lower power consumption. This is one advantage of using an independent charging and discharging system. If different HOT HEX are being used for CC and DC, the difference between high-pressure sides may be increased further to achieve even better performances.

Figure 79 shows the overall performance of the thermodynamic properties of the systems which include the COP of CC and the thermal efficiency of DC and RTE (both energetic and exergetic ones). Considering fixed pressure ratios for all analysed TES configurations, the efficiency of the DC largely depends on the turbine inlet conditions. Therefore, due to fixed pressure ratios, as the turbine inlet temperature increases, the efficiency of DC increases too: the trend for the efficiency can be observed as increasing from 23% to 28.80% for 400 °C to 600 °C, respectively. As a result of the recuperator in the DC, the CC has lower net power requirement. The recuperated heat increases the temperature at which $CO_2$ enters the HOT HEX in the DC while in CC such an unused amount of heat can be employed in a low temperature turbine, thus increasing the net power and consequently, COP. The COP also depends upon the temperature glide between WH and TES. Therefore, COP decreases by 2.26 points for TES temperature variations from 400 °C to 600 °C. Looking at DC efficiency increasing values and CC COP decreasing values with TES temperatures, it is relevant to highlight that the decline of the COP, however, is much higher than the increment in the efficiency, thus penalizing RTE while increasing the TES temperature. Therefore, for 400 °C, the value of RTE obtained is above 100% while for the other TES materials, RTEs are below 100%, decreasing further for higher temperatures following COP in a similar trend. The gap between the COP and RTE can be seen to increase in Figure 79 as we move to the higher temperature of TES, which shows that increasing TES temperatures does not compensate for the decrease in the power-to-heat COP, eventually bringing RTE down for the higher temperatures. In order to have higher RTE at high

temperatures, it would be possible to increase COP using a recuperator in the HP cycle too which is a possibility to be investigated in future studies.

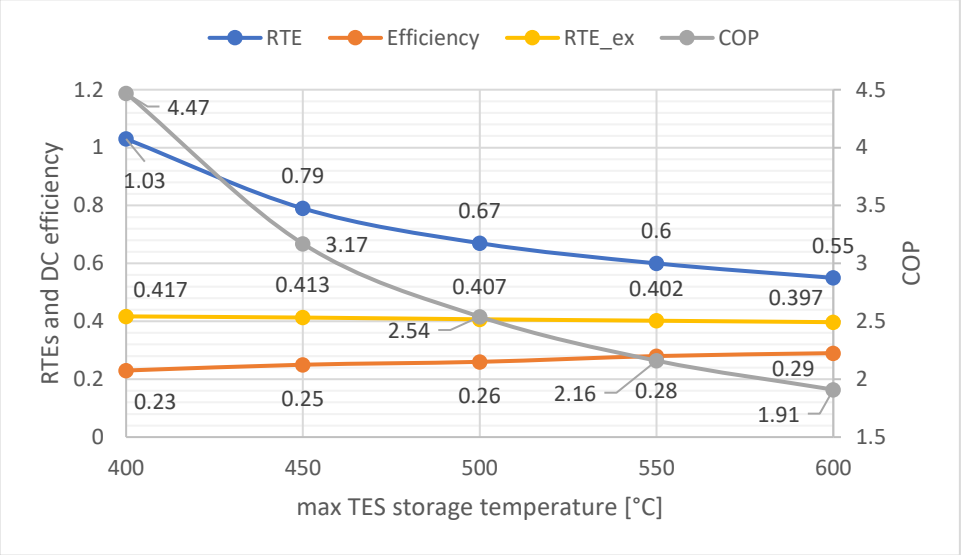


*Figure 79 - Performance of TI-PTES system with different TES materials and temperature levels.*

The exergetic RTE seems to decrease while the TES temperature is increasing. However, such a trend is barely visible compared to the electrical RTE one, even if the reason behind the exergetic RTE decrease is similar to the electrical RTE one. From an exergy point of view, there is not so much difference if a lower TES temperature configuration or a higher TES temperature configuration is promoted as the difference in the values is only about two percent (in Kelvin). From an exergy point of view, it can make sense to utilize higher-temperature TES storage and obtain higher DC efficiencies at the expense of almost similar exergy performance as compared to low-temperature TES.

Table 17 shows the thermal storage characteristics and sizing of all analysed PTES configurations. All the PTES are scaled based on equal amount of power consumption in CC and power production in DC, which is 10 MW in both cases. For the fixed amount of time of charging of 10 h, the amount of storage is determined for each case.

*Table 17 - TES parameters/performance for different TES materials for PTES.*

| TES Material | $T_{TES}$ [°C] | TES Capacity [$MWh_{th}$] | Charging Time [h] | Discharging Time [h] |
|---|---|---|---|---|
| Syltherm | 400 | 447 | 10 | 10.33 |
| Yara Salt | 450 | 317 | 10 | 7.91 |
| HitecXL | 500 | 253 | 10 | 6.71 |
| Solar salt | 550 | 215 | 10 | 5.99 |
| Concrete\air | 600 | 190 | 10 | 5.50 |

For equal power consumption or production for each TES case, the mass flow of $CO_2$ in CC and DC decreases for the increasing temperature of storages, which leads to lower energy storage capacity requirement as we move towards the higher temperature TES. By comparison, the required capacity is minimized by 57% for the concrete storage as compared to the Syltherm which can lead to smaller capital costs. The discharging time will change depending upon the RTE. As the RTE for 400 °C is higher, the DC for this configuration can run for a longer time, such as 10 h and 20 min for 10 h of charging, whereas the time of discharging becomes less and less for the higher temperature TES, with concrete being able to discharge for 5 h and 30 min for a 10 h charge.

## 6. Preliminary Economic Investigations

Starting from values presented in Table 17, Table 18 shows the capital cost of the components needed for the 10 MW scale system; all the values are in Million of USD (M$). The CAPEX of the overall proposed PTES system is calculated as the sum of the different components present in the plant layout, and separate turbomachinery for charging and discharging are considered.

Along with the costs of different PTES systems, the cost of the WH2P system has also been mentioned for comparison. It is clearly visible that despite the absence of the charging turbomachinery in the WH2P, the CAPEX calculated is much higher than all the PTES configurations. The justification is that the comparison is being made for the WH2P and WH+PTES for the same operating conditions of pressure and temperatures using the temperature 330 °C of waste heat to attain a set power output of 10 MW for all the configurations; the lower temperature configurations will require a larger mass flow rates and larger machines.

As the temperature of storages becomes higher, the same amount of power can be reached with a smaller mass flow rate in the machines. The scale of the mass flow rate determines the size of the machinery. For a larger mass flow rate, the size of the machines would be larger, thus bringing higher CAPEX. WH2P operates at the lowest temperature of 330 °C among all the other configurations, thus requiring the highest mass flow rate to guarantee a net power of 10 MW, leading to the highest CAPEX, even achieving values that go beyond the PTES configurations. DC cycle turbomachinery and HEX of all the configurations follow the same trend of cost reduction with higher temperatures as all the configurations are operating on same operating pressures, but with lower mass flow rates, while for CC turbomachinery there is a reverse trend not driven by mass flow rate reasons in this case. Indeed, although the mass flow rate is also decreasing in the CCs for higher temperature configurations, the pressure ratios in CC are different for each configuration, thus leading to higher turbomachinery CAPEX despite a decrease in the mass flow rate. The magnitude of the increase, however, is minimized by the positive counter effect that decreasing mass flow has on the cost of turbomachinery.

*Table 18 – Capital cost estimations for 10 MW power scaling of the proposed WH-driven PTES system with different TES materials.*

| **Components** | **Syltherm (400 °C)** | **YaraSalt (450 °C)** | **HitecXL (500 °C)** | **Solarsalt (550 °C)** | **Concrete\ Air (600 °C)** |
|---|---|---|---|---|---|
| CC_Compressor | 7.51 | 7.56 | 7.61 | 7.66 | 7.71 |
| CC_Turbine | 1.62 | 1.69 | 1.75 | 1.81 | 1.87 |
| WH_HEX(WH-$CO_2$) | 2.64 | 1.86 | 1.43 | 1.16 | 0.97 |
| WH_HEX(WH-TES) | - | - | - | - | - |
| DC_Compressor | 5.13 | 4.83 | 4.60 | 4.40 | 4.24 |
| DC_Turbine | 3.74 | 3.58 | 3.47 | 3.38 | 3.30 |
| DC_Air_HEX | 0.30 | 0.25 | 0.22 | 0.20 | 0.18 |
| DC_Recuperator | 1.11 | 0.88 | 0.74 | 0.63 | 0.56 |
| HOT_HEX | 9.06 | 7.24 | 6.46 | 6.01 | 5.65 |
| Thermal Storage | 13.54 | 6.52 | 6.25 | 4.10 | 10.39 |
| **Total CAPEX (M$)** | **44.65** | **34.43** | **32.54** | **29.35** | **34.88** |

The highest cost for all the components is of the TES heat exchanger. This is evident in Figure 80, which shows the internal features of the heat exchanger for 450 °C TES. The temperature difference between the hot side fluid and cold side fluid remain more or less 10 K for the whole duration of heat transfer, which tends to make the area of the heat exchanger very large. This TES heat exchanger is similar for the charge and discharge cycles, although the pressures

are not similar for charge and discharge with 280 bar for CC and 300 bar for DC. The parameters of pressure and mass flow rate are different whereas the temperature difference between the inlet and the outlet of TES HEX are the same for the CC and the DC. Except for the storage, the highest component cost for the PTES configuration is incurred by the 400 °C temperature configuration and the lowest by the 600 °C configuration which goes to show that although the RTE is lower for high-temperature configurations, the higher temperature configurations can be a better choice when CAPEX is the priority.

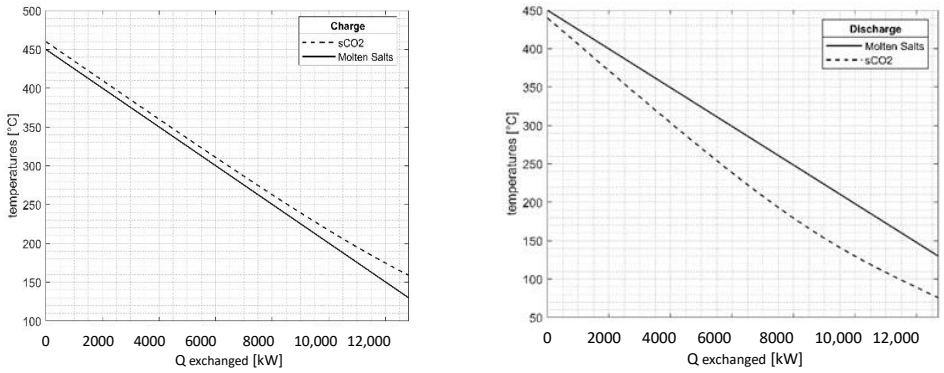


(a) (b)

*Figure 80 - High temperature (TES HEX) heat exchanger thermal exchange behaviour: **(a)** charging and **(b)** discharging (example for TES temperature at 450 °C).*

# 4 Dynamic behaviour of CO2 cycles

As introduced in the first chapter, the increasing share of non-dispatchable sources in the energy mix, as well as the need to manage the electricity production in critical times of the day (to compensate the so-called "duck curve"), lead to the need of fast-responsive power plant, and the sCO2 plant are possible candidates to play a role in this scenario. At the same time, the sCO2 systems need to operate under stringent operational constraints, especially when working close to the critical point, and exhibit distinct transient phenomena during load fluctuations. For these reasons, it is essential to analyse the dynamic behaviour of an sCO2 plant to fully understand its capabilities and advantages compared to conventional power plants. This understanding is also vital to design a control system that is both responsive and efficient.

This chapter briefly reports the work developed within the European Project SOLARSCO2OL [62], in which the University of Genova is partner, to develop a dynamic model of a simple recuperated sCO2 plant.

After a presentation of the research project, the main modifications to a pre-existing simulation tool are reported. Finally, some of the results achieved are presented.

## 4.1 The Demo-Cycle and the SOLARSCO2OL Project

The goal of the SOLARSCO2OL [61] Horizon 2020 EU research project is to build the first MW-scale sCO2-CSP plant in Europe and to demonstrate its operation. The layout of the demo plant is shown in Figure 81. It is based on a simple recuperated sCO2 Brayton cycle and it was designed, with the use of the TEMP-EVO tool and in agreement with the partner of the consortium, to generate a net power output of 1.6 MW, achieving a design cycle efficiency of 21.3%. However, the study by Guedez et al. [61] demonstrated that an upscaled version of this concept could reach efficiencies over 31%, and a slightly different

configuration that include a recompression to the plant could lead the efficiency to almost 50%.

The sCO2 plant will be coupled with the EMSP (Évora Molten Salt Platform) of the University of Evora [120]. Located in Evora, Portugal, the EMSP is a state-of-the-art industrial scale facility including parabolic trough solar collectors and high temperature thermal energy storage (TES). The solar field has a total length of almost 700 m and a thermal power output of 3.5 MW [121]. It is one of the first plants using directly molten salts as heat transfer fluid, allowing for lower costs and higher operative temperatures (up to 550°C). However, the use of molten salts poses some technological challenges related to the necessity of avoiding their solidification in any condition. The plant was carefully designed to comply with this requirement, including also an electric heater to heat up the salts if needed and always maintain them in a liquid state. Regarding the TES, it is composed by multiple tanks, where the molten salts can be stored for up to 12 h. In this way, it is possible to improve the dispatchability of the solar energy source, generating power under unfavourable weather conditions or at night.

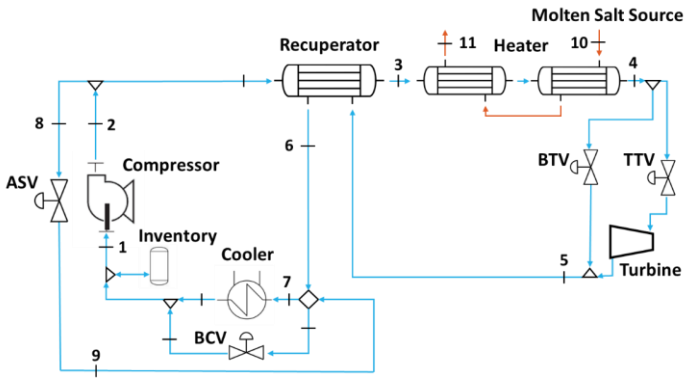


*Figure 81 – Plant layout of the SOLARSCO2OL demonstrator.*

CSP facility and sCO2 plant will be coupled via the "heater", which is composed by two shell-and-tube heat exchangers specifically sized for the SOLARSCO2OL project. After leaving the TES, the molten salts are heated up by the electrical resistance and enter the hot side of the heaters. Here, they transfer heat to the $CO_2$ flow in order to reach the desired temperature at the turbine inlet (565°C).

After the heater, the $CO_2$ flow is led to the turbine through the TTV (turbine throttling valve). The turbine can also be partially or entirely bypassed by opening the BTV (bypass turbine valve), a procedure that can be useful during plant start-up, transient and part load operation. In the analyses present here, since the focus is on the normal part-load operation, the BTV is always considered closed. The flow expands in the turbine which is connected to an electrical generator. Then, it enters the hot side of a recuperator (design effectiveness of 80%), where it transfers heat to the cold $CO_2$ flow entering the heater.

After leaving the recuperator, the temperature of the $CO_2$ is lowered to 33°C by an air cooler. Before entering the compressor, the $CO_2$ must reach very exact conditions of temperature and pressure: 33°C and 83 bar. In fact, the fluid is very close to the critical point at the cooler outlet (Figure 82) to minimize the compressor work, and any significant deviation from those values could bring the $CO_2$ in subcritical conditions at the compressor rotor inlet, or vice versa significantly decrease its density. The temperature can be regulated by varying the cooler air mass flow and, if necessary, partially bypassing the cooler through the BCV (bypass cooler valve). The pressure, instead, is kept constant by controlling the mass of $CO_2$ inside the loop, i.e. introducing more $CO_2$ from an inventory to increase it or venting into the ambient to reduce it. The compressor is equipped with an ASV (anti surge valve), which can be used to recirculate part of the pressurized flow at its inlet. This reduces the pressure losses in the loop, without significantly changing the compressor mass flow, thus increasing the distance from the surge line. Despite reducing the plant efficiency, this solution can guarantee safe operation at low power load or during fast transients. After being pressurized by the compressor, the $CO_2$ reaches the maximum pressure of the cycle, equal to 188 bar, enters the cold side of the recuperator and finally the heater. The compressor is not connected to the turbine, but to an electrical motor. In fact, compressor and turbine are mounted on separate shafts, a solution which maximizes the flexibility of the

demonstrator, and allow to control the plant mass flow rate through the compressor speed.

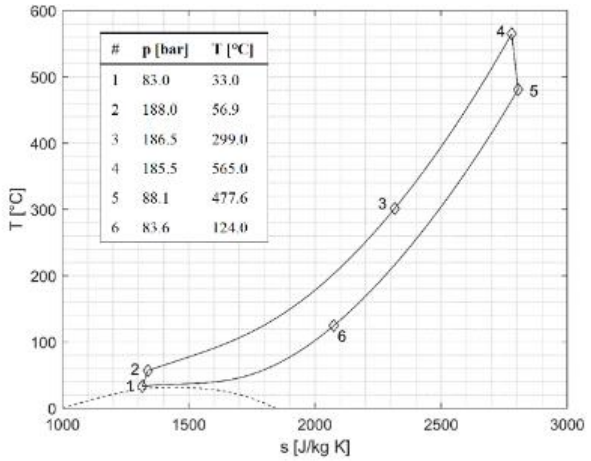


*Figure 82 – The SOLARSCO2OL simple recuperated Brayton thermodynamic cycle, represented on an entropy-temperature diagram.*

## 4.2 Demo-Cycle modelling methodology

The SOLARSCO2OL demo-plant is simulated using the TRANSEO tool, an existing in-house tool developed in MATLAB-Simulink. The tool is component-based, meaning that each component of the real plant is represented by a function, in which the characteristic dynamic equations are computed at each time step.

The components are usually simulated with an approach that uses a disk actuator (a function in which the characteristic of the component are computed) plus the integration with a lumped volume, in which the time delays are implemented. Further information can be found in [122].

It is important to highlight the information flow upon which it is based a simulated plant, and in particular the SOLARSCO2OL one analysed here. In fact, each component can act in an "active" or "inactive" way. If a component is set to active, then it will be a component that computes the mass flow rates based on the other information (pressure differences). If it is set to inactive, the

component will transfer the information of mass flow rate that has received from the near component (forward or backward). The only component that acts as sink of information on the mass flow rates is the Plenum component, which computes the pressures at which a specific section of the plant is, based on the amount of mass present.

In particular, the demo-plant analysed is simulated so that the turbomachinery act as active components, computing the mass flows based upon the pressure differences and their characteristic maps, and the heat exchangers are set into inactive behaviour. In Figure 83, the compressor is in yellow, the turbine in red, and before this two components two Plenum components are posed (in dark grey). The valves, in purple, have their active/inactive logic set accordingly.

Due to the fact that the plant operates with CO2 in condition with a strong real-gas behaviour, for all the component the original computation of the temperatures and specific heat to compute energy equations has been substituted using enthalpy and integrating the model with the REFPROP library [71].

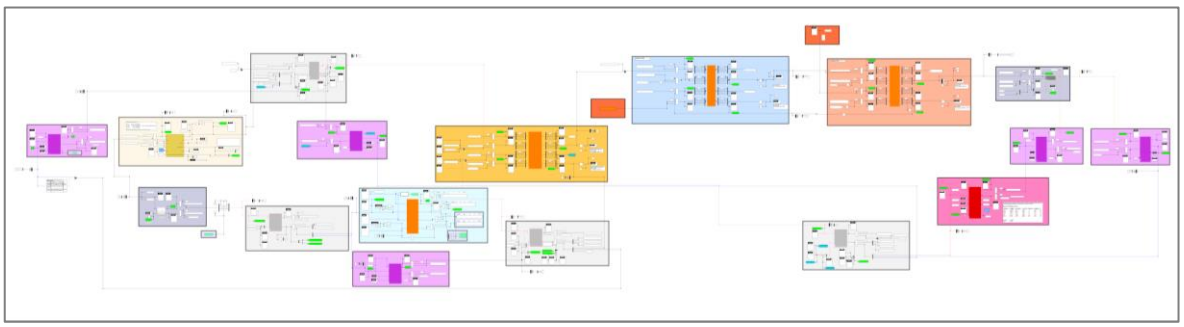

*Figure 83 – SOLARSCO2OL TRANSEO model screenshot*

### 4.2.1 Compressor Modelling

A Centrifugal Compressor (CC) coupled with variable speed electrical motor was designed by Baker Hughes for the SOLARSCO2OL cycle. The compressor suction condition was selected very close to the $CO_2$ critical point to both

optimize cycle efficiency; the selection of the exact pressure and temperature in the vicinity of this point was then done to optimize compressor operability. In these conditions (33°C, 83 bar) carbon dioxide attains a very high density, around 650 kg/m$^3$, significantly higher with respect to common applications for centrifugal compressors. In addition, a pressure ratio higher than 2.2 was required by the selected sCO2 Brayton cycle.

Compressor curves are provided by the manufacturer partner of the EU Project, and their implementation in the model is based on the approach of Lambruschini et al. [123], assuming the inlet as reference condition. The main characteristic parameters of the machine, the isentropic reduced head $\Delta h_{is}/(k_{in}Z_{in}\,T_{in})$ and the isentropic efficiency, are given versus the reduced mass flow $\dot{m}\,\sqrt{Z_{in}\,T_{in}}/(p_{in}\sqrt{k_{in}})$, and as a function of reduced speed $N/\sqrt{k_{in}Z_{in}\,T_{in}}$ (Table 19).

During the simulations it was suggested by manufacturers to maintain a proper margin to $CO_2$ saturation condition (density equal to 620 kg/s, pressure equal to 80 bar in case of temperature inlet set at 33°C, against a critical point of 73.8 bar and 31.0 °C), and this was suggested to avoid uncontrolled phase transitions. Indeed, from a centrifugal compressor standpoint, it is recommended to keep suction pressure and temperature as constant as possible, even in part-load and dynamic operations.

The TRANSEO compressor model computes new outlet condition and performance through characteristic curves interpolation and boundary conditions, considering the real gas effects [124]. The compressor model employed in this cycle simulation is not suitable for capturing the surge behaviour [125], but it can well indicate the surge margin, defined according to the following equations. This has been achieved employing the lumped-volume model (pipe of equivalent length and section) coupled with a disk actuator which responds according to the impeller characteristic curves [122]. So, at each time step of the simulation, the surge margin can be monitored and to verify that the compressor is kept in the safe region.

The compressor surge margin is an important parameter useful for the compressor control, referring the distance of the actual operating point from the surge conditions. Two different definitions are implemented in the model.

#### *4.2.1.1 Constant-head or Constant-PR Surge Margin*

The calculation of this type of surge margin, is based on the isentropic head (H), or on the pressure ratio, together with the mass flow rate. It is defined as the ratio between the mass flow rate of the actual operating point and the mass flow rate of the point, on the surge line on the compressor map, which presents the same isentropic head (or pressure ratio) as the actual operating point. The surge margins (Kp) are reported in Eq. (111) and (112). The surge margin should be greater than 1.1 to guarantee the compressor safe operation.

$$Kp_H = \frac{\dot{m}}{(\dot{m})_{@\ surgeH}} \tag{111}$$

$$Kp_{PR} = \frac{\dot{m}}{(\dot{m})_{@\ surgePR}} \tag{112}$$

Despite the two definitions being similar, since they are based on two different maps of the compressor their actual value differ slightly, suggesting that a control on both the values can result necessary to actually avoid compressor surge.

#### *4.2.1.2 Constant-RS Surge Margin*

The calculation of this type of surge margin, is based on the isentropic head (H), or pressure ratio, together with the mass flow rate . It is defined on the angular coefficient of the compressor maps, thus as the ratio between the isentropic head and the mass flow of the actual operating point, normalised on the same ratio, but considered for the point, having the same reduced compressor speed (RS, or N), which lies on the surge line; then the reciprocal of this number is considered in the definition, as shown in Eq. (113).

$$Kp_{N,H} = \frac{\left(\Delta h_{is}/\dot{m}\right)_{@\ surgeN}}{\Delta h_{is}/\dot{m}} \qquad (113)$$

### 4.2.2 Turbine Modelling

A sCO2 turbine was designed by Franco Tosi Meccanica for the SOLARSCO2OL cycle.

For the turbine, although it operates in a region where the compressibility factor Z is close to unity, the non-dimensional curves are implemented considering the exhaust flow as reference condition, which is a typical assumption used also in steam turbines, the most common turbines operating in closed cycles.

Similarly to what presented for the compressor, the turbine load parameter $\Delta h_{is}/(Z_{exh}\,T_{exh})$ and isentropic efficiency are given vs. the reduced flow $\dot{m}\sqrt{Z_{exh}\,T_{exh}}/p_{exh}$ as a function of $N/\sqrt{Z_{exh}\,T_{exh}}$ (Table 19). Moreover, a lumped-volume model coupled with a disk actuator which responds according to the expander characteristic curves have been developed and implemented, being satisfactory for cycle simulations.

*Table 19 – Supercritical reduced groups*

| | ***Compressor*** | ***Turbine*** |
|---|---|---|
| **Isentropic reduced head** | $\Delta h_{is}/(k_{in}Z_{in}\,T_{in})$ | $\Delta h_{is}/(Z_{exh}\,T_{exh})$ |
| **Reduced mass flow** | $\dot{m}\sqrt{Z_{in}\,T_{in}}/(p_{in}\sqrt{k_{in}})$ | $\dot{m}\sqrt{Z_{exh}\,T_{exh}}/p_{exh}$ |
| **Reduced speed** | $N/\sqrt{k_{in}Z_{in}\,T_{in}}$ | $N/\sqrt{Z_{exh}\,T_{exh}}$ |

### 4.2.3 Modelling of shell and tubes heat exchangers

High-Performance shell-and-tube heat exchanger technology was selected and sized for the SOLARSCO2OL project by the LOINTEK company for recuperator and the heaters. They consist of two independent pressure chambers (shell side and channel/tube side) through which two fluids flow in such a way that when there is a temperature difference between them, heat is exchanged without the media mixing.

Heat transfer coefficients and the heat exchanger geometry design data allow TRANSEO dynamic tool to emulate the counter-current flow heat exchanger as a quasi 2-D plate heat exchanger, using two plates whose areas (S) correspond to the total exchanging area; the numerical solution of differential equation is computed using convective heat transfer coefficients (h) and metal thermal conductivities (λ) in a finite difference scheme which is implicitly integrated along time, as shown in Figure 84. The model is structured in four layers (j), two for the flows and two for the metallic matrix, each of those is divided into N blocks (length equal to Δx) along the heat exchanger length. The temperature in each node is computed through thermal (q) balance equation in unsteady formulation.

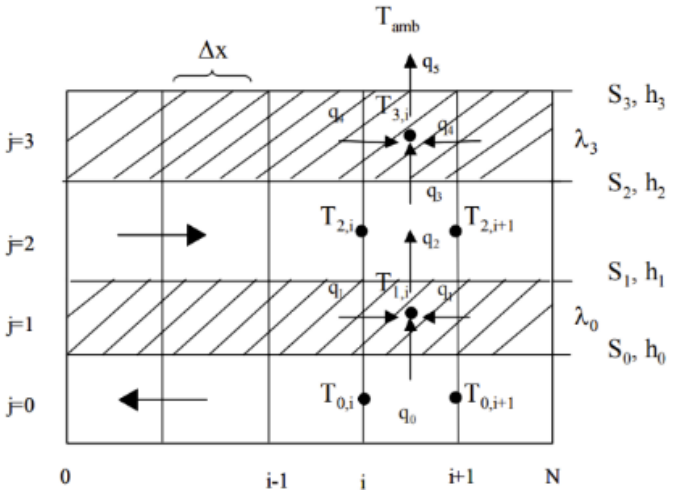


*Figure 84 – counter-current flow heat exchanger as a quasi 2-D plate heat exchanger, numerical finite difference scheme*

To emulate the shell and tube heat exchanger configuration, only the heat exchange of a single tube was modelled, in axial-symmetrical geometry (half of the longitudinal section in Figure 84), computing intensive properties and scaling up extensive ones. The same approach has been adopted for modelling both the recuperator and the heater, but using the different design data of the two heat exchangers.

### 4.2.4 Modelling of the Cooler

The cooler heat exchanger should control the temperature at the compressor inlet, keeping nominal value in steady-state operation. A Wet Surface Air Cooler (WSAC) [126] or an Adiabatic Cooler (AC) [127] could be suitable for this aim [128], while evaporative cooling towers could be disadvantageous for the high-water consumption: in this case, the adiabatic cooler was selected as best compromise between performance and cost. It delivers $sCO_2$ at 33°C at the compressor inlet during every season, since the wet bulb temperature is the minimum temperature achievable by the ambient air.

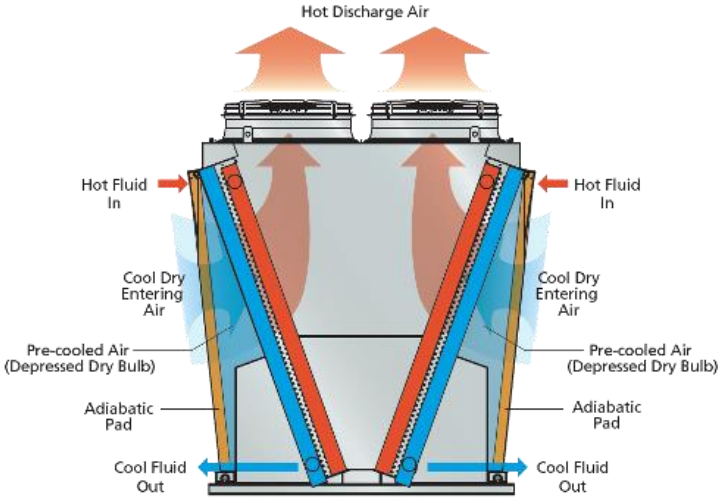


*Figure 85 - A general adiabatic cooler representation*

The air cooler model was developed starting from the equations implemented in the sizing tool by White et al. [128]. The equations were translated from Microsoft Excel to Matlab-Simulink and reorganized for the off-design simulation of a flat or V-shaped crossflow air cooler.

The air cooler used in the SOLARSCO2OL plant is a V-shaped dry (or adiabatic) air cooler, where the $CO_2$ makes six passes through a serpentine tube, while the air flows externally in the perpendicular direction. Therefore, a 2D numerical scheme was adopted, considering 6 passes and discretizing each pass in 10 elements.

Heat transfer coefficients are computed with different correlations depending on the configuration (flat or V-shaped) and the fluid (CO2 or air) [129] [98], following the approach by White at al. Heat exchange in each section is computed with the effectiveness-NTU method, relying on multiple iterative loops checking the convergence of temperatures and pressures.

The transient behaviour of the air cooler is simulated combining the steady-state model described above with first order delays. The time constant [122] governing the thermodynamics of the cooler, namely the output temperatures, is estimated from its metal mass, heat exchange areas and conductive coefficients, resulting in a value of 33 s, this being mainly driven by energy equation. The time constant related to the variations of CO2 pressure, instead, is computed based on the geometrical characteristics of the cooler and equal to 0.1 s, this being mainly driven by momentum equation.

### 4.2.5 Valves Modelling

The valve model assumes general characteristic curves for each type of valve, and the actual mass flow, at a certain value of the fractional opening [0,1], the mass flow rate depends on the inlet and outlet properties of the flow, such as temperature and pressure.

In the current model, the anti-surge valve (ASV) and the cooler-bypass valve (BCV) were selected as linear characteristic valves, while the other valves were selected to be choked-linear characteristics valves, i.e. capturing the orifice chocking, when sonic conditions are attained at the valve throat. The valves are not isothermal because of the non-ideal gas behaviour ($sCO_2$). The outlet temperature is computed with REFPROP [71] according to an iso-enthalpic transformation. At the steady-state nominal operating point, the valves the anti-surge (ASV) and the two bypass valves for turbine (TBV) and cooler (CBV) are closed, while the turbine throttling valve (TTV) is fully open.

### 4.2.6 Concentrated Volumes

#### *4.2.6.1 Plenum component modifications*

The so-called "Plenum" is a component already present in the TRANSEO library. It represent a certain volume of a section of the plant which is concentrated in a certain location in the simulation model, and it is aimed at the resolution of the equations of continuity and energy across all its inlets and outlets, in order to provide information on the pressure that characterises a certain section during each time step. It is thus a "sink" in terms of mass flow information, and a source of pressure information, thus operating in a compensatory way with respect to the active components (usually the turbomachinery) in the model, which instead set the information of mass flow, receiving the information on pressures.

In order to make this component operating with real-gases (thus when the compressibility factor Z is far from 1), this component had to be completely re-structured, solving the two conservation equations without the common assumptions and simplifications used in perfect gas applications. In the following are reported the equations implemented in the new Plenum component for real-gases.

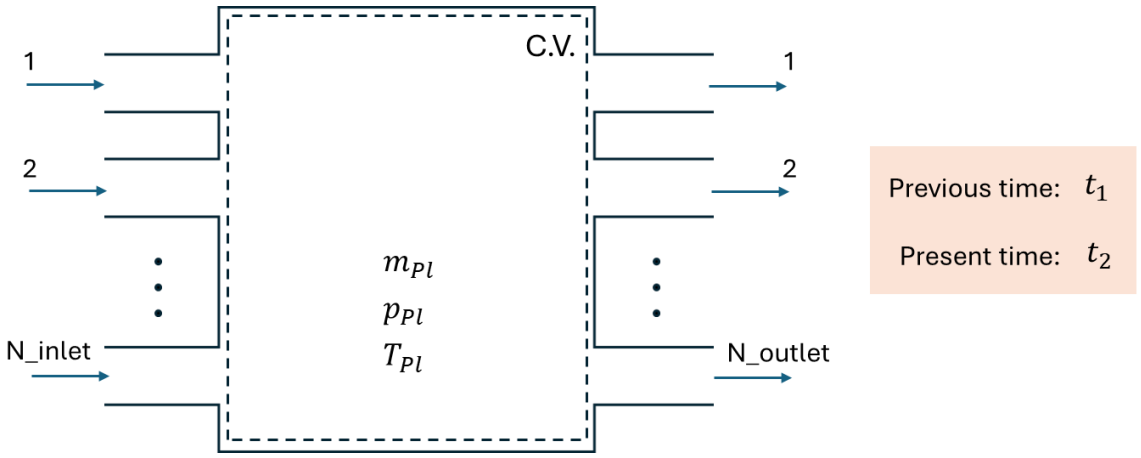


*Figure 86 - Control Volume for the Plenum equations*

Considering a control volume as represented in Figure 86, and a time step $\Delta t$:

$$t_2 = t_1 + \Delta t \tag{114}$$

The continuity equation allows to find the new mass in the plenum at the present time $(m_{Pl})_{t_2}$:

$$\frac{d(m_{Pl})}{dt} = \sum_{in} \dot{m}_{in} - \sum_{out} \dot{m}_{out} \tag{115}$$

$$(m_{Pl})_{t_2} \approx (m_{Pl})_{t_1} + \\ + \left( \left( \sum_{in} \dot{m}_{in} \right)_{t_2} + \left( \sum_{in} \dot{m}_{in} \right)_{t_1} \right) \cdot \frac{\Delta t}{2} - \left( \left( \sum_{out} \dot{m}_{out} \right)_{t_2} + \left( \sum_{out} \dot{m}_{out} \right)_{t_1} \right) \cdot \frac{\Delta t}{2} \tag{116}$$

The energy equation:

$$\frac{d(U_{Pl})}{dt} = \sum_{in} \dot{m}_{in} h_{in} - \sum_{out} \dot{m}_{out} h_{out} + \dot{Q}_{source} \tag{117}$$

Cannot be simplified as it would be with a perfect gas assumption, thus its resolution needs to rely on enthalpies instead of on temperatures. It is thus coupled in a system with the definition of enthalpy:

$$h = u + pv = u + \frac{p}{\rho} \quad (118)$$

And with the information on the volume of the Plenum $V_{Pl}$ (which is a parameter set by the user depending on the volumes of the real plant):

$$\rho = \frac{m_{Pl}}{V_{Pl}} \quad (119)$$

And leads to a system of coupled equations to compute the pressure inside the Plenum, solved numerically inside the component:

$$u_{Pl} = \left[ C - \frac{p_{Pl}}{\rho} \cdot \dot{m}_{out\_TOT} \cdot \frac{\Delta t}{2} \right] \Big/ \left( m_{Pl} + \dot{m}_{out\_TOT} \cdot \frac{\Delta t}{2} \right) \quad (120)$$

$$p_{Pl} = f(u_{Pl}, \rho) \quad (121)$$

Where C is a constant:

$$C = \left( \dot{H}_{in\_TOT} \right)_{t_2} \cdot \frac{\Delta t}{2} + \left( \dot{Q}_{source} \right)_{t_2} \cdot \frac{\Delta t}{2} + K_{t_1} \quad (122)$$

Where $K_{t_1}$ is the constant of all the information from the previous time step:

$$K_{t_1} = (U_{Pl})_{t_1} + \left( \dot{H}_{in\_TOT} \right)_{t_1} \cdot \frac{\Delta t}{2} - \left( \dot{H}_{out\_TOT} \right)_{t_1} \cdot \frac{\Delta t}{2} + \left( \dot{Q}_{source} \right)_{t_1} \cdot \frac{\Delta t}{2} \quad (123)$$

#### *4.2.6.2 Plant Equivalent Volumes*

An evaluation of the volumes used in the model has been made. Two concentrated volumes has been used, and their value has been computed starting from the pre-design of the plant, especially for what concerns the volumes of the heat exchangers and of the piping. As shown in Figure 87, each section has been linked to the volume value obtained form the pre-design, and for each section it was computed the relative value of average density to be found

in it. Then, two equivalent volumes are set up in the model, concentrating the mass information in two places, one in high pressure and one in low pressure. The information of the volumes is inserted in the model using two plenum components, and they are placed at the inlet of the compressor and at the inlet of the turbine, as presented (the two dark grey components) in Figure 83.

The estimated mass of CO2 in the loop, at nominal operating point, is equal to 1055 kg, while the detailed numerical results for each section are reported in Table 20.

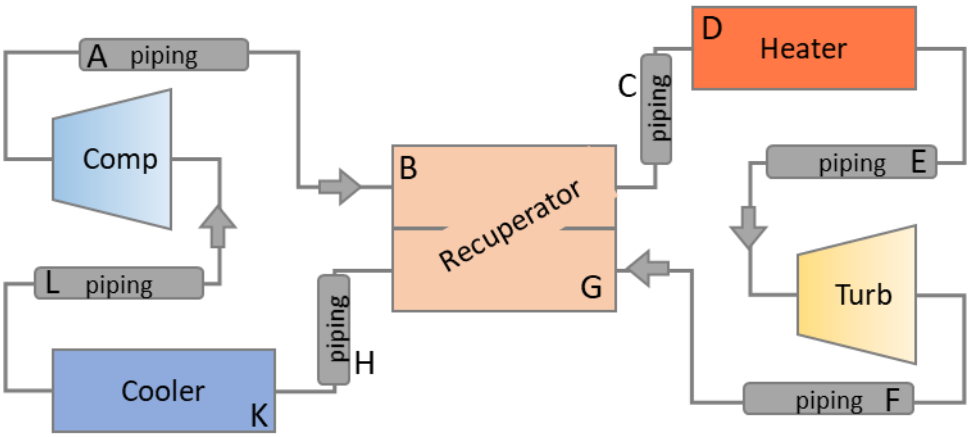


*Figure 87 - Considered sections with volumes*

*Table 20 – Calculation of equivalent volumes*

| ***Section*** | ***Volume [m³]*** | ***Average Density [kg/m³]*** | ***Equivalent Volume [m³]*** | |
|---|---|---|---|---|
| *A* | 0.09 | 723.798 | 4.3005 | *High pressure* |
| *B* | 0.1573 | 451.036 | | |
| *C* | 0.94 | 178.274 | | |
| *D* | 0.5562 | 145.885 | | |
| *E* | 0.91 | 113.496 | | |

| | | | | |
|---|---|---|---|---|
| *F* | 1.79 | 61.413 | | *Low Pressure* |
| *G* | 0.9248 | 96.576 | | |
| *H* | 0.44 | 131.739 | 0.86386 | |
| *K* | 0.2 | 392.525 | | |
| *L* | 0.35 | 653.310 | | |

## 4.3 Off-Design Analysis and control strategy of a simple recuperated cycle demo-plant

### 4.3.1 Control Variable Definition and Control Actuators

The first step in the development of a off-design analysis of a power plant is to identify the main variables that need to be controlled and their relative control loops. In Table 21 are detailed the control loops identified, the specific signal and the relative actuator is preliminary defined.

*Table 21 – Main control loops identified in the system*

| No | Description | Signal | Actuator |
|---|---|---|---|
| 1 | Compressor Inlet Temp. | Compressor Inlet Temperature | Cooler By-pass valve + Fans |
| 2 | Lower Pressure | Compressor Inlet Pressure | Inventory management system (and venting) |
| 4 | Mass flow rate in the loop | Compressor mass flow | Compressor speed |
| 6 | Anti-surge system and protection | Volume Flow rate, Temp, Pressure | Compressor control (Anti-surge valve) |
| 7 | Turbine control | Turbine Inlet Pressure | Turb Control Valve |

| | | | | |
|---|---|---|---|---|
| 9 | MS inlet temp to the MS-to-CO2 HX / (indirectly TIT) | Molten Salts Temperature | Inlet | Electric Heater |
| 10 | MS mass flow / (indirectly TIT) | Turbine Temperature | Inlet | Control valve (of MS pump) |

From this selection, the parameters that are most relevant for the plant operation are then analysed in detail in the following.

### 4.3.2 Off-Design steady-state analysis and main results

Starting from the control loops identified (listed in Table 21), the specific variables are further investigated. First of all, being one of the most important parameter, the temperature at the compressor inlet is kept constant through all the off-design analyses, since this is one of the main constraints that the controllers will have to respect; in particular, this behaviour will be guaranteed with a variation of parameters in the cooling system.

Then, among the possible control variables listed in Table 21, three main parameters are identified for the control of the cycle in part-load; for each of these, one or more control actuator are identified and are studied in the analysis, where are reported results coming from different combination of these parameters. In particular, the three degrees of freedom used in the analysis are explained below, and synthetised in Table 22:

- The heat power entering in the cycle from the Heater.
  It is controlled through the variation of the molten salts mass flow rate, which will be actually controlled with a recirculation system. In this analysis, the temperature of the molten salts at the inlet of the MS-sCO2 heater is selected to be constant and equal to 580°C.
- The total mass of CO2 in the cycle.
  This parameter is important to stabilise the operating pressures of the

cycle, in order to reach the desired values. In the simulation it is regulated through a connection between the lower pressure collector and an injection (positive input) or extraction (negative input) of mass.

- The CO2 mass flow rate evolving in the cycle.
  It can be regulated in two ways, using the variation of the speed of the compressor or using the opening of the anti-surge valve of the compressor in order to recirculate part of the mass flow itself.

*Table 22 - The main degrees of freedom of the plant and relative actuators*

| ***Degree of Freedom*** | ***Control Actuator*** |
|---|---|
| Heat power from the hot source | Molten Salts Mass flow rate |
| Total mass in the loop | Inventory Control |
| Mass flow rate | Compressor ASV Opening |
| | Compressor Speed |

Moreover, in the following Table 23 is reported the range analysed for each of the control variables analysed, while in Figure 88 is displayed a schematic of the analyses conducted to explore the part-load behaviour.

*Table 23 - Ranges analysed for each control variable*

| | ***Compressor Speed*** | ***ASV Opening*** |
|---|---|---|
| ***Molten Salts Mass flow rate*** | [100% 85% 70% 55% 40%] | [100% 85% 70% 55%] |
| ***Inventory Control (Mass variation)*** | [+5% +0% -2% -4%] | [+15% +0% -3%] |
| ***ASV Opening*** | 0% | [0% 15% 30% 45%] |
| ***Compressor Speed*** | [100% 90% 80% 70%] | 100% |

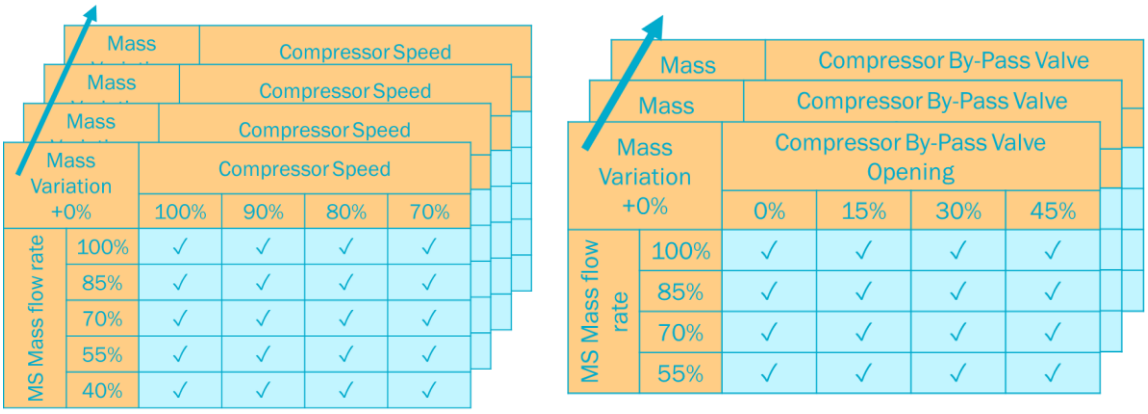


*Figure 88 - Schematic of the combination of the degree of freedom in the analyses*

The main objectives of the off-design analysis were to explore the operational envelope of the demonstration plant, and to establish a control strategy to be later tested with transient analyses.

A proper control philosophy must provide coordination of the available degrees of freedom guaranteeing efficiency and safety operation. Thus, two main strategies have been firstly analysed in off-design, decoupling the two actuators for the loop mass flow rate, and the focus was maintained on the most efficient one of the two, which is the one using the compressor speed variation to regulate the mass flow rate (and thus the power of the loop). Figure 89 shows the normalised efficiency for all the points analysed in off-design, also highlighting

two constrains that has to be considered during the actual selection of operating points. Starting from this results, a strategy to move between the different operating scenarios from the design point to half-load has been studied.

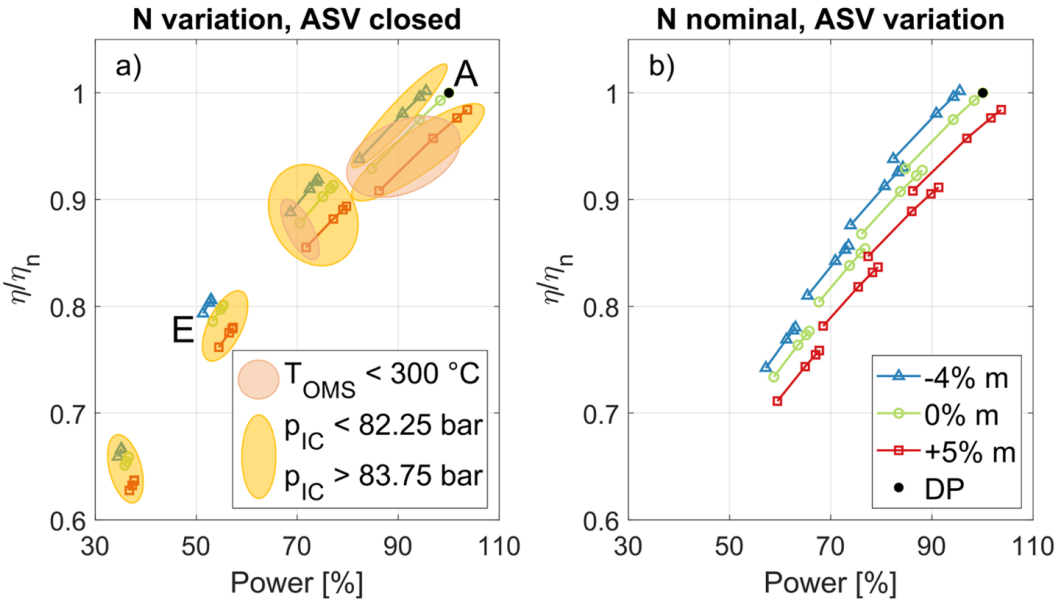


*Figure 89 - Strategies comparison of Off-design points*

### 4.3.3 Variable speed control strategy

Starting from the off-design results as described above, the main focus of the preliminary study of control strategy has been to select the steady state points that could represent the main control strategy for normal part-load operation. Table 24 resumes the control variable actuators and related monitored variables.

*Table 24 - Control variable actuator and monitored parameter*

| **Control Actuator** | **Monitored Parameter** |
|---|---|
| Compressor Speed ($sCO_2$ mass flow) | Regulate Power |
| MS mass flow | Control TIT setting |

The strategy analysed refers to the compressor speed, total mass, and molten salts mass flow rate variation, as showed in the left part of Figure 89. Five steady-state points, respecting the main constraints in temperature of the molten salts and compressor inlet pressure, are highlighted and presented in Table 25.

*Table 25 - Preliminary Control Strategy points*

| *Steady-State Points* | $N/N_n$ *[%]* | $\dot{m}_{MS}/\dot{m}_{MSn}$ *[%]* | $m/m_n$ *[%]* | $P_{el}/P_{eln}$ *[%]* |
|---|---|---|---|---|
| ***A*** | 100 | 100 | 100 | 100 |
| ***B*** | 95 | 88.75 | 99 | 87 |
| ***C*** | 90 | 77.5 | 98 | 75 |
| ***D*** | 85 | 66.25 | 97 | 73 |
| ***E*** | 80 | 55 | 96 | 51 |

In the following figures, different results for the points in the control strategy are reported. The main driver of the load variation is the mass flow of CO2 in the loop, as highlighted in Figure 90, where at 51% load, the normalized efficiency decreases by 20%. The same behaviour is showed for the pressure ratio, in fact at 51% load the pressure ratio decreases linearly by 20% compared to the nominal point, from 2.31 to 1.84, as showed in Figure 91, which also shows the behaviour of compressor inlet pressure, regulated through the variation of the total $CO_2$ mass in the loop by injecting or extracting $CO_2$ with the inventory. Figure 92a shows the moderate variation of the TIT, which is almost constant and thus helps to maintain high efficiency, and of the MS outlet temperature,

never crossing its lower boundary value (300° C); besides, Figure 92b shows that the machines work with an efficiency value almost constant.

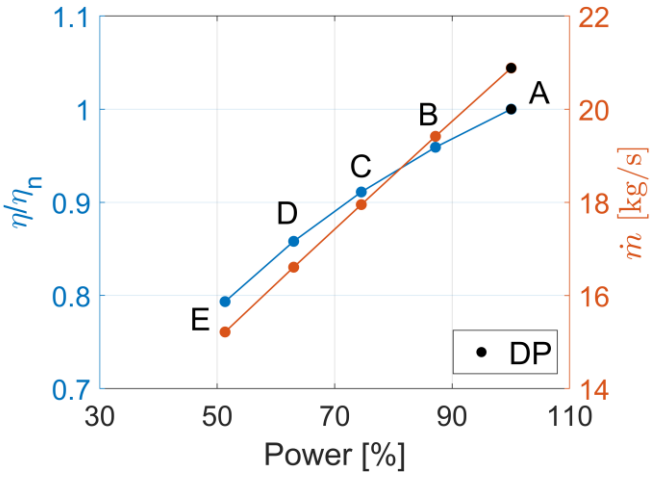


*Figure 90 - Normalized efficiency and mass flow in control strategy as a function of power*

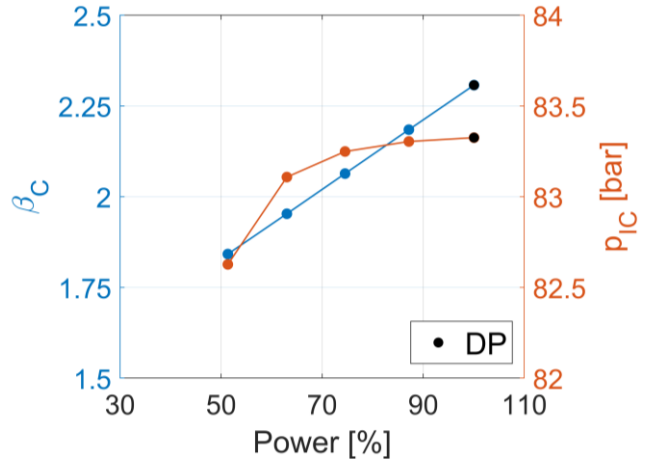


*Figure 91 - Pressure ratio and compressor inlet pressure in control strategy as a function of power*

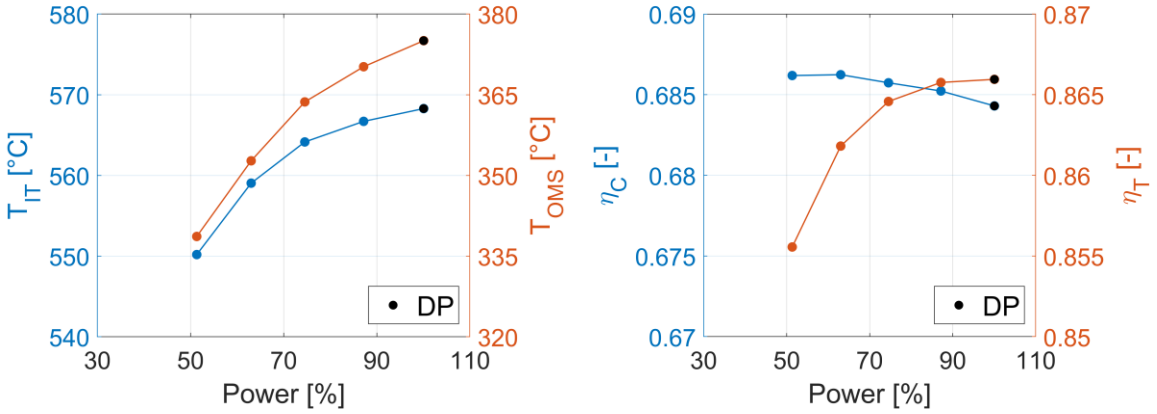


*Figure 92 - a) turbine inlet temperature and MS outlet temperature and b) compressor and turbine efficiency, in control strategy as a function of power*

## 4.4 Dynamic Analyses: Step responses of the main variables of the demo-plant

In this section are presented the responses of relevant parameters to a step variation of the main control variables, namely the compressor speed, the molten salts mass flow rate, the total mass of $CO_2$ in the loop, the anti-surge valve fractional opening, and the air mass flow rate in the cooler.

The value chosen for the control variables are roughly the ones of the points A and B of the abovementioned control strategy, in Table 25. The analysis on the control of the compressor inlet temperature was added at this point, and to characterise it, it has been analysed the response to the step variation of the air mass flow rate in the air cooler.

Since a step variation of the control variables from the design point to lower loads caused the system to incur in physical instabilities mainly due to compressor surge, the step variation of the compressor speed was made up towards an increase of mass flow, because an increase in mass flow rate did not cause the instable behaviour of the compressor even when sudden variations of the controlled values occurred.

Thus, in the next paragraphs are reported the separate variations of compressor speed N (from 95% to 100% of the nominal velocity), of the MS mass flow rate (from 100% to 90% of the full load value), of the $CO_2$ mass in the loop, analysed with a variation of 1% of the total nominal value of $CO_2$ mass, injected with a step variation in a timespan of 5 seconds.

Along with these, simulations were made analysing the variation of the mass flow of air in the fans of the air cooler (from a value of 100% to 90% with respect to the full load value), and the variation of the Anti-Surge Valve fractional opening (from a value of 0% to 10% with respect to the nominal one of the valve, the same as the compressor).

All these results are of paramount importance to understand and to characterise the behaviour of the main parameters in response to the control variables, and will be also used to set appropriately the controllers and develop the actual control logics.

### 4.4.1 Compressor speed

The compressor speed has been pre-selected as the main parameter to control the power output of the system. The parameter immediately influenced by the variation of the compressor speed is the mass flow rate of $CO_2$ in the cycle, which in cascade is the main driver of the total cycle power variation. Figure 93 shows the variation of mass flow rate with a fast response, and the final value reached is the one leading to an increase in the power output.

The step variation in compressor speed clearly causes a sudden increase in the mass flow evolved in the compressor, which explain also the behaviour of the compressor inlet pressure in Figure 94; in fact, the increase in mass flow causes the concentrated volume to empty and decrease its pressure, that is then stabilised to a new and lower value. Despite the safe margin from the $CO_2$ critical pressure, this aspect needs further study, as this behaviour could be an indication of the ramp limits for compressor operation, to not harm the inlet

vanes by possibly causing liquid formation; these will also be the main ramp limits for the load variation, once regulated the other constrained parameters.

Figure 94 also clearly shows the increase of the higher pressure of the cycle, and thus of the pressure ratio, which further increase the power output. Finally, the behaviour of the compressor inlet pressure highlights that a combined strategy with other control variables, to regulate the lower pressure level, needs to be carefully developed.

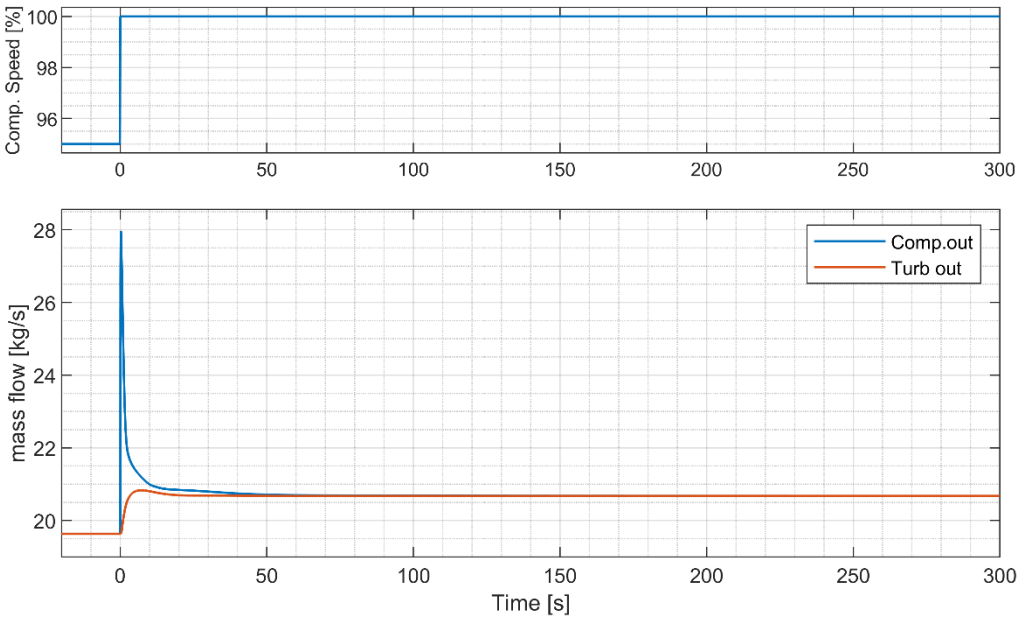


*Figure 93 – Mass flow rates variations*
*in response to a compressor speed step variation from 95% to 100%*

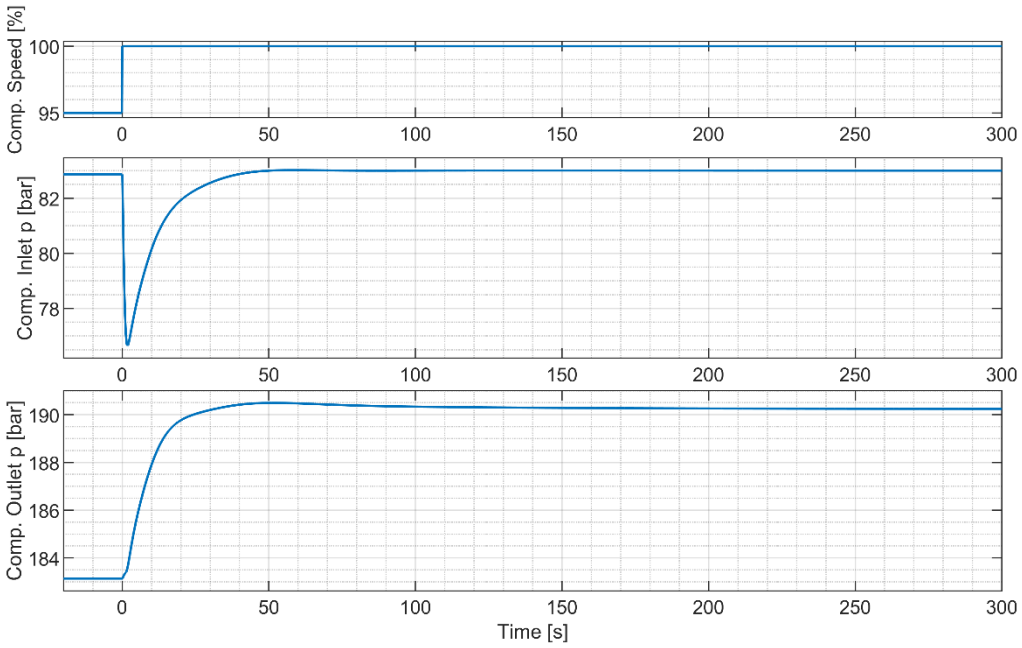


*Figure 94 – Compressor pressures variations*
*in response to a compressor speed step variation from 95% to 100%*

### 4.4.2 Molten salts mass flow rate

In the analysed range, between the two operating points A and B, the MS mass flow rate has a lower influence on all the cycle parameters. However, this variable is proved to be effective in regulating the turbine inlet temperature as MS mass-flow rate will mostly control the amount of heat that will be provided from the MS Tank/solar input to the power cycle.

Figure 95 shows a larger characteristic time of the temperature variation (due to thermal inertia of MS mostly) with respect to other parameters. Consequently, the system shows a slower general dynamic behaviour when the driver of the simulation is the MS mass flow rate.

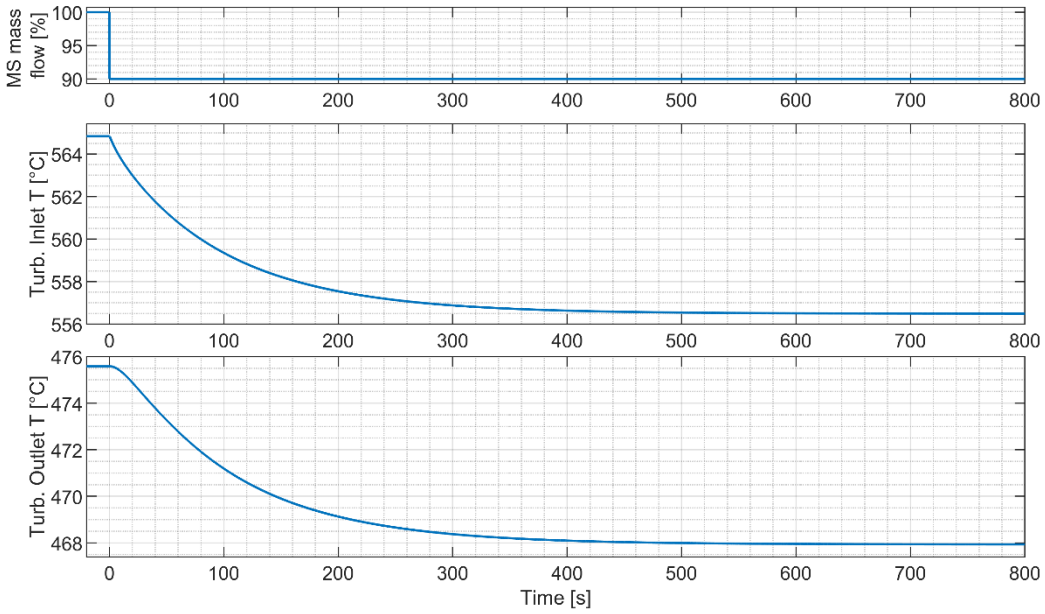


*Figure 95 – Turbine temperatures variations*
*in response to a MS mass flow rate step variation from 100% to 90%*

### 4.4.3 Carbon Dioxide total mass in the loop

The quantity of CO2 in the loop directly impacts on the average cycle pressure, therefore it can help to keep constant the compressor intake pressure at part-load.

Figure 96 shows the mass injection process and its influence on the mass flow rates in the cycle. Instability spikes are present and due to the sudden variation of the variable. In the actual control logic a selection of mass injection/subtraction ramps is needed.

Figure 97 shows the consequent increase in the pressure levels of the cycle, with a slower variation of the compressor inlet pressure. In general it can be noticed again a slower dynamic response with respect to the compressor speed variation.

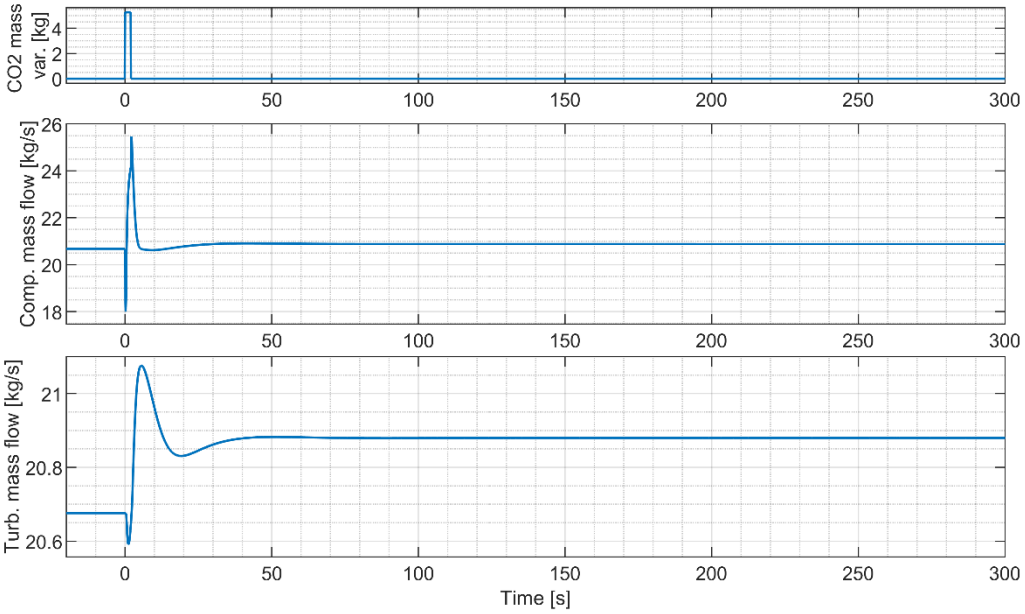


*Figure 96 - Mass flow rates variations*
*in response to a "step" injection of 1% of total mass in 2 seconds*

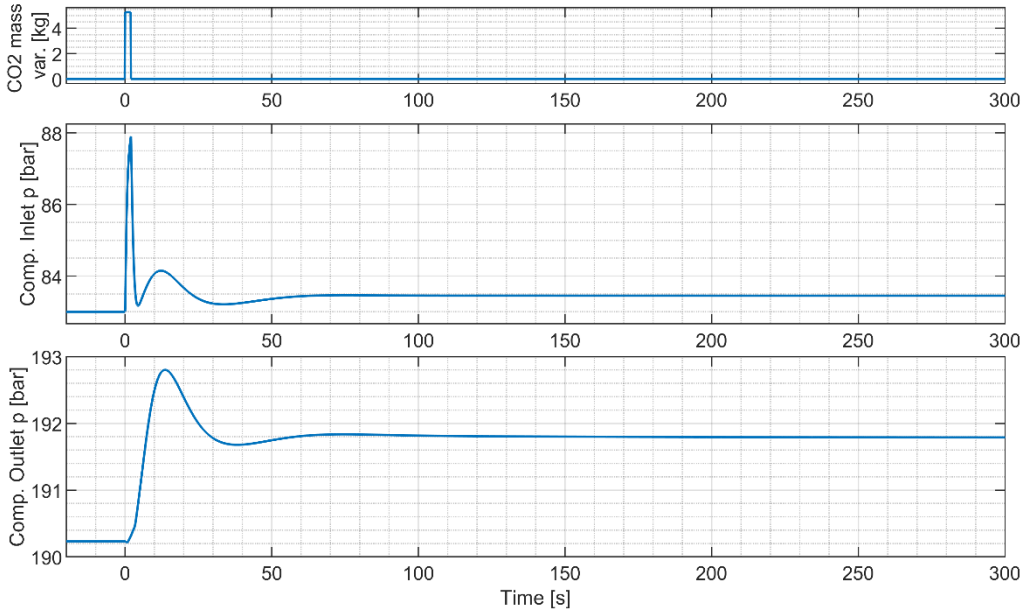


*Figure 97 - Compressor pressures variations*
*in response to a "step" injection of 1% of total mass in 2 seconds*

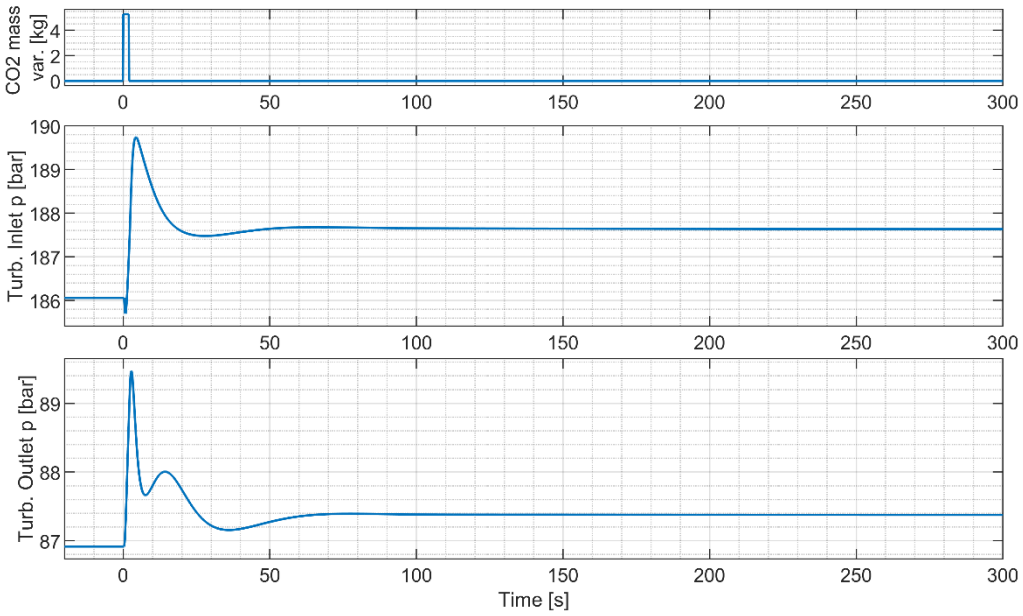


*Figure 98 - Turbine pressures variations*
*in response to a "step" injection of 1% of total mass in 2 seconds*

### 4.4.4 Anti-Surge Valve fractional opening

The opening of the ASV causes the recirculation of part of the mass flow, and thus an increase of the compressor mass flow rate and a decrease of the turbine one, as shown in Figure 99.

Figure 100 shows the behaviour of the pressures of the cycle, with a decrease of the pressure ratio. In particular, the spike response in the compressor inlet pressure and its slow regime dynamic, needed further study and attention.

Finally, Figure 101 presents the surge margin (in the definition at constant pressure ratio). The graph shows an increase in the surge margin with an opening of the ASV, but the dynamic behaviour characterised by an undershoot could have caused problems and was carefully managed during the control tuning phase.

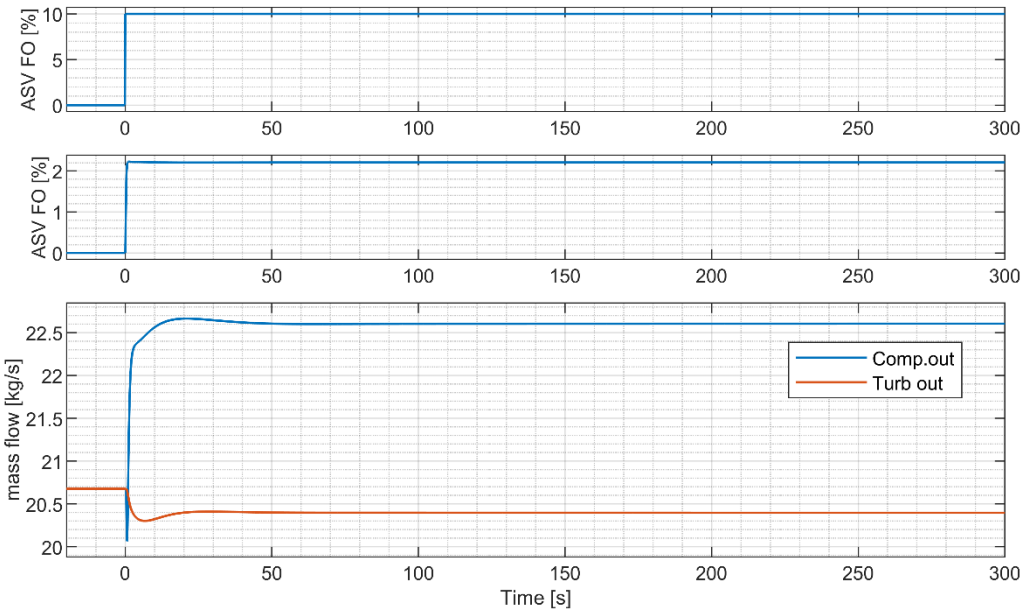


*Figure 99 - Mass flow rates variations*
*in response to a step variation of ASV FO from 0% to 10%*

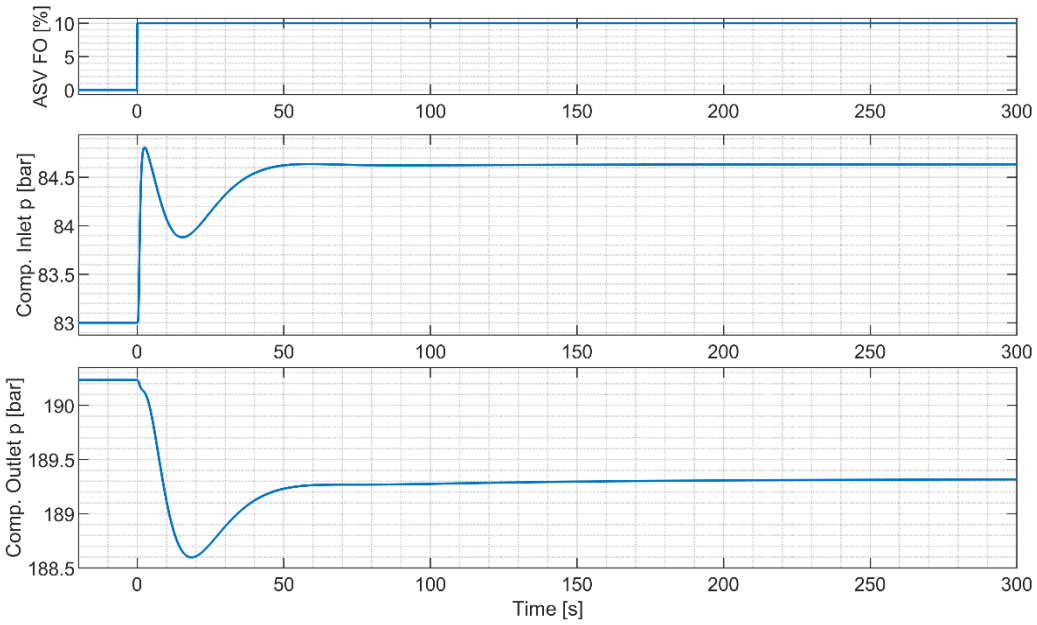


*Figure 100 - Compressor pressures variations*
*in response to a step variation of ASV FO from 0% to 10%*

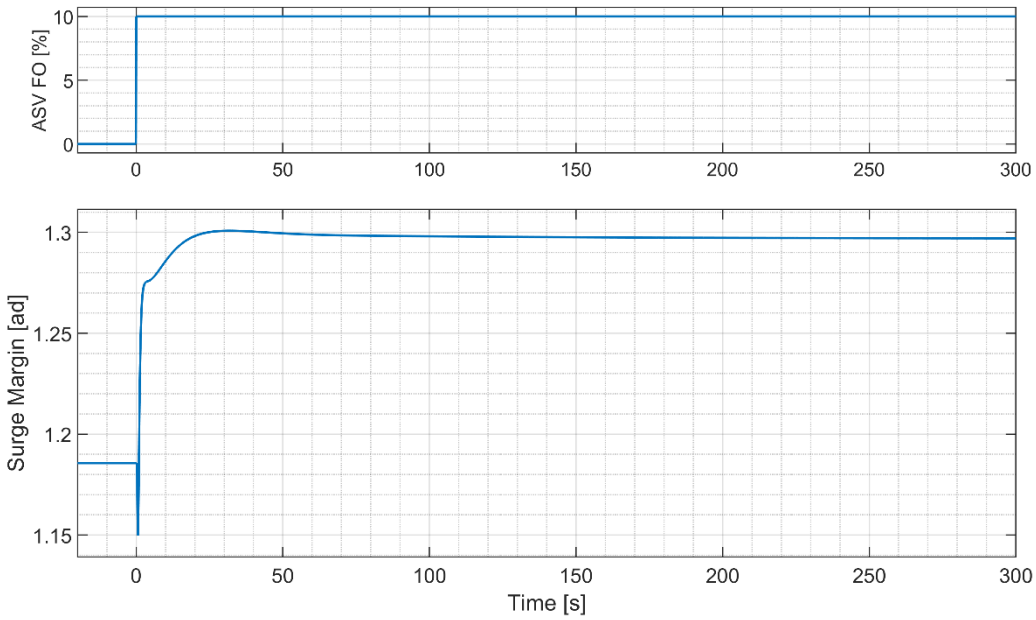


*Figure 101 - Surge Margin (const. PR) variation*
*in response to a step variation of ASV FO from 0% to 10%*

### 4.4.5 Fan air mass flow of the adiabatic cooler

The mass flow rate of the fans of the adiabatic cooler is used to regulate the compressor inlet temperature. Figure 102 shows the variation of the temperatures of the compressor given a variation of the air flow in the fans of the adiabatic cooler. A 10% reduction with respect to the full load conditions returns a variation of 1.5°C around the design point value.

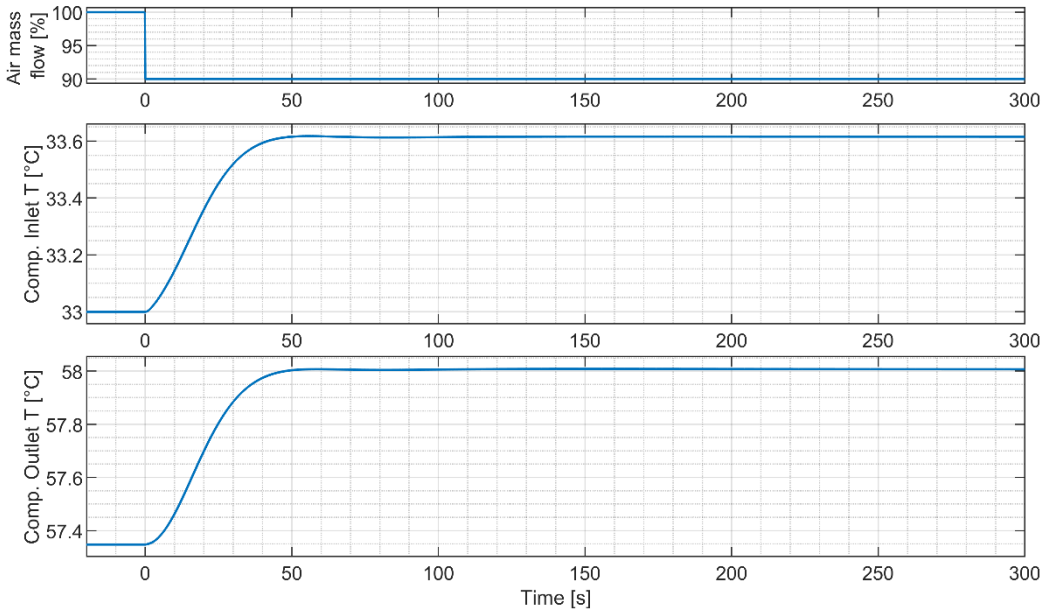


*Figure 102 - Compressor temperatures variation in response to a step variation of air mass flow rate from 100% to 90%*

## 4.5 Control development and implementation

After the analysis of the responses of the plant to changes in the main control variables, actual controllers were implemented in the model to finally test the controlled behaviour of the demo-plant.

Controllers are fundamentals to operate the plant while also respecting all the strict constraints that operating this supercritical plant requires. In fact, during the operation of the plant, it is necessary to maintain a safety margin in the compressor intake from the $CO_2$ critical point; however, at the same time, inlet pressure and temperature must be always kept as close as possible to the design point, even during transients, for performance maximisation. Moreover, compressor surge must be prevented, thus the surge margin $K_p$ needs to be tracked and it is assumed that values over 1.1 can ensure safe operation of the compressor.

Given all these constraints, it is necessary to design a control philosophy able to regulate the plant and guarantee an efficient and safe operation. Based on previous off-design analyses, a control strategy has been proposed, and it is resumed in Table 26, with the addition of the controller of the compressor inlet temperature, which has to be regulated through the mass flow rate of air through the cooler.

*Table 26 - Control philosophy.*

| **Controlled variable** | **Manipulated variable** |
|---|---|
| Plant net power ($P_{net}$) | Compressor speed |
| Turbine inlet temperature ($T_{T,in}$) | MS mass flow rate |
| Compressor inlet pressure ($p_{C,in}$) | Total $CO_2$ mass in the loop |
| Compressor inlet temperature ($T_{C,in}$) | Air mass flow rate |

In this chapter and the following, the controllers of $P_{net}$, $T_{T,in}$, $T_{C,in}$, and $p_{C,in}$ are designed, implemented and tested on the dynamic model, following a well-established tuning procedure.

Due to small misalignments in mass flows and in the design of the main components, and uncertainties in the balance of plant and auxiliaries of the plant, the design point condition that can be obtained in the dynamic model, where the actual designs are implemented, is slightly different from the theoretical design point that was selected for the demo-plant. For this reason, the definition of design point is replaced by the one of Full Load condition, being the latter the one that is obtained from the dynamic model developed, and shown in Table 27.

*Table 27 – Comparison between Parameters in Full Load (100%) Condition and their Design Values*

| *Parameter* | *Design Point* | *Full Load* | *Unit* |
|---|---|---|---|

| | | | |
|---|---|---|---|
| *Compressor Inlet Temperature* | 33 | 33 | °C |
| *Compressor Inlet Pressure* | 83 | 83 | bar |
| *Turbine Inlet Temperature* | 565 | 565 | °C |
| *CO2 Mass Flow Rate* | 21 | 20.65 | kg/s |
| *MS Mass Flow Rate* | 22.148 | 19.37 | kg/s |
| *Fan Air Mass Flow Rate* | 72.104 | 70.25 | kg/s |
| *Compressor Speed* | 12761 | 12761 | rpm |

The full load condition selected has been achieved by connecting the components and letting the model settling, and later aligning the main controlled values to the desired on-design ones. The so defined Full Load condition has been selected as reference in the further simulations.

During the previously shown off-design analysis, it has been found that a control with a constant turbine inlet temperature leads to the best cycle efficiency; moreover, avoiding great temperature variations, a faster response is expected. For this reason, and also considering that small deviations from the nominal temperature are possible, a simple feed-forward controller determines the MS mass flow necessary to maintain the turbine inlet temperature sufficiently close to the design value, as a function of the $CO_2$ mass flow entering the heat exchangers.

### 4.5.1 Control Tuning

Figure 103 shows the steady-state data implemented as the feed-forward controller, in terms of percentage of the full load (FL) values. The feed-forward controller uses the mass flow rate of $CO_2$ at the turbine inlet to determine the appropriate mass flow rate of the molten salt through the heater, as a fraction of the mass flow rate at full load. For increased precision, the $T_{T,in}$ controller is then adjusted by a proportional-integral-derivative (PID) controller, which acts

on approximately one-twentieth of the nominal feed-forward controller value, and was tuned using the Cohen-Coon step response method, then scaled down by a factor of 20.

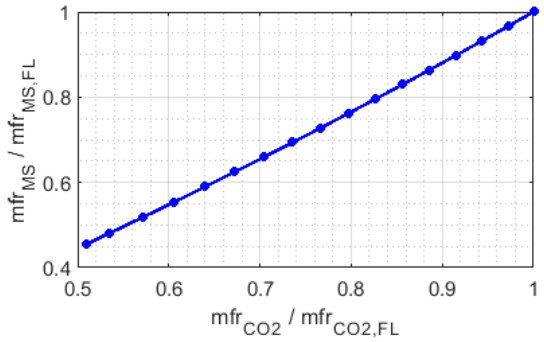


*Figure 103 - The turbine inlet temperature feed-forward controller map*

In a similar manner, another feed-forward controller is used to change the compressor rotational speed based on the net power demand; this steady-state map is shown in Figure 104. In this feed-forward controller it is implemented a map which from the information on the required power output of the plant, changes the compressor speed accordingly.

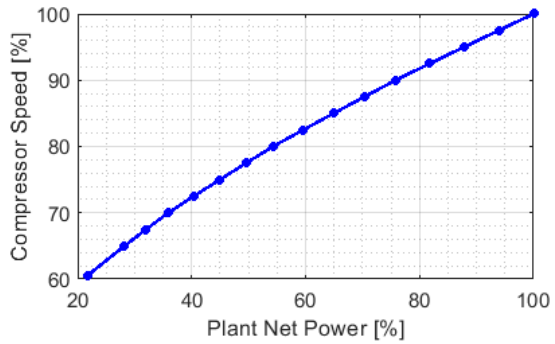


*Figure 104 - The net power feed-forward controller*

The controller of the compressor inlet temperature ($T_{C,in}$) consists of a proportional-integral (PI) controller, which acts on the mass flow rate of air through the cooler, tuned using the Cohen-Coon step response method and scaled down by a factor of 0.6. It is assumed that the controller is able to adjust the flow rate of air continuously and immediately between 10% and 150% of its design value of 72.104 kg/s.

Three different mechanisms were considered for the controller of the compressor inlet pressure ($p_{C,in}$):

1) a simple feedback on-off controller, which changes the internal mass of the loop if the difference between actual pressure and its setpoint (83 bar) exceeds a certain limit (± 0.05 bar);
2) a proportional-integral-derivative (PID) controller, tuned by the Ziegler-Nichols oscillation method and scaled by a factor of 0.1 for stable performance;
3) a feedforward controller, based on the change in compressor speed or power setpoint at each timestep, in conjunction with a steady-state map from compressor speed or power setpoint to total mass in the loop.

Both $p_{C,in}$ feedback controllers (2 and 3) follow the same method of action: if the pressure is too low, more $CO_2$ is introduced from the inventory, and if it is too high, some $CO_2$ is expelled through a venting valve. According to the plant requirements, the control can be considered effective if the pressure is always kept within ± 0.75 bar from the setpoint value.

## 4.6 Dynamic analyses of normal operation: ramp variation of load

In this chapter are reported some of the preliminary analysis on the dynamic controlled behaviour of the plant, analysed in normal operation. In particular, it was analysed the response of the demo-plant to a ramp change in the load (or required power).

First of all, the model was used to simulate the full load (FL) condition (see also Table 27). In this case, the mass flow of $CO_2$ circulating in the plant is equal to 20.65 kg/s, and the mass of molten salts to be provided to the heater is 19.35 kg/s. The simulation showed a generated net power ($P_{net}$) of 1456 kW with an total efficiency ($\eta$) of 21.64%. Then the model was used to define the off-

design performance of the plant, at steady-state, changing the compressor speed between 100% and 60% of its FL value.

Figure 105 shows the values of the total efficiency of the plant, normalised over full-load conditions, with respect to the variation of net power. Finally, the model was used to simulate the transient operation of the plant and to verify the proper operation of the control logics.

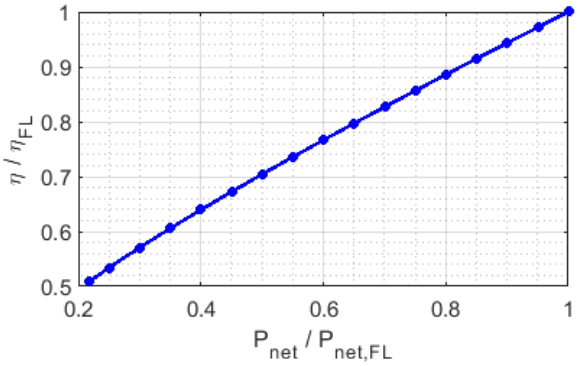


*Figure 105 - Efficiency variation at part load*

### 4.6.1 Tests structure and results

As said, it was important in this analysis to verify the proper operation of the control logic built upon the results from the off-design analysis and the step responses of the plant. To do this, tests were carried out in different conditions, varying the net power of the plant from 100% to 50% of the FL value. The power variation follows a ramp performed over 15 minutes. Some of these tests were designed to also analyse the behaviour of the plant without some of the controllers. Table 28 shows the conditions adopted in each test. The options listed for the $p_{C,in}$ control refer to the various control types presented in the previous chapter: "on-off, 0.1 kg/s" refers to the use of an on-off controller with a mass flow rate of 0.1 kg/s; "on-off, 0.2 kg/s" refers to the use of an on-off controller with a mass flow rate of 0.2 kg/s; "PID" refers to the use of the oscillation-tuned PID controller; "Feedforward" refers to the use of a feedforward controller based on the change in net power setpoint. When the temperature controllers are listed as inactive ("No") in the table, this means that

the mass flow rate of the air (in the cooler) or molten salt (in the heater) is left constant, at its nominal flow rate. When the $p_{C,in}$ controller is listed as inactive, no inventory action is taken.

*Table 28 – Conditions of the different transient tests.*

| *Test case* | *Load setpoint variation* | *Ramp duration* | *$p_{C,in}$ control* | *$T_{T,in}$ control* | *$T_{C,in}$ control* | *$T_{Air}$, inlet of Cooler* |
|---|---|---|---|---|---|---|
| *Test z* | 100% to 75.1% | 448 s | No | No | No | 299.15 K |
| *Test a* | 100% to 50% | 900 s | on-off, 0.1 kg/s | Yes | Yes | 299.15 K |
| *Test b* | 100% to 50% | 900 s | on-off, 0.2 kg/s | Yes | Yes | 299.15 K |
| *Test c* | 100% to 63.9% | 650 s | No | Yes | Yes | 299.15 K |
| *Test d* | 100% to 50% | 900 s | PID | No | Yes | 299.15 K |
| *Test e* | 100% to 73.9% | 469 s | PID | Yes | No | 299.15 K |
| *Test f* | 100% to 50% | 900 s | PID | Yes | Yes | 299.15 K |
| *Test g* | 100% to 50% | 900 s | PID | Yes | Yes | 301.15 K |
| *Test h* | 100% to 50% | 900 s | PID | Yes | Yes | 297.15 K |
| *Test i* | 100% to 50% | 900 s | Feedforward | Yes | Yes | 299.15 K |

Tests (a), (b), (c), (f), (i), and (j) compare the various options for $p_{C,in}$ control. Tests (d) and (f) evaluate the $T_{T,in}$ control. Tests (e) and (f) evaluate the $T_{C,in}$ control, and tests (f), (g), and (h) show the effect of the ambient air temperature on cooler performance. Tests (z), (c), (d), (e), and (f) compare the performance of the uncontrolled system with the system when only one control is inactive, and finally the system with all controls active.

During each test, the ramp variation of $P_{net}$ setpoint translates into a variation of the compressor speed. This allows to change the mass flow rate of $CO_2$ in the whole cycle, which is what actually drives the net power variation, and, as a

consequence, the variations of pressure ratio in the closed cycle and of temperature at the turbine inlet.

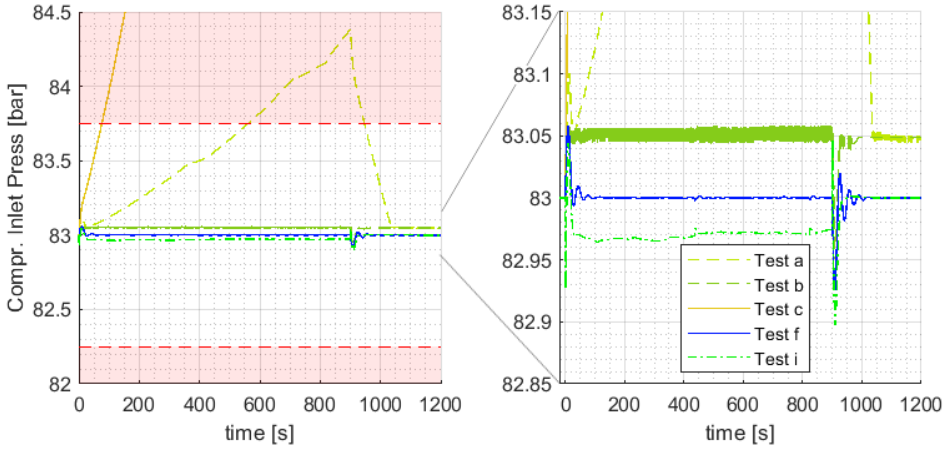


*Figure 106 - Compressor inlet pressure with and without pC,in control implementation. Test a: on-off control with inventory flow rate of 0.1 kg/s. Test b: on-off control with inventory flow rate of 0.2 kg/s. Test c: No pC,in control. Test f: All controls active. Test i: Feed-forward control from the load setpoint.*

Figure 106 shows the $p_{C,in}$ during the tests. Test (c) shows the uncontrolled behaviour of the pressure, with a variation of 4 bar in response to a variation of 50% of the load. Tests (a) and (b) show the effectiveness of the implemented pressure control. In particular, test (a) shows that with a $CO_2$ mass venting of 0.01 kg/s, the pressure value deviates from the setpoint value during the ramp, exceeding the limit of ±0.75 bar by almost 0.65 bar, reaching a peak of 84.4 bar before finally returning to the setpoint almost two minutes after the end of the ramp. On the other hand, test (b) shows that a mass variation of 0.02 kg/s leads to successful regulation of $p_{C,in}$, which stays within 0.01 bar of the minimum pressure required to activate venting (setpoint +0.05 bar) for the duration of the ramp. However, this is achieved through sudden and sometimes continuous shifts of the inventory venting valve during its operation. Moreover, at the moment of this analysis this model did not account for any delay between the controller action and the increase of mass flow at the compressor inlet, so it is likely that this behaviour would be difficult if not impossible to achieve in a physical system.

Figure 107 shows the surge margin ($K_p$) behaviour during the tests with at least one control inactive. It is important to recall that values over 1.1 represent a safe operative condition. Thus, since values of $K_p$ lower than 1.1 were reached during most tests, further simulations will be necessary to include the action of the anti-surge valve. Moreover, the graph shows once again how the influence of the stability of the compressor inlet point is paramount in these plants. Indeed, without a control either on the temperature or the pressure, at the inlet of the compressor, the plant is lead into instability through the compressor surge behaviour.

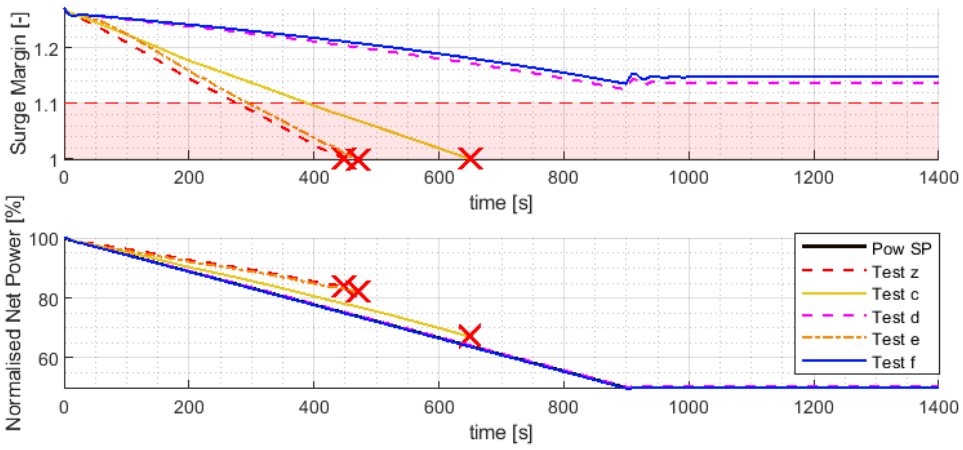


*Figure 107 - Surge margin with and without control implementation. Test z: No controls. Test c: No pC,in control. Test d: No TT,in control. Test e: No TC,in control. Test f: All controls active.*

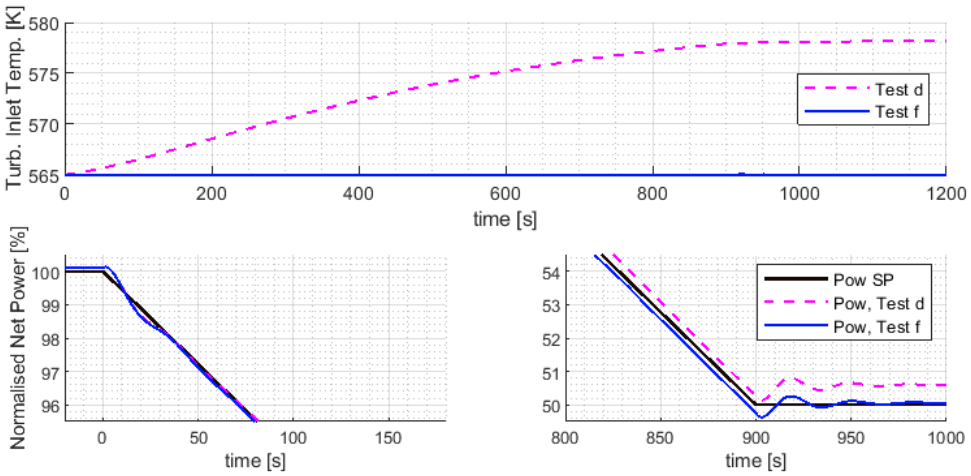


*Figure 108 - Turbine Inlet Temperature ($T_{T,in}$) with and without control implementation. Test d: No $T_{T,in}$ control. Test f: All controls active.*

Figure 108 shows the effectiveness of the control on $T_{T,in}$ behaviour, obtained through the correlation between $CO_2$ and molten salts mass flow rates at the inlets of the heaters: this is evident by comparing the results of test (b) with the ones of test (d), which shows the behaviour of the temperature without a controller. In the uncontrolled case (test d) the $T_{T,in}$ tends to the temperature of the molten salts, fixed at 580°C. It is important to clarify that, if a reliable measurement of the $CO_2$ mass flow at the heater inlet were not available in the real system, a different controller should be implemented, like a PID following the $T_{T,in}$ setpoint.

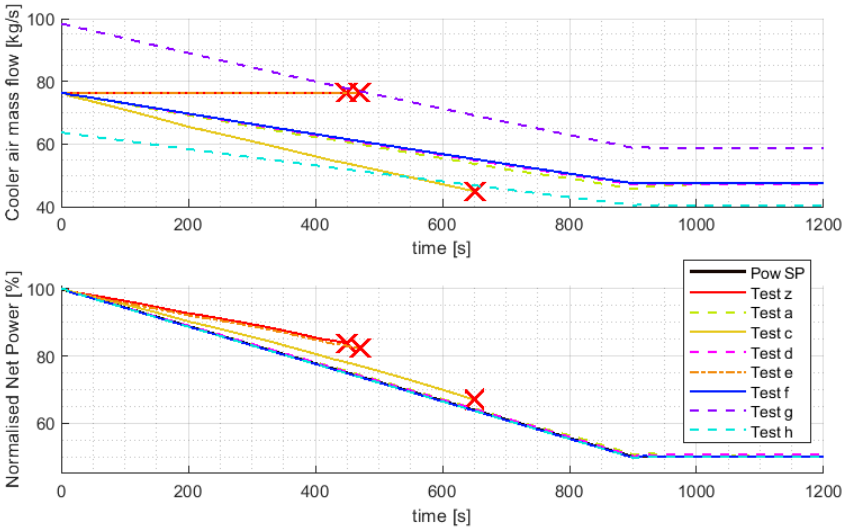


*Figure 109 – Cooler behaviour with different air temperatures*

Figure 109 shows the power ramping down and the behaviour of the main control actuator of the cooler in this analysis, thus the mass flow rate of air (that can be controlled through the fans of the cooler). The same tests as before are shown, and also compared with the case of different ambient temperatures. Since the condition of all the tests and of the test f in particular are the Full Load conditions, at 100% FL the cooler uses only about the 80% of its rated value, which has been designed on the cycle design point DP.

Test a, which was not able to maintain the CIP during the ramp, can be seen in this figure requiring slightly less airflow to achieve the controlled CIT. Tests z and e are horizontal lines, as an "uncontrolled" cooler in this case refers to a constant flow rate for the entire duration of the test.

Test g (+2K to $T_{amb}$) and Test h (-2K to $T_{amb}$) show the dramatic dependence of required cooler air flow on the ambient temperature, mainly due to the fact that the high values of specific heat of the $CO_2$ near the critical point, mean that a small change in temperatures can only be obtained with a consistent change in the amount of exchange heat.

# 5 Conclusion

In this dissertation, it has been presented the development of a simulation tool aiming at the design and optimisation of energy systems, focusing in particular on the study of closed cycles, or processes, at fixed composition.

The need of such a tool has been promoted by the study of closed power cycles evolving carbon dioxide, especially in supercritical state. In fact, the interest in the evaluation of the possible layouts and applications of such cycles in different fields of the energy production, with a focus on their techno-economic performances, drove the development of a way to evaluate this technology in different aspects and compare it with more traditional ones.

Given the large variation of the thermophysical properties of the chosen fluid, the thermo-economic tool TEMP-EVO, evolution of the preexisting WTEMP in TPG, has been newly developed in MATLAB and integrated with thermophysical libraries.

The TEMP-EVO tool implements a modular system in order to let the user assembly the desired process using the predesigned components, that resolve simple characteristic equations of the real equipment associated with them. The tool is structured so that all the information that characterise the cycle is collected and stored in few data (such as the *cycle definition structure* and the *properties matrix*) that are passed through the blocks in which the tool is composed (inputs, thermodynamics, economic analysis, etc). This also allows for the definition of different key performance indicators depending on the process of interest to the user, and to establish sensitivity and optimisation analyses on the desired values.

The thermodynamic resolution is available in two possible methods, to favour either speed, with the passing-information logic, or user-friendliness and freedom in the layout choice, with the complete-system logic. The solvers implemented are developed to be able to take advantage of the native MATLAB

functions to increase the robustness of the code, as well as to be able to follow the in-house developed resolution method (such as the modified Newton method) to allow more control to the experienced user. For both of these options some mathematical methods have been studied and implemented, mainly resulting in the management of the initial guess values and in the equation ordering. In this way, the resolution methods have been managed to increase the robustness and affordability of the solution, as well as to increase the performance and modularity of the code itself.

The modularity, not only of the implemented components, but also of the structure of the code also, allows for partial use of the code itself, and most of all allows for easiness in the development of future upgrades as well as in the modification of existing code. Since the problem definition (thus the definition of the process/cycle of interest) is quite disconnected to the resolution of the problem itself, modifications and improvements can be done separately without affecting all the general structure of the code. Moreover, adding new components can be done by simply changing the characteristic equations to the copy of an existing component function, keeping the same structure for interface with the rest of the tool. Similarly, adding new features to an equipment already existing in the tool can be done by adding a new component function for the same real equipment that includes more (or different) characteristic equations.

The tool has been used to perform mainly analyses of closed cycles, some of them reported in this dissertation. Different configurations of sCO2 cycles have been studied and also compared with traditional technologies such as steam. Comparable results between these technologies were achieved from a performance and economical point of view, also showing the simplest cycles to be competitive from a techno-economical point of view. Despite this result, new analyses (together with technological considerations on the feasibility and unexpected costs) are necessary to assess the main target markets and applications in which the sCO2 technology can provide advantages to investors. One of such applications can be the thermo-mechanical storage technologies,

and an example of that is provided in the last application showed in this thesis, regarding a Thermally-Integrated PTES. Aiming at providing also flexibility to process industries, high value of RTE for this kind of battery were achieved; the exergetic analysis showed good performance as well, even though the advantages of this technology have to be studied with the development of dispatch strategies, and analysed in favourable markets were long-term energy storage (LDES) is required, such as electricity markets with high renewable energy penetration and with high price span.

Next steps in the enhancements of the tool can be identified in the development of a graphical interface, as well as in the upgrade towards an object-oriented approach, that would fits well with the modular approach developed. On the general structure, also a method to manage the variation of fluids composition inside the loops (e.g., treating it as new fluid parameters) can unlock the development of new components and new processes that can be analysed with the tool. Finally, in a separate way also improvements to the solver methods can be performed, such as a combination between the two approaches presented, to increase the speed and robustness of the iterative process and of the solution.

Finally for what concerns not only the thermo-economic aspects of sCO2 cycles but also their dynamic performances and operational management, the latest chapter of the this dissertation presents the work related to the application of the existing TRANSEO tool, a tool for dynamic analysis of energy systems, to adapt it to the use of sCO2. In particular this work was carried out in the framework of the EU Project SOLARSCO2OL, and aimed at the evaluation of sCO2 cycles not only at a techno-economic level, as done with TEMP-EVO, but also to their evaluate dynamic behaviour. A simple recuperated cycle was thus implemented in a modified version of TRANSEO, and finally controllers were implemented, tuned, and tested. Despite the results are still preliminary and need further study and verification on the demonstration site of the project, the first results highlight the capability of such plants of having a fast response, possibly being an advantage against the more traditional technologies.

# Bibliography


[1] IEA, 2024, *World Energy Outlook 2023*, Paris.

[2] Manabe, S., 2019, "Role of Greenhouse Gas in Climate Change**," Tellus, Series A: Dynamic Meteorology and Oceanography, **71**(1), pp. 1–13.

[3] Blunden, J., Boyer, T., and Bartow-Gillies, E., 2023, "State of the Climate in 2022," Bull Am Meteorol Soc, **104**(9), pp. S1–S516.

[4] Dyurgerov, M. B., and Meier, M. F., 2000, "Twentieth Century Climate Change: Evidence from Small Glaciers," Proceedings of the National Academy of Sciences, **97**(4), pp. 1406–1411.

[5] Burrell, A. L., Evans, J. P., and De Kauwe, M. G., 2020, "Anthropogenic Climate Change Has Driven over 5 Million Km2 of Drylands towards Desertification," Nat Commun, **11**(1), p. 3853.

[6] Wright, L. P., Zhang, L., Cheng, I., Aherne, J., and Wentworth, G. R., 2018, "Impacts and Effects Indicators of Atmospheric Deposition of Major Pollutants to Various Ecosystems - A Review," Aerosol Air Qual Res, **18**(8), pp. 1953–1992.

[7] Barna, C., 2020, "Current Socio-Economic Challenges. Approaching Sustainability and Social Economy. Guest Editor's Note.," Management Dynamic in the Knowledge Economy, **1**(8), pp. 7–9.

[8] European Commission, 2019, "The European Green Deal" [Online]. Available: https://commission.europa.eu/strategy-and-policy/priorities-2019-2024/european-green-deal_en. [Accessed: 12-Feb-2024].

[9] Hainsch, K., Göke, L., Kemfert, C., Oei, P., and Von Hirschhausen, C., 2020, "European Green Deal: Using Ambitious Climate Targets and Renewable Energy to Climb Out of the Economic Crisis," DIW Weekly Report, **28+29**, pp. 303–310.

[10] European Commission, 2020, "Horizon Europe" [Online]. Available: https://research-and-innovation.ec.europa.eu/funding/funding-opportunities/funding-programmes-and-open-calls/horizon-europe_en. [Accessed: 12-Feb-2024].

[11] European Commission, 2020, "NextGenerationEU" [Online]. Available: https://commission.europa.eu/strategy-and-policy/recovery-plan-europe_en. [Accessed: 12-Feb-2024].

[12] Sun, K., Xiao, H., Liu, S., You, S., Yang, F., Dong, Y., Wang, W., and Liu, Y., 2020, "A Review of Clean Electricity Policies—From Countries to Utilities," Sustainability, **12**(19), p. 7946.

[13] IRENA, 2014, *Renewable Energy Prospects: China*.

[14] Bilgili, M., Ozbek, A., Sahin, B., and Kahraman, A., 2015, "An Overview of Renewable Electric Power Capacity and Progress in New Technologies in the World," Renewable and Sustainable Energy Reviews, **49**, pp. 323–334.

[15] IEA, 2024, *Renewables 2023*, Paris.

[16] Batalla-Bejerano, J., and Trujillo-Baute, E., 2016, "Impacts of Intermittent Renewable Generation on Electricity System Costs," Energy Policy, **94**, pp. 411–420.

[17] White, M. T., Bianchi, G., Chai, L., Tassou, S. A., and Sayma, A. I., 2021, "Review of Supercritical CO 2 Technologies and Systems for Power Generation," **185**(December 2020).

[18] Dostal, V., Driscoll, M. J., and Hejzlar, P., 2004, “Advanced Nuclear Power Technology Program A Supercritical Carbon Dioxide Cycle for Next Generation Nuclear Reactors.”
[19] Dostal, V., Hejzlar, P., and Driscoll, M. J., 2006, “The Supercritical Carbon Dioxide Power Cycle: Comparison to Other Advanced Power Cycles,” Nucl Technol, **154**(3), pp. 283–301.
[20] Angelino, G., 1968, “Carbon Dioxide Condensation Cycles For Power Production,” Journal of Engineering for Power, **90**(3), pp. 287–295.
[21] Feher, E. G., 1968, “The Supercritical Thermodynamic Power Cycle,” Energy Conversion, **8**(2), pp. 85–90.
[22] Ahn, Y., Bae, S. J., Kim, M., Cho, S. K., Baik, S., Lee, J. I., and Cha, J. E., 2015, “Review of Supercritical CO<inf>2</Inf> Power Cycle Technology and Current Status of Research and Development,” Nuclear Engineering and Technology, **47**(6), pp. 647–661.
[23] Crespi, F., Gavagnin, G., Sanchez, D., and Martinez, G. S., 2018, “Analysis of the Thermodynamic Potential of Supercritical Carbon Dioxide Cycles : A Systematic Approach,” **140**(May), pp. 1–10.
[24] Baik, Y.-J., Kim, M., Chang, K. C., and Kim, S. J., 2011, “Power-Based Performance Comparison between Carbon Dioxide and R125 Transcritical Cycles for a Low-Grade Heat Source,” Appl Energy, **88**(3), pp. 892–898.
[25] Liu, Y., Wang, Y., and Huang, D., 2019, “Supercritical CO2 Brayton Cycle: A State-of-the-Art Review,” Energy, **189**, p. 115900.
[26] Wright, S. A., Davidson, C. S., and Scammell, W. O., “Thermo - Economic Analysis of Four SCO2 Waste Heat Recovery Power Systems,” pp. 1–16.
[27] Alfani, D., Binotti, M., Macchi, E., Silva, P., and Astolfi, M., 2021, “SCO2 Power Plants for Waste Heat Recovery: Design Optimization and Part-Load Operation Strategies,” Appl Therm Eng, **195**.
[28] Cho, S. K., Kim, M., Baik, S., Ahn, Y., and Lee, J. I., 2015, “Investigation of the Bottoming Cycle for High Efficiency Combined Cycle Gas Turbine System with Supercritical Carbon Dioxide Power Cycle,” *Proceedings of the ASME Turbo Expo*.
[29] Kim, M. S., Ahn, Y., Kim, B., and Lee, J. I., 2016, “Study on the Supercritical CO<inf>2</Inf> Power Cycles for Landfill Gas Firing Gas Turbine Bottoming Cycle,” Energy, **111**, pp. 893–909.
[30] Bae, S. J., Lee, J., Ahn, Y., and Lee, J. I., 2014, “Preliminary Studies of Compact Brayton Cycle Performance for Small Modular High Temperature Gas-Cooled Reactor System,” Ann Nucl Energy, **75**, pp. 11–19.
[31] Le Moullec, Y., 2013, “Conceptual Study of a High Efficiency Coal-Fired Power Plant with CO2 Capture Using a Supercritical CO2 Brayton Cycle,” Energy, **49**, pp. 32–46.
[32] Yin, J., 2020, “Review of Supercritical CO 2 Power Cycles Integrated with CSP,” (May 2019), pp. 1337–1369.
[33] Crespi, F., Sanchez, D., Rodríguez, J. M., and Gavagnin, G., 2020, “A Thermo-Economic Methodology to Select SCO 2 Power Cycles for CSP Applications,” **147**, pp. 2905–2912.
[34] Turchi, C. S., Ma, Z., Neises, T. W., and Wagner, M. J., 2013, “Thermodynamic Study of Advanced Supercritical Carbon Dioxide Power Cycles for Concentrating Solar Power Systems,” Journal of Solar Energy Engineering, Transactions of the ASME, **135**(4).

[35] Neises, T., and Turchi, C., 2014, "A Comparison of Supercritical Carbon Dioxide Power Cycle Configurations with an Emphasis on CSP Applications," *Energy Procedia*, pp. 1187–1196.
[36] Glos, S., Hansper, J., Grotkamp, S., and Wechsung, M., 2019, "Assessment of Performance and Costs of CO2 Based Next Level Geothermal Power (NLGP) Systems," *3rd European Supercritical CO2 Conference, September 19-20, 2019, Paris, France*, Paris.
[37] McTigue, J., Farres-Antunez, P., Ellingwood, K., Neises, T., and White, A., 2020, "Pumped Thermal Electricity Storage with Supercritical CO2 Cycles and Solar Heat Input," *The Vii International Young Researchers' Conference – Physics, Technology, Innovations (Pti-2020)*, p. 190024.
[38] Astolfi, M., Rizzi, D., Macchi, E., and Spadacini, C., 2022, "A Novel Energy Storage System Based on Carbon Dioxide Unique Thermodynamic Properties," J Eng Gas Turbine Power, **144**(8).
[39] Trevisan, S., Shamsi, S. S. M., Maccarini, S., Barberis, S., and Guedez, R., 2023, "Techno-Economic Assessment of CO2-Based Power to Heat to Power Systems for Industrial Applications," J Eng Gas Turbine Power, **145**(12).
[40] Barberis, S., Maccarini, S., Shamsi, S. S. M., and Traverso, A., 2023, "Untapping Industrial Flexibility via Waste Heat-Driven Pumped Thermal Energy Storage Systems," Energies (Basel), **16**(17).
[41] Liu, L., Yang, Q., and Cui, G., 2020, "Supercritical Carbon Dioxide(S-Co<inf>2</Inf>) Power Cycle for Waste Heat Recovery: A Review from Thermodynamic Perspective," Processes, **8**(11), pp. 1–18.
[42] "Alfa Laval Wet Surface Air Cooler" [Online]. Available: https://www.alfalaval.co.uk/products/heat-transfer/wet-surface-air-heat-exchangers/wet-surface-air-heat-exchangers/niagara-wet-surface-air-coolers/. [Accessed: 13-Feb-2024].
[43] Moisseytsev, A., and Sienicki, J. J., 2014, "Recent Developments in SCO2 Cycle Dynamic Modeling and Analysis at ANL," *The 4th International Symposium - Supercritical CO2 Power Cycles, September 9-10, 2014, Pittsburgh, Pennsylvania*, Pittsburgh, Pennsylvania.
[44] Marchionni, M., Bianchi, G., and Tassou, S. A., 2021, "Transient Analysis and Control of a Heat to Power Conversion Unit Based on a Simple Regenerative Supercritical CO<inf>2</Inf> Joule-Brayton Cycle," Appl Therm Eng, **183**.
[45] Trinh, T. Q., 2009, *Dynamic Response of the Supercritical CO2 Brayton Recompression Cycle to Various System Transients*.
[46] Luu, M. T., Milani, D., McNaughton, R., and Abbas, A., 2017, "Analysis for Flexible Operation of Supercritical CO2 Brayton Cycle Integrated with Solar Thermal Systems," Energy, **124**, pp. 752–771.
[47] Luu, M. T., Milani, D., McNaughton, R., and Abbas, A., 2018, "Advanced Control Strategies for Dynamic Operation of a Solar-Assisted Recompression Supercritical CO2 Brayton Power Cycle," Appl Therm Eng, **136**, pp. 682–700.
[48] Liese, E., Albright, J., and Zitney, S. A., 2020, "Startup, Shutdown, and Load-Following Simulations of a 10 MWe Supercritical CO2 Recompression Closed Brayton Cycle," Appl Energy, **277**, p. 115628.
[49] Avadhanula, V. K., and Held, T. J., 2017, "Transient Modeling of a Supercritical CO2 Power Cycle and Comparison with Test Data," *Proceedings of the ASME Turbo Expo*.

[50] Lock, A., and Bone, V., 2022, "Off-Design Operation of the Dry-Cooled Supercritical CO2 Power Cycle," Energy Convers Manag, **251**, p. 114903.
[51] Neises, T., 2020, "Steady-State off-Design Modeling of the Supercritical Carbon Dioxide Recompression Cycle for Concentrating Solar Power Applications with Two-Tank Sensible-Heat Storage," Solar Energy, **212**, pp. 19–33.
[52] Yang, J., Yang, Z., and Duan, Y., 2020, "Off-Design Performance of a Supercritical CO2 Brayton Cycle Integrated with a Solar Power Tower System," Energy, **201**, p. 117676.
[53] Yu, H., Hartanto, D., Moon, J., and Kim, Y., 2015, "A Conceptual Study of a Supercritical CO2-Cooled Micro Modular Reactor," Energies (Basel), **8**(12), pp. 13938–13952.
[54] Utamura, M., Hasuike, H., Ogawa, K., Yamamoto, T., Fukushima, T., Watanabe, T., and Himeno, T., 2012, "Demonstration of Supercritical CO2 Closed Regenerative Brayton Cycle in a Bench Scale Experiment," *Volume 3: Cycle Innovations; Education; Electric Power; Fans and Blowers; Industrial and Cogeneration*, American Society of Mechanical Engineers, pp. 155–164.
[55] Cho, J., Shin, H., Ra, H.-S., Lee, G., Roh, C., Lee, B., and Baik, Y.-J., 2016, "Development of the Supercritical Carbon Dioxide Power Cycle Experimental Loop in KIER," *Volume 9: Oil and Gas Applications; Supercritical CO2 Power Cycles; Wind Energy*, American Society of Mechanical Engineers.
[56] Ahn, Y., Lee, J., Kim, S. G., Lee, J. I., Cha, J. E., and Lee, S.-W., 2015, "Design Consideration of Supercritical CO2 Power Cycle Integral Experiment Loop," Energy, **86**, pp. 115–127.
[57] Wright, S., Radel, R., Vernon, M., Pickard, P., and Rochau, G., 2010, *Operation and Analysis of a Supercritical CO2 Brayton Cycle.*, Albuquerque, NM, and Livermore, CA (United States).
[58] Kriz, D., Vlcek, P., and Frybort, O., 2023, "SYSTEM ANALYSIS OF EXPERIMENTAL SCO2 CYCLE SOFIA," *Conference Proceedings of the European SCO2 Conference*, pp. 84–92.
[59] Marion, J., Kutin, M., McClung, A., Mortzheim, J., and Ames, R., 2019, "The STEP 10 MWe SCO2 Pilot Plant Demonstration," *Proceedings of the ASME Turbo Expo 2019: Turbomachinery Technical Conference and Exposition. Volume 9: Oil and Gas Applications; Supercritical CO2 Power Cycles; Wind Energy.*, American Society of Mechanical Engineers.
[60] "STEP Project Website" [Online]. Available: https://www.gti.energy/step-demo/step-demo-project/. [Accessed: 22-Jan-2024].
[61] Guédez, R., Barberis, S., Maccarini, S., López-Román, A., Milani, A., Pesatori, E., Oyarzábal, U., and Sánchez, A., 2022, "Design of a 2 MW Molten Salt Driven Supercritical CO2 Cycle and Turbomachinery for the SOLARSCO2OL Demonstration Project," *Proceedings of the ASME Turbo Expo 2022: Turbomachinery Technical Conference and Exposition. Volume 9: Supercritical CO2.*
[62] "SOLARSCO2OL Project Webpage" [Online]. Available: https://www.solarsco2ol.eu/. [Accessed: 15-Jan-2024].
[63] "STEAG EBSILON" [Online]. Available: https://www.ebsilon.com/en/. [Accessed: 14-Feb-2024].
[64] "GateCycle" [Online]. Available: http://www.wyattllc.com/GateCycle/GateCycle.html. [Accessed: 14-Feb-2024].

[65] “IPSEpro” [Online]. Available: https://www.simtechnology.com/cms/ipsepro/process-simulation-and-heat-balance-software. [Accessed: 14-Feb-2024].
[66] “Thermoflow” [Online]. Available: https://www.thermoflow.com/. [Accessed: 14-Feb-2024].
[67] “Aspen Plus” [Online]. Available: https://www.aspentech.com/en/products/engineering/aspen-plus. [Accessed: 14-Feb-2024].
[68] “ProSim” [Online]. Available: https://prosim-ar.com/. [Accessed: 14-Feb-2024].
[69] Traverso, A., Massardo, A. F., Cazzola, W., and Lagorio, G., 2004, “WIDGET-TEMP: A Novel Web-Based Approach for Thermoeconomic Analysis and Optimization of Conventional and Innovative Cycles,” *Volume 7: Turbo Expo 2004*, ASMEDC, pp. 623–631.
[70] Bell, I. H., Wronski, J., Quoilin, S., and Lemort, V., 2014, “Pure and Pseudo-Pure Fluid Thermophysical Property Evaluation and the Open-Source Thermophysical Property Library CoolProp,” Ind Eng Chem Res, **53**(6), pp. 2498–2508.
[71] Lemmon, Bell, Huber, and McLinden, 2018, “NIST Standard Reference Database 23: Reference Fluid Thermodynamic and Transport Properties-REFPROP, Version 10.0, National Institute of Standards and Technology,” Standard Reference Data Program.
[72] Span, R., and Wagner, W., 1996, “A New Equation of State for Carbon Dioxide Covering the Fluid Region from the Triple-Point Temperature to 1100 K at Pressures up to 800 MPa,” J Phys Chem Ref Data, **25**(6), pp. 1509–1596.
[73] Assadi, M., 2000, “Methods and Tools for Analysis and Optimization of Power Plants,” Lund Institute of Technology.
[74] “MATLAB Fsolve” [Online]. Available: https://it.mathworks.com/help/optim/ug/fsolve.html. [Accessed: 14-Feb-2024].
[75] Lukšan, L., and Vlček, J., 2017, “New Quasi-Newton Method for Solving Systems of Nonlinear Equations,” APPLICATIONS OF MATHEMATICS, **62**(2), pp. 121–134.
[76] Polyak, B. T., 2006, “Newton-Kantorovich Method and Its Global Convergence,” Journal of Mathematical Sciences, **133**(4), pp. 1513–1523.
[77] Brewster, M. E., and Kannan, R., 1984, “Nonlinear Successive Over-Relaxation,” Numer Math (Heidelb), **44**(2), pp. 309–315.
[78] “MATLAB Cond” [Online]. Available: https://it.mathworks.com/help/matlab/ref/cond.html. [Accessed: 14-Feb-2024].
[79] Saad, Y., and Schultz, M. H., 1986, *GMRES: A GENERALIZED MINIMAL RESIDUAL ALGORITHM FOR SOLVING NONSYMMETRIC LINEAR SYSTEMS**.
[80] “MATLAB Gmres” [Online]. Available: https://it.mathworks.com/help/matlab/ref/gmres.html. [Accessed: 14-Feb-2024].
[81] Foncubierta Blázquez, J. L., Rodríguez Maestre, I., González Gallero, F. J., and Mena Baladés, J. D., 2016, “Reduction of Computation Time in Building Energy Performance Simulation Programs by Applying Tearing Techniques,” Energy Build, **130**, pp. 667–675.
[82] Pissanetzky Sergio, 1984, *Sparse Matrix Technology*, Elsevier.
[83] Baharev, A., Domes, F., and Neumaier, A., 2017, “A Robust Approach for Finding All Well-Separated Solutions of Sparse Systems of Nonlinear Equations,” Numer Algorithms, **76**(1), pp. 163–189.
[84] Dulmage, A. L., and Mendelsohn, N. S., 1958, “Coverings of Bipartite Graphs,” Canadian Journal of Mathematics, **10**, pp. 517–534.

[85] “DMPERM MATLAB Dumalge-Mendelsohn Permutation” [Online]. Available: https://it.mathworks.com/help/matlab/ref/dmperm.html. [Accessed: 13-Feb-2024].
[86] Pothen, A., and Fan, C.-J., 1990, “Computing the Block Triangular Form of a Sparse Matrix,” ACM Transactions on Mathematical Software, **16**(4), pp. 303–324.
[87] Tarjan, R., 1972, “Depth-First Search and Linear Graph Algorithms,” SIAM Journal on Computing, **1**(2), pp. 146–160.
[88] Kuczenski, B., 2024, “Tarjan(e), MATLAB Central File Exchange.” [Online]. Available: https://www.mathworks.com/matlabcentral/fileexchange/50707-tarjan-e. [Accessed: 13-Feb-2024].
[89] Guccione, S., Trevisan, S., Guedez, R., Laumert, B., MacCarini, S., and Traverso, A., 2022, “TECHNO-ECONOMIC OPTIMIZATION OF A HYBRID PV-CSP PLANT WITH MOLTEN SALT THERMAL ENERGY STORAGE AND SUPERCRITICAL CO2 BRAYTON POWER CYCLE,” *Proceedings of the ASME Turbo Expo*.
[90] Shi, D., Zhang, L., Xie, Y., and Zhang, D., 2019, “Aerodynamic Design and Off-Design Performance Analysis of a Multi-Stage S-CO2 Axial Turbine Based on Solar Power Generation System,” Applied Sciences, **9**(4), p. 714.
[91] Kalra, C., Sevincer, E., Brun, K., Hofer, D., and Moore, J., 2014, “DEVELOPMENT OF HIGH EFFICIENCY HOT GAS TURBO-EXPANDER FOR OPTIMIZED CSP SUPERCRITICAL CO2 POWER BLOCK OPERATION,” *The 4th International Symposium - Supercritical CO2 Power Cycles, September 9-10, 2014, Pittsburgh, Pennsylvania*, Pittsburgh, Pennsylvania.
[92] Glos, S., Lippe, P. R., Schlehuber, D., Kobler, S., and Wechsung, M., “DESIGN CONSIDERATIONS OF SCO SCO2 TURBINES DEVELOPED WITHIN THE CARBOSOLA PROJECT,” *The 4th European SCO2 Conference for Energy Systems, March 23-24, 2021, Online Conference*, Online.
[93] Bidkar, R., Mann, A., Singh, R., Sevincer, E., Cich, S., Day, M., Kulhanek, C. D., Thatte, A., Peter, A. M., Hofer, D., and Moore, J., 2016, “Conceptual Designs of 50MWe and 450MWe Supercritical CO2 Turbomachinery Trains for Power Generation from Coal. Part 1: Cycle and Turbine,” *The 5th International Symposium - Supercritical CO2 Power Cycles March 28-31, 2016, San Antonio, Texas*, San Antonio, Texas.
[94] Brun, K., Friedman, P., and Dennis, R., 2017, *Fundamentals and Applications of Supercritical Carbon Dioxide (SCO₂) Based Power Cycles*, Woodhead Publishing.
[95] Guo, J., 2016, “Design Analysis of Supercritical Carbon Dioxide Recuperator,” Appl Energy, **164**, pp. 21–27.
[96] Incropera, F. P., DeWitt, D. P., Bergman, T. L., and Lavine, A. S., 1996, *Fundamentals of Heat and Mass Transfer*, Wiley, New York.
[97] Churchill, S. W., and Bernstein, M., 1977, “A Correlating Equation for Forced Convection From Gases and Liquids to a Circular Cylinder in Crossflow,” J Heat Transfer, **99**(2), pp. 300–306.
[98] Gnielinski, V., 1976, “New Equations for Heat and Mass Transfer in Turbulent Pipe and Channel Flow,” International Journal of Chemical Engineering.
[99] Kandlikar, S. G., 1990, “A General Correlation for Saturated Two-Phase Flow Boiling Heat Transfer Inside Horizontal and Vertical Tubes,” J Heat Transfer, **112**(1), pp. 219–228.
[100] Chato, J., 1960, “Laminar Condensation inside Horizontal and Inclined Tubes,” Massachusetts Institute of Technology.

[101] Jiang, Y., Liese, E., Zitney, S. E., and Bhattacharyya, D., 2018, “Optimal Design of Microtube Recuperators for an Indirect Supercritical Carbon Dioxide Recompression Closed Brayton Cycle,” Appl Energy, **216**, pp. 634–648.
[102] Turton, R., Bailie, R. C., Whiting, W. B., and Shaeiwitz, J. A., 2018, *Analysis, Synthesis and Design of Chemical Processes.* , Prentice Hall.
[103] Weiland, N. T., Lance, B. W., and Pidaparti, S. R., 2019, “SCO2 Power Cycle Component Cost Correlations From DOE Data Spanning Multiple Scales and Applications,” *Volume 9: Oil and Gas Applications; Supercritical CO2 Power Cycles; Wind Energy*, American Society of Mechanical Engineers.
[104] Bejan, A., Tsatsaronis, G., and Moran, M. J., 1996, *Thermal Design and Optimization*.
[105] Guthrie, K., 1974, *Process Plant Estimating, Evaluation, and Control*, Craftsman Book Company of America.
[106] “CEPCI - The Chemical Engineering Plant Cost Index ® ” [Online]. Available: https://www.chemengonline.com/pci-home. [Accessed: 14-Feb-2024].
[107] “Cost Indices - CEPCI” [Online]. Available: https://toweringskills.com/financial-analysis/cost-indices/. [Accessed: 14-Feb-2024].
[108] Del Turco, P., Asti, A., Scotti Del Greco, A., Bacci, A., Landi, G., and Seghi, G., 2011, “The ORegen$^{TM}$ Waste Heat Recovery Cycle: Reducing the CO2 Footprint by Means of Overall Cycle Efficiency Improvement,” *Volume 3: Controls, Diagnostics and Instrumentation; Education; Electric Power; Microturbines and Small Turbomachinery; Solar Brayton and Rankine Cycle*, ASMEDC, pp. 547–556.
[109] Kimzey, G., 2012, *Velopment of a Brayton Bottoming Cycle Using Supercritical Carbon Dioxide as the Working Fluid.*, Palo Alto, CA.
[110] Cho, S. K., Kim, M., Baik, S., Ahn, Y., and Lee, J. I., 2015, “Investigation of the Bottoming Cycle for High Efficiency Combined Cycle Gas Turbine System With Supercritical Carbon Dioxide Power Cycle,” *Volume 9: Oil and Gas Applications; Supercritical CO2 Power Cycles; Wind Energy*, American Society of Mechanical Engineers.
[111] Ginosar, D. M., Petkovic, L. M., and Guillen, D. P., 2011, “Thermal Stability of Cyclopentane as an Organic Rankine Cycle Working Fluid,” Energy & Fuels, **25**(9), pp. 4138–4144.
[112] Walter, H., and Hofmann, R., 2011, “How Can the Heat Transfer Correlations for Finned-Tubes Influence the Numerical Simulation of the Dynamic Behavior of a Heat Recovery Steam Generator?,” Appl Therm Eng, **31**(4), pp. 405–417.
[113] de Campos, G. B., Bringhenti, C., Traverso, A., and Tomita, J. T., 2020, “Thermoeconomic Optimization of Organic Rankine Bottoming Cycles for Micro Gas Turbines,” Appl Therm Eng, **164**, p. 114477.
[114] Kakaç, S., Liu, H., and Pramuanjaroenkij, A., 2012, *Heat Exchangers*, CRC Press.
[115] Marchionni, M., Bianchi, G., and Tassou, S. A., 2018, “Techno-Economic Assessment of Joule-Brayton Cycle Architectures for Heat to Power Conversion from High-Grade Heat Sources Using CO 2 in the Supercritical State,” Energy, **148**, pp. 1140–1152.
[116] Biondi, M., Giovannelli, A., Di Lorenzo, G., and Salvini, C., 2020, “Techno-Economic Analysis of a SCO2 Power Plant for Waste Heat Recovery in Steel Industry,” Energy Reports, **6**, pp. 298–304.
[117] Caraballo, A., Galán-Casado, S., Caballero, Á., and Serena, S., 2021, “Molten Salts for Sensible Thermal Energy Storage: A Review and an Energy Performance Analysis,” Energies (Basel), **14**(4), p. 1197.

[118] Shamsi, S. S. M., Maccarini, S., Trevisan, S., Barberis, S., and Guedez, R., 2023, "SCO2 BASED PUMPED HEAT THERMAL ENERGY STORAGE SYSTEMS VALORIZING INDUSTRIAL WASTE HEAT RECOVERY: A TECHNO-ECONOMIC ANALYSIS OF THE ROLE OF HIGH TEMPERATURE TES," *Proceedings of the ASME Turbo Expo*.
[119] Maccarini, S., Barberis, S., Shamsi, S. S. M., Gini, L., and Traverso, A., 2023, "PERFORMANCE ANALYSIS OF PTES LAYOUTS EVOLVING SCO<inf>2</Inf> FOR INDUSTRIAL WHR INTEGRATION," *Conference Proceedings of the European SCO2 Conference*.
[120] Guedez, R., Guccione, S., Trevisan, S., Horta, P., Stengler, J., Martins, P., Meyer-Grünefeldt, M., Lopez-Roman, A., Barberis, S., and Xhani, I., 2022, "Demonstration of the SOLARSCO2OL SCO2 Power Cycle for Future Hybrid CSP-PV Plants at the Évora Molten Salt Platform," *28th International Conference on Concentrating Solar Power and Chemical Systems, SolarPACES*.
[121] "DLR – Salt Makes Solar Thermal Power More Cost-Effective" [Online]. Available: https://www.dlr.de/en/latest/news/2022/02/20220428_salt-makes-solar-thermal-power-more-cost-effective. [Accessed: 19-Feb-2024].
[122] Traverso, A., 2005, "TRANSEO Code for the Dynamic Performance Simulation of Micro Gas Turbine Cycles," *Volume 5: Turbo Expo 2005*, ASMEDC, pp. 45–54.
[123] Lambruschini, F., Liese, E., Zitney, S. E., and Traverso, A., 2016, "Dynamic Model of a 10 Mw Supercritical CO<inf>2</Inf> Recompression Brayton Cycle," *Proceedings of the ASME Turbo Expo*.
[124] Baltadjiev, N. D., Lettieri, C., and Spakovszky, Z. S., 2015, "An Investigation of Real Gas Effects in Supercritical CO2 Centrifugal Compressors," J Turbomach, **137**(9).
[125] Reggio, F., Silvestri, P., Ferrari, M. L., and Massardo, A. F., 2022, "Operation Extension in Gas Turbine-Based Advanced Cycles with a Surge Prevention Tool," Meccanica, **57**(8), pp. 2117–2130.
[126] Maclaine-cross, I. L., and Banks, P. J., 1981, "A General Theory of Wet Surface Heat Exchangers and Its Application to Regenerative Evaporative Cooling," J Heat Transfer, **103**(3), pp. 579–585.
[127] Moisseytsev, A., Lv, Q., and Sienicki, J. J., 2017, "Heat Exchanger Options for Dry Air Cooling for the SCO2 Brayton Cycle," *Proceedings of the ASME Turbo Expo*.
[128] White, C. W., Pidaparti, S., O'Connell, A. C., and Weiland, N., 2019, *Cooling Technology Models for Indirect SCO2 Cycles (No. NETL-PUB-22604)*, Pittsburgh, PA, Morgantown, WV, and Albany, OR (United States).
[129] Kays, W. M., and London, A. L., *Compact Heat Exchangers*, McGraw-Hill, New York, NY.